PERIPHERAL NERVE TISSUE ENGINEERING: STRATEGIES FOR REPAIR AND REGENERATION

by

Mitra Lavasani

Bachelor of Science in Molecular Biology, San Jose State University, 1998

Master of Science in Bioengineering, University of Pittsburgh, 2005

Submitted to the Graduate Faculty of

Swanson School of Engineering in partial fulfillment

of the requirements for the degree of

Doctor of Philosophy

University of Pittsburgh

2008

UNIVERSITY OF PITTSBURGH

SWANSON SCHOOL OF ENGINEERING

This dissertation was presented

by

Mitra Lavasani

It was defended on

November 21, 2008

and approved by

Robert J. Goitz, PhD, Assistant Professor, Department of Orthopaedic Surgery

Kacey G. Marra, PhD, Assistant Professor, Departments of Surgery and Bioengineering

Bruno Péault, PhD, Professor, Departments of Pediatrics and Bioengineering

Jonathan B. Pollett, PhD, Assistant Professor, Department of Orthopaedic Surgery

Dissertation Director: Johnny Huard, PhD, Professor, Departments of Orthopaedic Surgery, Molecular Genetics and Biochemistry, and Bioengineering

PERIPHERAL NERVE TISSUE ENGINEERING:
STRATEGIES FOR REPAIR AND REGENERATION

Mitra Lavasani, PhD

University of Pittsburgh, 2008

Peripheral nerve injuries are frequently encountered in trauma, sports accidents, military activities, and degenerative muscle diseases. Like most neurological conditions, patients exhibit pain, sensory and motor deficits, and functional disability. Despite all the advances in biomedical science and technology, achieving full function and organ reinnervation after these injuries remains a major challenge. High costs of healthcare, loss of employment, and social disruption have provided the impetus for active research focusing on improved strategies for repair and regeneration. Stem cell therapy holds tremendous potential for the treatment of pathologic conditions and has consequently emerged as a new area of focus in regenerative medicine. Stem cells isolated from skeletal muscle have been shown to be both pluripotent and of significant therapeutic value; however, their ability to undergo neurogenic differentiation has yet to be investigated. Here, we report that progenitor cells isolated from skeletal muscles of both mouse and human, using our established preplate technique, adopt neuronal and glial phenotypes under controlled culture conditions. Transplantation of these cells into a critical-size sciatic nerve defect allowed full nerve restoration with induction of axonal regeneration through myelin-producing Schwann-like cells. Functional recovery resulted in improved gait of cell-transplanted mice.

Multi-lineage progenitor cells have been recently identified in blood vessel walls, notably in skeletal muscle, and venous grafts have been used effectively to bridge nerve defects

experimentally and clinically, through unknown cellular mechanisms. In a sex-mismatch model, we identified donor-derived Y chromosomes co-localized with host Schwann cells' nuclei, indicating nerve repair through vein grafting are mediated by vascular cells. A sustained decrease in nerve regeneration by decellularized or irradiated venous grafts also highlights the contribution of blood vessel-derived cells to nerve repair. Together, these findings not only identify the cellular basis for the efficacy of therapeutic vein wrapping, but also reinforce the emerging view of muscle cell-mediated therapy for peripheral neuropathies.

TABLE OF CONTENTS

LIST OF TABLES

LIST OF FIGURES

NOMENCLATURE

ACRONYMS, ABBREVIATIONS, AND SYMBOL DEFINITIONS

7-AAD	7-Amino-ActinomycinD
APC	Allophycocyanin
b-FGF	basic Fibroblast Growth Factor
ß-gal	ß-galactosidase
BMP	Bone Morphogenetic Protein
CD34	Cluster Differentiation 34
CD45	Cluster Differentiation 45
CNPase	2', 3'-Cyclic-nucleotide 3'-phosphodiesterase
CNS	Central Nervous System
DAPI	4′, 6′ diamidino-2-phyenylindole
DMD	Duchenne Muscular Dystrophy
DMEM	Dulbecco's Modified Eagle's Medium
DS	Donkey Serum
EGF	Epidermal Endothelial Growth Factor
ELISA	Enzyme-Linked Immunosorbent Assay
EP cells	Early Preplate cells

FACS	Fluorescence Activated Cell Sorting
FBS	Fetal Bovine Serum
FGF-2	Fibroblast Growth Factor-2
FISH	Fluorescent *in situ* hybridization
FITC	Fluorescein Isothiocyanate
f-MyHC	fast Myosin Heavy Chain
FN-MDSCs	Female Newborn-MDSCs
FNr-MDSCs	Female Newborn retroviral Vector Transduced MDSCs
GFAP	Glial Fibrillary Acidic Protein
GS	Goat Serum
HBSS	Hanks' Balanced Salt Solution
H&E	Hematoxylin and Eosin
HSCs	Hematopoietic Stem Cells
HS	Horse Serum
ITS	Intermediate Toe Spread
LTP	Long-Term Proliferating
LP cells	Late Preplate cells
LTP cells	Long-Term Proliferating cells
MAP2ab	Microtubule Associated Protein 2ab
MDSCs	Muscle-Derived Stem Cells
MS	Mouse Serum
MTT	Malignant Triton Tumor
NF	Neurofilament

NGF	Nerve Growth Factor
nLacZ	nuclear *LacZ* reporter gene
NSE	Neuron-Specific Enolase
NS	Neurospheres
PBS	Phosphate Buffered Saline
PCNA	Proliferating Cell Nuclear Antigen
PE	Phycoerythrin
PL	Print Length
PM	Proliferation Medium
PNS	Peripheral Nervous System
RACs	Rapidly Adhering Cells
RI	Regeneration Index
SACs	Slowly Adhering Cells
Sca-1	Stem cell antigen-1
SCID	Severe Combined Immunodeficiency
SFI	Sciatic Functional Index
TD	Terminal differentiation
TDCs	Tumor-Derived Cells
TEM	Transmission Electron Microscopy
TrkA	Tyrosine Kinase receptor A
TS	Toe Spread
UN	Undifferentiated
VEGF	Vascular Endothelial Growth Factor

PREFACE

"I am always doing things I can't do, that's how I get to do them." **Pablo Picasso**

I like to dedicate this work to my beloved mother, brother, sister and my dear nephew and niece. I would like to express my sincere appreciation to my mother for her unconditional love and sacrifices, her commitment as a dedicated parent, and most importantly for being a great friend. You taught me how to be strong, never to give up on my faith, and keep my hopes and dreams alive by overcoming my life challenges. I also dedicate this work to my father, whom I lost at very early age, but I know he would be proud of my accomplishments as he valued education tremendously. Bijan, thank you for giving me the love of a big brother, being supportive, and putting a smile on my face when things got tough while I was confronting my daily educational challenges. You always believed in me even when I was in doubt. Minoo, I appreciate your reassuring words to continue pursing my education and your love as a wonderful sister. Shawn and Zhaleh, I am proud of both of you and hope I have been an inspiration toward your future academic achievements.

I am forever grateful to my mentor, Dr. Johnny Huard, for giving me a second chance and the freedom to experience the beauty and power of scientific discoveries. Your passion for science, generosity, and dedication to students is admirable. Because of your efforts, the doors of opportunity are always open to anyone who likes to seize the challenge and work hard. You have consistently helped me to reach my full potential and beyond. You are both a great mentor and a friend and I look forward to our future collaborations. I offer sincere thanks to all my doctoral committee members. Dr. Kacey Marra, I value your support for women scientists. Dr. Bruno Péault, thank you for sharing your expertise and appreciation of scientific writing. Dr. Robert Goitz, thank you for providing an opportunity for me to use scientific methods to explain a

clinical application. Dr. Jonathan Pollett, I enjoyed our scientific discussions creating new ideas and appreciate your trust in my scientific data and your friendship.

Many thanks to talented and dedicated surgeons Drs. Arvydas Usas, Robert Kaufmann, and Sebastian Gehrmann who helped me to make impossible rather possible.

I would like to thank the chairman of bioengineering, Dr. Harvey Borovetz for his devotion to bioengineering students from diverse background. Many thanks to Dr. David Vorp, for providing an environment where students' concerns and suggestions are always welcome. Special thanks to Lynette Spataro for her willingness to help students and her patience when faced with endless questions. I am blessed to also know you in a personal level and have your love as a close friend.

To all the members of Stem Cell Research Center – both past and present – thank you for providing a friendly and supportive environment. It was truly a pleasure to work with such talented and intelligent individuals with such diverse backgrounds. Dr. Moreland, thank you for your advice and thoughtfulness. Special thanks must go to Drs. Bridget Deasy, Burhan Gharaibeh, and Denise Barry for participating in helpful scientific discussions and Jim Cummins for his thoughtful scientific reasoning. I like to thank Aiping Lu, Marcelle Pellerin, Maria Branca, Joseph Feduska, Jessica Tebbets, Michelle Witt, Alison Logar, Lynn Bauer, Ying Tang, Bin Sun, and Katie Clark for their consideration, willingness to help and sharing their expertise. Joe, thanks for being there for me when I needed a hand or a friend to talk to. Dr. Aiping Lu, thanks for your help throughout these many years. You are a special friend and a wonderful listener. Our old and new supportive administrators, Barbara Lipari, Melanie Predis, Matt Bosco, Paul Loedding, and Michele Keller for offering outstanding assistance and support behind the scene. Michele, thanks for providing a friendly environment in the office. Thanks to Timo Brown, James Panichella, and Matt Yee for their help with my computer glitches. Thanks to Greg Botta, Maria and Jessica, who taught me how to be a Steelers-fan.

To all old and new graduate students who I am delighted to get to know particularly Jenny Zhu, Karin Corsi, Thomas Payne, Tea Soon Park, Bonnie Teng, Ken Urish, Tiffany Sellaro, Lauren Drowley, Jeff Jasko, Rehka Rapaka, and Mihaela Crisan – I appreciate your advice, kindness, and the time spends together.

Especial thanks to Dr. Theresa Cassino and Lauren Drowley for providing and encouragement while I was close to the finishing line of my dissertation, and for their friendship

and willingness to help edit my writings. Drs. Masaho Okada and Masa Nozaki, thanks for sharing Japanese words of wisdom and cultures and being good work companions. Dr. Sheila Ingham, thanks for sharing your time so I get to experience a unique opportunity in the Pittsburgh Zoo. Georgia Pambianco and Tina thanks for your friendship and time spent together.

It was a privilege to be invited by Drs. Ronald Heberman and Devra Davis at the Hillman Cancer Center to attend and present my findings at the UPCI scientific conference. Dr. Davis, you saw teaching ability in me, and I promise if the opportunity presents itself I will gladly teach. I would like to thank Dr. Aran Pollett for providing the differential diagnostic of tumors, Dr. Susanne Gollin and Dale Lewis for their help with the cytogenetic analyses, Dr. Paul Robbins for providing the *nLacZ* virus, and Dr. Simon Watkins, the director of Center for Biological Imaging at University of Pittsburgh, for his resources with the electron microscopy.

I am also grateful to all my undergraduate professors at San Jose State University, particularly Drs. Chris Brinegar, Daniel Holley, and Michael Sneary who helped me to build a solid academic foundation. I appreciate Dr. Donato Di Monte, director of the Basic Research at Parkinson's Institute, for his guidance and trust on my work throughout my early time of research on models of the Parkinson's disease. I would also like to thank my best friend, Nina Sahakian and Drs. Amy Manning-Bog and Daniel Togasaki for believing in me and encouraging me to further pursue my passion to be a scientist.

Coming from California, I have experienced being under the weather some days in Pittsburgh. Luckily, I had my dear skin and cosmetics counselors Trena Sepos, Ellen Borg, and Christine Brososky who made it all melt away. It always made me wonder why Chanel cosmetics experts would be so interested in what I do. They all would welcome me with sparkles in their beautiful and elegantly made-up eyes when we would gather by the Chanel counter at Saks Fifth Avenue in downtown Pittsburgh and discuss my scientific adventures, successes, and setbacks. Thank you all for your kindness, hospitality, and encouraging words. Special thanks to Meagan Oakleys – I always had a great time discussing science with you while shopping for my favorite Sisley brand. Good luck with the school of your dreams.

Lastly, I would like to acknowledged funding support from the Henry J. Mankin Endowed Chair for Orthopaedic Research at the University of Pittsburgh, the William F. and Jean W. Donaldson Chair at Children's Hospital of Pittsburgh, the Hirtzel Foundation, and grants

awarded to Dr. Huard from the NIH (R01AR049684, and R01AR047973) and the Department of Defense (W81XWH04-0003), and to Dr. Robert Goitz from the Foundation of Hand Research.

1.0 BACKGROUND

1.1 ORGANIZATION OF THE NERVOUS SYSTEM

The nervous system is classified into the central nervous system (CNS) and the peripheral nervous system (PNS). The CNS, which includes the brain, spinal cord, optic, and olfactory and auditory systems, conducts and interprets signals as well as provides excitatory stimuli to the PNS. The PNS consists of the cranial nerves arising from the brain, the spinal nerves arising from the spinal cord, and sensory nerve cell bodies (dorsal root ganglia) and their processes. Peripheral nerves innervate muscle tissue, transmitting sensory and excitatory input to and from the spinal column.

1.2 CELLULAR COMPONENTS OF THE NERVOUS SYSTEM

The nervous system is composed of two cell types: neurons and neuroglia. Neurons are the basic structural and functional elements of the nervous system and consist of a cell body (soma) and its extensions (axons and dendrites). Clusters of sensory nerve soma, known as ganglia, are located just outside the spinal column. Dendrites transmit electrical signals to the neuron cell body and the axon conducts impulses away. Glial cells, or neuroglia, are support cells that aid the function of neurons and include Schwann cells in the PNS and astrocytes and oligodendrocytes in the

CNS. Glial cells are more abundant than neurons, and undergo mitosis (cell division) when needed. Unlike neurons, glial cells do not conduct electrical impulses [1].

In the PNS, many axons are surrounded by an insulating myelin sheath formed from multiple layers of successive wrappings of the cell membrane of specialized living cells called Schwann cells (PNS) or oligodendrocytes (CNS). Myelin serves to increase the propagation velocity of the nerve impulse (action potential), which is particularly important for those axons in PNS that extend long distances [1, 2]. These motor neurons relay messages from brain or spinal cord to the muscles and organs and can be over 1 meter long (**Figure 1.1**). Action potential conduction velocity is proportional to axon diameter and also increases as a result of myelination [1].

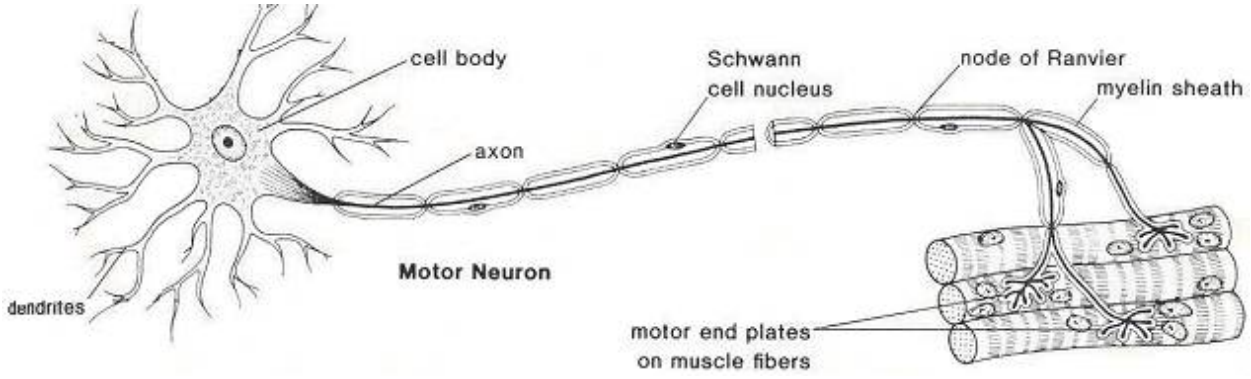

Figure 1.1: Motor neuron with myelinated axon
A typical motor neuron has few processes called dendrites which extend out from the cell body and branch out extensively. It also has a long fibrous axon which originates from a somewhat thickened area of the cell body. A short distance from its origin, the axon acquires a sheath of myelin, a protein- lipid complex made up of many layers of unit membrane. The myelin sheath envelopes the axon except at its ending and at periodic constrictions about 1mm apart called nodes of Ranvier. The axon ends in a number of synaptic knobs at motor end plates. (Figure adapted from www.biologymad.com).

1.3 ANATOMY OF THE PERIPHERAL NERVE

A peripheral nerve consists of motor and sensory axons bundled together by support tissue into an anatomically defined nerve trunk (**Figure 1.2**). In myelinated axons, a single Schwann cell provides insulation to only one axon, while in unmyelinated axons, one Schwann cell envelops several axons [1, 2]. Endoneurium surrounds individual axons and their Schwann cell sheaths and is composed predominantly of oriented collagen fibers. Next, the perineurium, formed from many layers of flattened cells (i.e., fibroblasts) and collagen, surrounds groups of axons to form fascicles. Finally, epineurium, an outer sheath of loose fibrocollagenous tissue, binds individual nerve fascicles into a nerve trunk. Peripheral nerves are well vascularized by capillaries within the support tissue of the nerve trunk or by vessels that penetrate the nerve from surrounding arteries and veins [3].

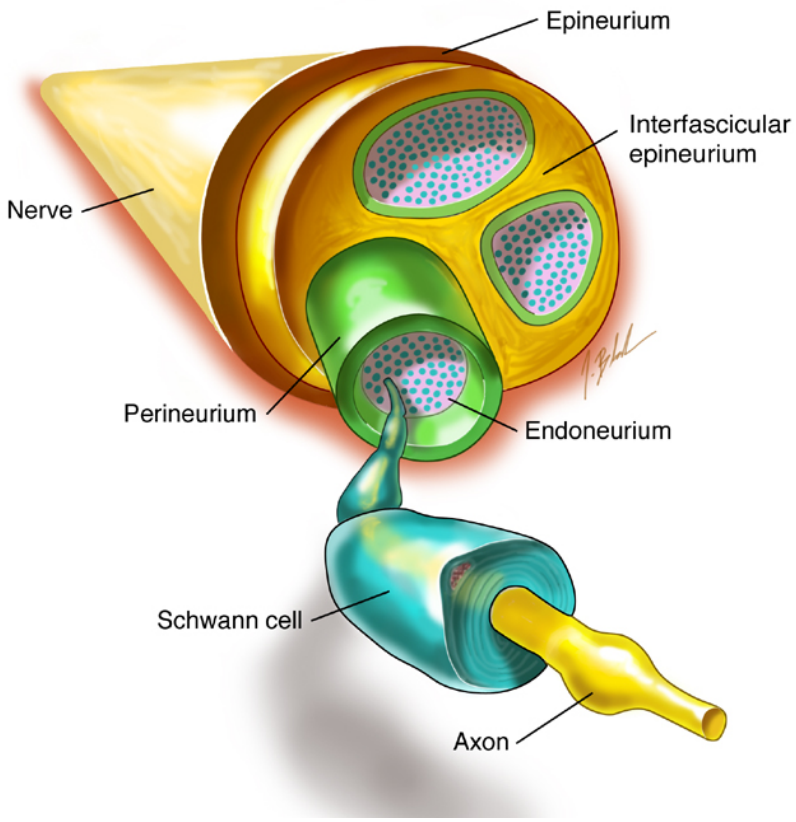

Figure 1.2: Anatomical overview of the PNS
Axons, surrounded by myelinated Schwann cell sheaths, are enclosed by endoneurium. Next, the perineurium binds individual axons together to form fascicles. Several axons are contained in each fascicle. Lastly, epineurium groups fascicles to one another, forming the nerve cable. (Figure adapted from www.backpain.guide.com/Chapter 10-1/Internal Structure of Peripheral Nerves).

1.4 PERIPHERAL NERVOUS SYSTEM INJURY

The most severe injury is a complete nerve transection. When the axon is disconnected from the cell body by injury, its distal segment and myelin sheath gradually degenerates, a feature known as Wallerian degeneration (**Figure 1.3**). As the degeneration of the distal nerve segment continues, connection with the target organ such as muscle is lost, leading to muscle atrophy and fibrosis. The early phase of the degeneration process includes the breakdown of the cytoskeleton,

dissolution of the cell membrane, and the Schwann cells surrounding the axons shedding off their myelin lipids. The proximal end of the nerve stump starts to swell but experiences only minimal damage via retrograde degradation (**Figure 1.3, Step 1**). After the cytoskeleton and membrane degradation, phagocytic macrophages and Schwann cells remove myelin and axonal debris [4] and produce cytokines, which enhance axonal growth [5] (**Figure 1.3, Step 2**). Schwann cells proliferate in the distal nerve segment and when contacted by an axon sprout, undergo a cascade of changes that trigger the production of myelin [6] and form a cell strand called Schwann cell column or band of Büngner [7]. These bands, together with the basal lamina sleeve that surrounds them, guide regrowing axons toward their original innervation [8-15]. Following debris clearance, regeneration begins at the proximal end by the Schwann cells and continues toward the distal stump by phenomenon known as chemotaxis (tropism) [16, 17]. Activation of Schwann cells occurs as early as 12 hours after injury [17]. New axonal sprouts with a fingerlike growth cone usually emanate from nonmyelinated areas of axons called the nodes of Ranvier, located between Schwann cells, and advance using Schwann cells as guides (**Figure 1.3, Step 3**). Conduction of action potentials only occurs at the nodes; this is called saltatory conduction. This mechanism increases the velocity of nerve as much as 5-fold to 50-fold (up to 200 meters per second) and explains the speed at which we can react to potentially harmful stimuli [2]. These sprouts are thinly myelinated by numerous new, but smaller Schwann cells, due to the very limited amount of amino acids produced by the cells at this stage [17] (**Figure 1.3, Step 4**). Functional reinnervation requires that these axons extend until they reach their distal target and the target organ (e.g. skeletal muscle), this usually takes a long period of time (2-5 mm/day in human), and significant injuries can take many months to heal [18].

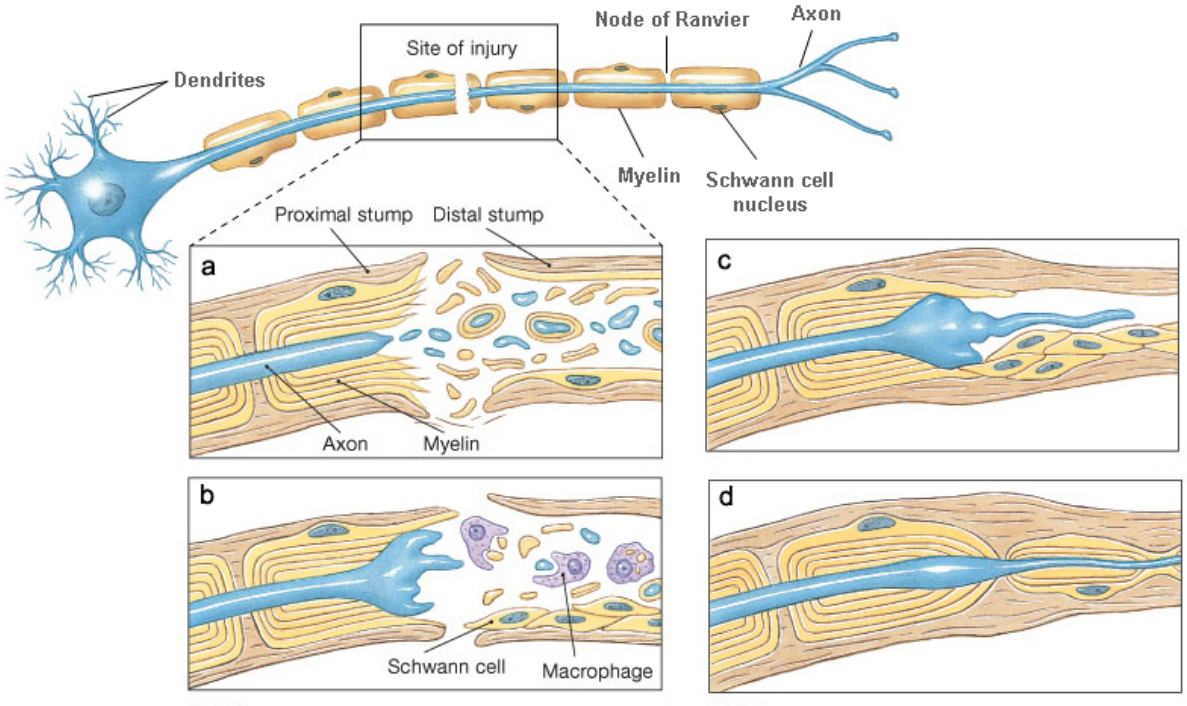

Figure 1.3: Illustrations showing the Wallerian degeneration of the peripheral nerve.
After significant injury, the axon and surrounding myelin break down. (b) Schwann cells form a solid cellular core along the axonal path to unite the stumps while releasing many growth factors, and Macrophages engulf degenerated axon and myelin. (c) Axon send buds into network of Schwann cells and advance along cord of Schwann cells using it as a guide. (d) Axon continues to grow into distal stump and is enfolded by Schwann cells. The newly connected axon to the target organ matures and the pre-injury and the tissue architecture and function are restored. Figure adopted and modified from www.biomed.metu.edu.

1.5 CURRENT TREAMENTS AND THEIR CHALLANGES

For peripheral nerve injury, treatment typically consists of either direct end-to-end surgical reconnection of the damaged nerve ends or the use of an autologous nerve graft. Suturing the ends of the two nerve ends together can repair small defects or gaps in the nerve. For longer nerve gaps, this approach is not desired because any tension introduced into the nerve cable would inhibit nerve regeneration [19]. Thus, for a larger nerve defect, an autologous nerve graft

that is harvested from another site in the body is used to span the injury site [20, 21]. Disadvantages of this technique include loss of function at the donor site and the need for multiple surgeries. Bioengineering strategies for the PNS have focused on developing alternative treatments to the nerve graft (e.g., nerve guidance channels and vein grafts), especially for larger defects, and improving recovery rates and functional outcome. These challenges provide fertile ground for the development of therapies to enhance regeneration.

1.5.1 Guidance therapies

Physical guidance of axons is a vital component of nerve repair. During the nineteenth century, many materials were used in an attempt to physically guide the regeneration of damaged peripheral nerves, including autologous nerve grafts [22], bone [23], metal tubes [24], and fat sheaths [25]. It was not until the 1960s that Millesi pioneered microsurgical techniques to accurately align nerve fascicles in the direct resection of nerve ends, with improved functional outcomes [19]. He also determined that the use of nerve grafts reduced tension on the damaged nerves in many cases and further enhanced functional recovery. These results also supported the need for physical guidance as an essential element in nerve regeneration. Later research demonstrated that biochemical signals as well as physical guidance are critical for nerve regeneration [26-29]. Current research is focused on developing improved “nerve guides” or “nerve conduits” that can be used to physically guide regeneration of nerves across lesions. Past research in this area has focused either on existing natural or synthetic materials; however, none of the materials studied to date have matched or exceeded the performance of the nerve autograft. As a result, researchers are now focusing on the combination of materials and desired biomolecules to create new composite materials that can actively stimulate nerve regeneration. In

addition, methods to minimize the immune response to nonautologous tissue could provide a source of natural material for nerve repair.

1.5.1.1 Autologous tissue grafts

The employment of an autologous nerve segment as an autograft was first reported in 1878, but used widely during World War II [30, 31] and became a standard technique for repairing nerve gaps since the 1970s [32]. For a more thorough synopsis of the early history of nerve repair using nerve grafts, refer to the review by Chiu et al. [33]. For additional information on the surgical techniques used in nerve grafting see references [21, 34-37]. Natural materials are more likely to be biocompatible than artificial materials, are less toxic, and provide a support structure to promote cell adhesion and migration. However, this technique is limited as it entails the sacrificing of healthy donor tissue, the need for multiple surgical procedures, and possible formation of painful neuroma (a bulb-shaped thickening created by improperly and irregularly regenerating nerve fibers). These significant drawbacks have prompted a search for alternative types of non-nervous tissue-engineered guides for repairing nerve defects that could serve to direct axons sprouting from the proximal to the distal end, provide a conduit for the diffusion of growth factors secreted by the injured nerve ends to facilitate restoration, reduce the infiltration of scar tissue, reduce denervation-induced atrophy of muscles, and minimize pain.

In addition to the nerve graft, other natural tissues, such as autologous muscle [38, 39] and vein grafts [33, 40-42], have been used in the clinic. Furthermore, some current research efforts are focused on natural tissue grafts for peripheral nerve repair, including the use of epineurial sheaths [43], tendon grafts [44], muscle-vein combined grafts [45, 46], inside-out vein grafts [47], and vein grafts impregnated with autologous Schwann cells [48]. All have exhibited encouraging results in research but still suffer from the key drawback that tissue must be

removed from the patient. Moreover, veins may also collapse especially when bridging long gaps because of their thin wall and absence of pressure from inside, while the surrounding scar tissue can cause constriction. Using the combined muscle-vein technique has helped to prevent collapsing of the vein wall, but the nerve fibers can easily divert from the muscle tissue and form neuroma in continuity.

1.5.1.2 Non-autologous tissue grafts

Other natural tissues including small intestinal submucosa (SIS) and amniotic tissue grafts have been explored for nerve repair applications. SIS is an acellular matrix derived from small intestine, typically of porcine origin. SIS is prepared from the mucosa and muscle layers of the small intestine, which are treated with a hypotonic solution to lyse and wash away the cells. The resultant ECM material is composed of collagen, fibronectin, growth factors, glycosaminoglycans, proteoglycans, and glycoproteins [49, 50]. Recently, SIS derived from rats has been used in conjunction with Schwann cells to create nerve grafts that promote regeneration almost as well as the nerve autograft [51].

Amnion harvested from human placental tissues has also received attention for its potential use in nerve regeneration applications [52-57]. The amnion is a natural, biodegradable tissue that exhibits low immunogenicity and stimulates new vascularization [58]. This material is also readily available and does not require surgical procedures for harvesting. This tissue is processed by removal of the epithelial cell layer from the amnion membrane while the basement membrane and stromal surfaces remain intact. The resulting acellular connective tissue matrix are manufactured into thin dry sheets and then subsequently processed into conduits. Comparable to the nerve autograft, amnion tubes have been shown to promote regeneration across 1 cm defects in the sciatic nerves of rats, and completely degrade by 4 months [54].

1.5.1.3 Synthetic materials

Research is growing to identify synthetic materials that can be used for nerve repair applications. The earliest of these was made of silicone. However, this non-biodegradable material eventually produces nerve constriction resulting in pain and partial destruction of the regenerated axons [59]; for this and other reasons, the focus of the search was shifted to nerve guides composed of biodegradable material. Biodegradable natural materials such as collagen, fibronectin, and laminin, as well as biodegradable synthetic materials such as polyesters, polyurethanes, and poly (organo) phosphazenes, have all been investigated as autograft substitutes. All of these materials can be used to provide a scaffold for axonal regeneration but lack the ability to actively stimulate nerve regeneration with the support cells and neurotrophic factors found in autologous grafts. For this reason, simple nerve guides have been effective only for short defects and are therefore of limited value in clinical practice particularly for large nerve defects [60-62]. But, synthetic materials are still attractive choice because their chemical and physical properties (e.g., degradation rate, porosity, mechanical strength) can be specifically optimized for a particular application.

According to Hudson *et al.* [63], the desired physical properties of a nerve guidance channels include: a biodegradable and porous channel wall (to allow diffusion of nutrients and elimination of waste products); the ability to deliver bioactive factors such as growth factors; the incorporation of support cells; an internal oriented matrix to support cell migration; intraluminal channels to mimic the structure of nerve fascicles; and electrical activity. For detail reviews of different synthetic materials used in aiding nerve regeneration refer to review paper by Hudson and Schmidt [63]. Despite the combined efforts of scientists and engineers from a variety of disciplines to design sophisticated synthetic nerve guides, the outcome after peripheral nerve

repair has not been satisfactory. Functional recovery is not always obtained, reinnervation may be unsatisfactory, and neuroma and scar tissue formation are common. In addition, the biocompatibility of synthetic materials poses a challenge because of inflammatory response causing immunorejection. More research is required to discover synthetic materials that are tolerated by the immune system and are more "cell friendly" in order to achieve functional recovery of peripheral nerve through combined therapies.

1.5.2 Cellular therapies

Independently of the type of non-nervous conduit employed to bridge a nerve gap, it was soon became clear to researchers that the availability of an adequate number of Schwann cells along the entire graft length to support axon regeneration was the critical point, as judged by the eventual success of the nerve repair. In fact, when non-nervous guides are used, Schwann cells that are required for successful axon regeneration inside the tube originate from bilateral migration from both severed nerve stumps [12, 64-67]. Consequently, there has been growing enthusiasm for the use of cell-based therapies for peripheral nerve regeneration. This concept is based upon the ability of transplanted cells to differentiate into specific tissue cell types or participate in the recovery process by cell fusion and/or differentiation, cell-to-cell contact, or sustained release of neurotrophic factors. These properties may be the premise of an early regenerative stage that leads to accurate target reinnervation, and, thus, less axonal dieback.

1.5.2.1 Schwann cells

Schwann cells are prime providers of the supportive environmental milieu for peripheral nerve tissue, as they produce neurotrophic factors, neural adhesion molecules, and extracellular

matrix proteins [68, 69]. These cells play a critical role in leading peripheral axons to the distal nerve stump and synapse formation [70], and are consequently integral to peripheral nerve regeneration [71]. Nerve grafts without viable Schwann cells have shown an inferior axonal regeneration caused by a decrease in neurotrophic and neurotrophic influence [72, 73]. For all of these reasons, the ability of Schwann cells to promote nerve regeneration has been a research area of intense focus [74-77]. There are two major difficulties in using Schwann cells for nerve guides in clinical situations. First, autologous Schwann cells need to be harvested from the injured patient, requiring nerve tissue that is difficult to obtain without morbidity. Second, human Schwann cells are difficult to isolate and expand *in vitro*, requiring elaborate mitogenic cocktails and prolonged periods of growth to obtain sufficient cultures for nerve guide construction. These difficulties significantly limit the clinical feasibility of a nerve guide containing autologous Schwann cells. Therefore, researchers continue to pursue the development of cellular therapies based on populations of stem cells capable of Schwann cell differentiation.

1.5.2.2 Stem cells

Stem cells play a critical role during embryo and tissue formation throughout development. Due to their multipotentiality, the ability to give rise to different lineages of mature cells, and to an extensive capacity for self-renewal and expansive growth, stem cells can also contribute to the maintenance of tissue integrity in adulthood. Historically, it has been held that fetal and adult (somatic) stem cells are tissue-specific 'entities' whose differentiation potential is limited to the generation of mature cell types of the tissue/organ in which they reside. Yet, recent years have seen the publication of an impressive sequence of reports detailing what is now emerging as one of the most striking functional attributes of somatic stem cells, the capacity to undergo transdifferentiation. This peculiar characteristic allows adult stem cells to display an

unexpected ability to give rise to differentiated cells of tissues and organs different from those in which they reside.

It is postulated that adult stem cells may provide promise for improving functional outcomes after peripheral nerve injuries by a combination of many factors. Stem cells can act as surrogate Schwann cells and supply neurotrophic factors and cell adhesion molecules to aid axonal outgrowth over long distances, prevent degeneration of distal ends, restore growth-promoting ability via differentiation toward glial cells (especially Schwann cells), and deliver supportive ECM components [78]. The utility of stem cell therapy is based on variety of their unique characteristics and behaviors: (i) self-renewal that results in a large number of progeny; (ii) long-term proliferation while in a transient quiescent state; and, (iii) multilineage differentiation that increases the efficiency of transplanted stem cells to differentiate into tissue-specific cell types.

Research in the use of adult-derived stem cells for regenerative medicine is rapidly progressing. Post-natal cells can circumvent some of the problems associated with embryonic stem cells, such as immunologic incompatibility, and ethical issues. Recent investigations have clearly demonstrated that multiple types of pluripotent stem cells exist in various types of postnatal tissues [79-83]. Neural stem cells, which are imprinted to generate neurons and glial cells, can differentiate into blood [84] and skeletal muscle cells [81, 82] as well as give rise to cell types found in all germ layers when implanted within the amniotic cavity of chick embryos [81]. Bone marrow stem cells, which are mainly destined to replenish blood cell populations, can contribute to the formation of various cell types in skeletal muscle [79, 80], the liver [85], and the brain [83, 86-89]. However, recent studies have called into question the observations of bone marrow cells dedifferentiation into neurons [90, 91]. Adipose-derived stem cells from mice and

human have also been shown to undergo osteogenic, myogenic, chondrogenic, and neurogenic differentiation [92-100]; for review papers refer to Kokai *et al.*, and Safford *et al.* [101, 102].

Skin-derived precursors can proliferate and differentiate in culture to produce neurons, glial, smooth muscle cells, and adipocytes [103]. Hair follicle stem cells have been shown to differentiate into neurons, glial, keratinocytes, smooth muscle cells, and melanocytes *in vitro* [104] and contributed in regeneration of severed peripheral nerve by differentiation toward Schwann cells [105]. Together, these studies indicate that different tissues contain a small population of pluripotent stem cells with the capacity to generate the tissue in which they reside and the ability to differentiate into diverse lineages when stimulated by appropriate environmental cues. Therefore, stem cells are being extensively investigated as transplants to support nerve regeneration.

1.6 STEM CELLS AND THEIR MICROENVIRONMENTAL NICHE: AN INSEPARABLE RELATIONSHIP

The concept of a niche as a specialized microenvironment housing stem cells was first proposed by Schofield almost 30 years ago in reference to mammalian haematology [106]. In the respective organs, tissue-specific stem cells are often localized in specific compartments (termed stem cell niches) where they are provided with the environmental requirements for their proliferation and differentiation [107]. The simple location of stem cells is not sufficient to define a niche. The niche is both anatomically and functionally dimensioned, specifically enabling stem cells to reproduce and self-renew [108]. The survival, expansion and differentiation of stem cells appear to be regulated by environmental signals as well as potential

of the cells themselves [109-111]. Different growth factors, cytokines, extracellular matrix proteins, and neurotransmitter have been implicated in the epigenetic regulation of the proliferation and differentiation processes [112-115]. Because cell fate conversion occurs when stem cells are transplanted to different environments, it has been proposed that stem cells are extremely plastic and have the ability to respond to various environmental signals that regulate their change in commitment. This cell fate conversion or trans-differentiation capacity of stem cells represents an emerging and promising area of study because of its therapeutic implications (for reviews refer to [107, 116]. Perhaps the niche may become a guide to novel way to enhance the regenerative capacity of normal stem cells and limit the malignant potential of cancerous ones. This interplay between stem cells and their niches may create the dynamic system necessary for sustaining tissues, and for the ultimate design of stem-cell therapeutics or anti-cancer drugs.

2.0 SIGNIFICANCE

Each year, over 50,000 peripheral nerve repair procedures are performed in the United States (*National Center for Health Statistics based on Classification of Diseases*, *Ninth Revision;* Clinical Modification for ICD-9 CM codes 04.3, 04.5, 04.6) due to physical injuries, systemic diseases, and inherited peripheral neuropathies. Peripheral nerve injuries are commonly encountered clinical problems that often lead to long-term functional deficits and expensive health care, lost employment, and social disruption [117]. Patients with peripheral nerve problems, like most neurological conditions, exhibit pain, sensory and motor deficit due to loss of axonal continuity, and functional disability.

Despite recent advances in microsurgical techniques and improved understanding of nerve regeneration, functional recovery following repair of peripheral nerves often remains poor [118, 119] due to many factors: (i) a progressive decline in the ability of motor neurons to sustain axonal growth; (ii) denervated Schwann cell atrophy and failure to provide a supportive growth environment; (iii) slow rate of axonal regeneration across the gap; (iv) misdirection of regenerating axons due to random reinnervation; and, (v) the formation of painful neuroma [16]. Therefore, achieving full function and accurate reinnervation after these injuries continues to be a major challenge. These consequently exacerbated burdens on patients and society have provided the impetus for research into reconstructive strategies for repairing peripheral nerve injuries.

2.1 SKELETAL MUSCLE-DERIVED STEM CELLS: POTENTIAL CANDIDATE FOR TISSUE ENGINEERING

In 1993, Langer and Vacanti [120] defined tissue engineering as "an interdisciplinary field that applies the principles of engineering and life sciences toward the development of biological substitutes that restore, maintain, or improve tissue or organ function." Tissue engineering has now emerged as a potential alternative to tissue or organ transplantation and stem cell therapy emerged as an area of focus in regenerative medicine. Cells play a key in tissue engineering and repair due to active participation by proliferation and differentiation, cell-to-cell signaling, biomolecule production, and formation of extracellular matrix, or indirect contribution by triggering the recruitment and activation of the host cells at the site of injury vital to aiding the process of regeneration. Skeletal muscle is as an accessible source from which somatic stem cells with the capacity to undergo multilineage differentiation could be isolated for utilization in cell replacement therapies [80, 121-127]. Muscle-derived stem cells (MDSCs) isolated from skeletal muscle by a modified preplate technique have been recognized by the Huard group for sustained self-renewal and proliferation, plasticity, and most recently resistance to oxidative/hypoxic stress [124, 128-130]. MDSCs differentiate into several cell types, including skeletal muscle, osteogenic, hematopoietic, and vascular endothelial cells [122, 124, 127]. Furthermore, MDSCs have been used to regenerate skeletal and cardiac muscle as well as bone and cartilage *in vivo*, and to replenish the bone marrow of lethally-irradiated mice [122, 124, 131, 132].

MDSCs can be an attractive candidate for clinical use in regenerative medicine because they can be easily obtained by a relatively non-invasive superficial muscle biopsy, readily expanded *in vitro*, and transplanted in an autologous manner. Following transplantation, MDSC most likely enhance restoration of damaged tissue by differentiation toward the necessary

lineages and secreting trophic factors. In case of neuronal tissue engineering, we desire these cells to restore the neural and vascular supply during nerve regeneration by undergoing multipotent differentiation into endothelial, neural and Schwann cell-like phenotypes, the primary types of tissue required for proper nerve healing. Furthermore, the application of exogenous neurotrophic factors by MDSCs could be an effective means of promoting regeneration in an *ex vivo* gene therapy approach to deliver therapeutic factors that would enhance the effect of cell transplantation. Transplanted MDSCs pose advantages as a means of delivering a continual supply of active neurotrophins [133], which promote the recruitment of macrophages and Schwann cells at the site of injury, thereby facilitating more active and directed axonal growth and promoting regeneration. They may also contribute by differentiating toward a neuronal/glial lineage themselves.

2.2 PROJECT OBJECTIVES

The overall objective of this research project is to determine the potential of murine muscle-derived stem cells (mMDSCs) and human muscle-derived progenitor cells (hMDPCs) isolated via the modified preplate technique to adopt neuronal and glial (in particular Schwann cell) phenotypes *in vitro*, and examine the capacity to support peripheral nerve regeneration and remyelination *in vivo*. In addition, cellular mechanism behind the efficacy of vein grafts applied as nerve conduits in clinic is also investigated. The objectives outlined below will help to test our hypotheses at all three levels: histological, biochemical, and functional.

2.2.1 Objective 1: Investigation of mMDSCs to adopt neuronal and glial phenotypes, and regenerate peripheral nerve defects

Our group has previously shown that cultured mMDSCs can differentiate toward skeletal muscle, bone, cartilage, endothelial, and hematopoietic cell lineages [122, 124, 127, 131, 132]. However, their capacity for neuronal and glial differentiation is unknown. It has been postulated that the microenvironment dictates the fate of stem cells, therefore we hypothesized that mMDSCs undergo mature neuronal and glial lineages differentiation under controlled culture conditions. Also, transplantation of mMDSCs accelerates the regeneration and functional recovery of critically sized sciatic nerve defects in mice following injury. The expression level of a population of mMDSCs for mature neuronal and glial-specific cell markers was screened in pre- and post-differentiation culture conditions, by means of immunocytochemical staining. Additionally, the process of nerve regeneration, including the proper regeneration and degree of myelination, as well as mMDSCs contribution through differentiation, was evaluated by histology, immunohistochemistry, and electron microscopy. Functional recovery of the severed sciatic nerve was determined using walking track assessment to evaluate nerve to muscle reinnervation.

2.2.2 Objective 2: Evaluation of hMDPCs for neuronal and glial differentiation, and nerve regeneration capacity

There is growing evidence to suggest that reservoirs of stem cells may reside in human skeletal muscle that can retain the potential to transdifferentiate from one phenotype to another,

presenting exciting possibilities for cellular therapies. The optimal cell type for neural tissue engineering would be progenitor/stem cells that survive, migrate, and engraft to promote regeneration. We hypothesized that hMDPCs isolated using our established modified preplate technique are capable of neuronal and glial differentiation. In addition, transplantation of these cells will improve the regeneration and functional recovery of critically sized sciatic nerve defects following injury.

Under controlled cultural conditions, we evaluated the capacity of hMDPCs to adopt neuron, astrocytes, oligodendrocytes, and Schwann cell phenotypes. Our proposed stem cell-based therapy relied on the ability of transplanted hMDPCs to facilitating the axonal regeneration, remyelination, and reduction of neuroma formation in our murine sciatic nerve defect model. Hence, the efficacy in achieving sciatic nerve regeneration following hMDPCs implantation was evaluated quantitatively by assessing motor function and improvement of gait as well as histological characterization of the regenerated nerve. The data generated from these experiments will further elucidate multipotentiality of hMDPCs and may help facilitate their usage potential candidate in cell-mediated therapies and tissue engineering applications for peripheral nerve injuries.

2.2.3 Objective 3: To identify cellular mechanisms for the efficacy of venous grafts in peripheral nerve reconstruction

Venous grafts are used experimentally and clinically to bridge peripheral nerve defects. This alternative strategy rely on the fact that the donor vein is easily withdrawn in close proximity to the involve nerve with minimal complications eliminating the sacrifice of healthy nerve. This approach has been highly conducive to tissue regeneration, and shows great promise for repair of

damaged nerves. However, exactly why vein wrapping or the use of venous nerve conduits is so successful in regenerating peripheral nerve is a question that remains, as yet, unanswered. In addition, a recent study has identified endothelial cells as critical components of the neural stem cell niche and their self-renewal [134]. A novel subset of cells overlapping phenotype between myogenic and endothelial cells was recently reported by our group to exhibit strong myogenic potential in skeletal muscle [135]. Interestingly, human endothelial cells and vascular pericytes were recently documented to be capable of generating various mesodermal derivatives, primarily skeletal muscle [136]. These results let us postulate that blood vessels may harbor a reserve of multi-lineage stem cells that play an active role in the process of regeneration.

Therefore, we hypothesized that venous nerve guides might improve healing of peripheral nerve defects due to contribution of stem/progenitor cells that reside in donor blood vessels. This may elucidate the rationale behind efficacy of using venous nerve conduits in surgical procedures to bridge peripheral nerve damage. Hence, we aimed to investigate this underlying principle by using a rat sex mismatch model and fluorescence in situ hybridization to detect donor-derived Y chromosomes in regions of host regenerated nerve. In doing so, we may uncover useful information to explain the cellular basis for the success of such clinical treatments, and provide the cornerstone for future work intended to explore the relationship between stem/progenitor cells, cell differentiation and/or fusion, and nerve regeneration.

3.0 FATE OF MDSCS IS MICROENVIRONMENT DEPENDENT

3.1 INTRODUCTION

Cell-to-cell interaction, cell-to-tissue matrix contact, and the presence of certain factors and signaling molecules together within the stem cell niche/compartment regulate stem cell homeostasis and determine their fate [137, 138]. Stem cells are engaged in constant cross-talk with their environment, and are influenced by the signals that they receive [137]. In 1968, investigators revealed that bone marrow possessed unique and potent attributes; hematopoietic stem cells (HSCs) that resided there appeared to be able to live forever. Once HSCs left the marrow environment, the cells immediately began to differentiate [139]. It has consequently been suggested that the environment is a greater factor in neural stem cell fate than the intrinsic properties of the cell [140]. More and more researchers are embracing the ecological concept of the niche and have begun to equate niche with the microenvironment in which the stem cells reside. Hence, it is believed that the interplay between stem cells and their niche creates key fate-determining events necessary for sustaining tissues [108, 141].

Muscle-derived stem cells (MDSCs) isolated from the skeletal muscle of normal mice (mMDSCs) have been recognized by our group for their sustained self-renewal and proliferation, developmental plasticity, and most recently resistance to oxidative/hypoxic stress [124, 128, 129]. Cultured MDSCs can differentiate into several cell types, including skeletal muscle,

osteogenic, hematopoietic, and vascular endothelial cells [122, 124, 127]. Furthermore, we have used these cells to regenerate skeletal and cardiac muscles as well as bone and cartilage, and to replenish the bone marrow of lethally-irradiated mice [122, 124, 131, 132]. Prior studies in our laboratory have also examined the roles of bone morphogenetic protein (BMP)4, nerve growth factor (NGF), and vascular endothelial growth factor (VEGF) on MDSCs fate [122, 124, 133]. Namely BMP4 induced osteogenesis [122], while NGF and VEGF induced neurogenic and endothelial differentiation of MDSCs [122, 124]. In addition, NGF stimulation of MDSCs significantly improved their engraftment in dystrophic muscles of *mdx* mice [133], suggesting a link between neurogenesis and myogenesis, and substantiating the role of the environment in stem cell differentiation. However, the potential involvement of mMDSCs in neurogenesis remains undetermined. The objective of this study was to investigate differentiation ability of mMDSCs toward neuronal and glial cell lineages in culture, and explore their regeneration efficiency *in vivo* using a sciatic nerve defect model in mice.

3.2 RESULTS

3.2.1 Myogenic differentiation

3.2.1.1 FNr-MDSCs display stable cell marker profile

Using a modified preplate technique, we have previously isolated MDSCs from wild-type skeletal muscle according to their adhesion and proliferation characteristics [122, 124, 142]. MDSCs differentiate to multiple cell lineages *in vitro* and *in vivo* [124, 127]. We employed this technique on skeletal muscle from a female newborn (FN) C57BL/10J mouse to isolate FN-

MDSCs. Similar to previously reported isolates [124], most of these cells were positive for the stem cell surface markers CD34 (88.5%) and Sca-1 (87%), showing 78% CD34/Sca-1 double-positive cells by flow cytometry, and very few cells expressed myogenic cell marker desmin (<1.5%), as observed following immunofluorescence staining. The cells were initially plated at a density of 250 cells/cm^2 and 20-30% confluency, and transduced with a retroviral vector containing a nuclear *LacZ* reporter gene (*nLacZ*) [122, 124, 131] for donor cell tracking. The cells were subcloned to obtain a population (FNr-MDSCs) that was over 90% ß-gal-positive (**Figure 3.1a**). We found no significant difference in cell marker expression compared to the parental FN-MDSCs, suggesting the stability of FNr-MDSCs *in vitro*.

3.2.1.2 FNr-MDSCs display a high myogenic potential *in vitro* and *in vivo*

As it has been previously reported that MDSCs generally have a high myogenic index [122, 124], the ability of FNr-MDSCs to undergo myogenesis was assessed. FNr-MDSCs were cultured in myogenic differentiation medium (2% FBS in DMEM) for 5 days. After cultivating the cells under low-serum conditions, myotube formation was detected by immunocytochemical staining for expression of fast myosin heavy chain (f-MyHC), a marker of terminal myogenic differentiation. As expected, FNr-MDSCs fused and formed multinucleated myotubes expressing f-MyHC (**Figure 3.1b**). Myogenic potential of FNr-MDSCs was further evaluated by their ability to regenerate dystrophin-positive muscle fibers after intramuscular implantation in dystrophin-deficient *mdx* mice was examined. Fourteen days post-implantation, many dystrophin-positive myofibers could be found within the injected muscle (n = 10; three independent experiments, **Figure 3.1c**). Furthermore, donor-derived *nLacZ*-positive nuclei could be observed within the regenerated myofibers 17 weeks (120 days) post-implantation (**Figure 3.1d**).

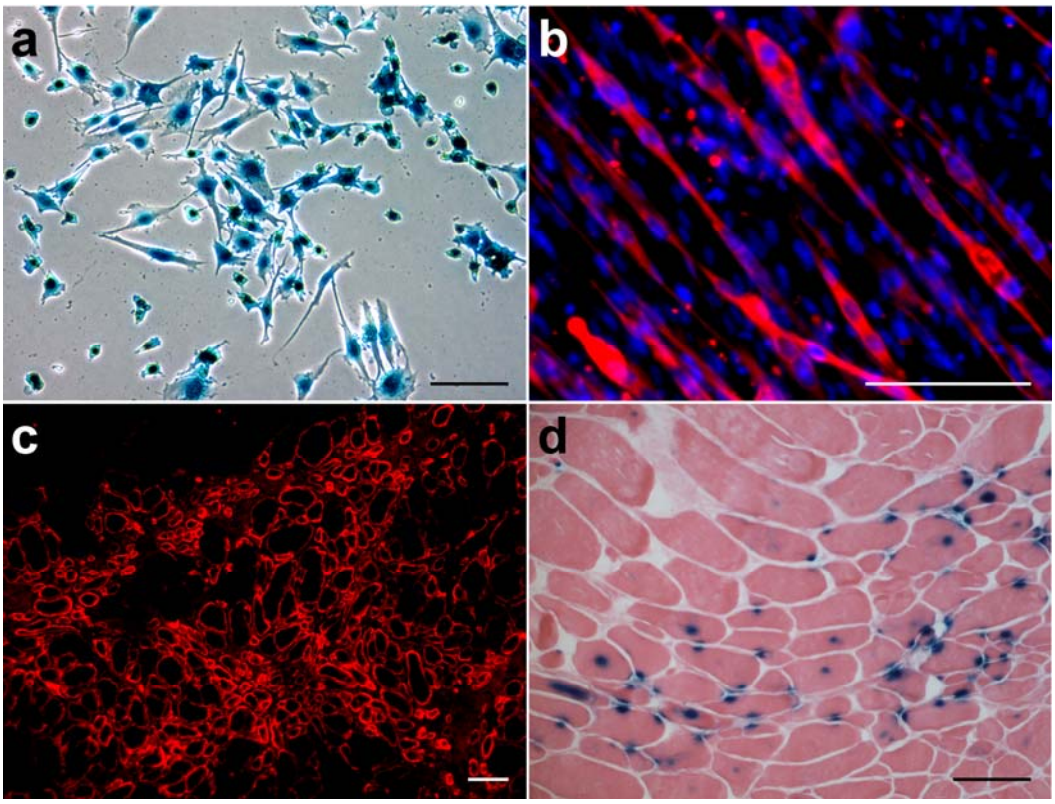

Figure 3.1: FNr-MDSCs exhibit myogenic differentiation potential *in vitro* and *in vivo*
(**a**) A population of female newborn MDSCs (FN-MDSCs) was genetically engineered to express a retroviral vector containing a nuclear *LacZ* reporter gene (*nLacZ*). Positive staining (blue) is localized to the nucleus of the cells. (**b**) Ten days after culture in low serum differentiation medium, FNr-MDSCs differentiated into multinucleated myotubes expressing f-MyHC (red) (overlaid on nuclear counterstain [DAPI; blue]). (**c**) Fourteen days after injection, cryosections of the gastrocnemius muscle of *mdx* mice immunostained for dystrophin expression show large numbers of regenerated dystrophin-positive myofibers (red). (**d**) The *nLacZ*-positive donor-derived FNr-MDSCs (blue) could be detected in regenerated myofibers 17 weeks after injections. Scale bars represent 100 μm.

3.2.2 Neuronal and glial cell differentiation

3.2.2.1 FNr-MDSCs express both neuronal and glial cell markers and can undergo neuronal and glial differentiation *in vitro*

Though MDSCs are myogenic both *in vitro* and *in vivo* [122, 124], the purpose of this work was to ascertain the potential involvement of MDSCs in neurogenesis. FNr-MDSCs were screened by immunocytochemistry for a series of neurogenic and glial cell markers prior to

differentiation. Most undifferentiated FNr-MDSCs (96% ± 4.9) were positive for nestin (a neuroepithelial progenitor marker), CNPase, a marker of oligodendrocytes (88% ± 9.0), and 53% ± 14.0 positive for neurofilament (NF, a postmitotic neuronal cell marker); but negative for other cell markers of neuronal maturity, such as neuronal nuclei (Neu-N), suggesting the phenotypic heterogeneity of FNr-MDSCs. In defined serum-free medium supplemented with growth factors (EGF and bFGF) [125], FNr-MDSCs generated free-floating clusters of cells (FNr-MDSC-derived neurospheres) within 7 to 10 days (**Figure 3.2a**, bright-field) with many cells on the outer surface displaying microspikes; a characteristic of neurospheres evident at higher magnification [125]. These clusters were successfully passaged and expanded as single cell suspension. Three to five days after each passage, all cells formed neurospheres. These FNr-MDSC-derived neurospheres expressed neuronal markers (β-tubulin III, NF, and Neu-N), a marker for myelin producing oligodendrocytes and Schwann cells (CNPase), and the astrocytic marker, glial fibrillary acidic protein (GFAP) (**Figure 3.2a**). Though FNr-MDSC-derived neurospheres expressed lineage commitment markers, the expression of neuroendothelial progenitor marker nestin was also retained (**Figure 3.2a**).

The FNr-MDSCs, unlike some neural stem cells derived from the developing brain [143], appear to require exogenous factors to trigger commitment to a neurogenic cell lineage. Elimination of mitogens, a negatively charged surface (poly-D-lysine), and high serum levels (10% FBS) were required to induce further neuronal and glial differentiation of our adult stem cells. After 3 days in differentiation medium, FNr-MDSC-derived neurospheres induced cells with diverse morphology, including small and round, large and flat, spindle-shaped cells, and round cell bodies with thin extended processes (**Figure 3.2b**, bright-field). Over 70% of cells were positive for the neuronal markers β-tubulin (**Figure 3.2b**, N) and NF, and 88% were

positive for the astrocyte marker GFAP (**Figure 3.2b**, A), while 22% expressed the immature oligodendrocyte cell marker NG2 (**Figure 3.2b**, O), and 65% displayed the mature oligodendrocyte marker-O4. The expression of both neuronal and astrocyte cell markers simultaneously has been observed previously *in vitro* in hippocampal stem cells after treatment with bFGF in a serum-free medium [144], in the rat embryonic striatum at early stages of differentiation [145], and in immortalized embryonic mesencephalic mouse cells [146]. Similarly, postnatal forebrain neural progenitors can display mixed glial and neuronal properties *in vitro* when they co-express neuron-specific enolase (NSE), NF, and GFAP [147]. Thus, co-expression of glial and neuronal cell markers seems to reflect multipotentiality at early stages of neurogenic differentiation *in vitro*.

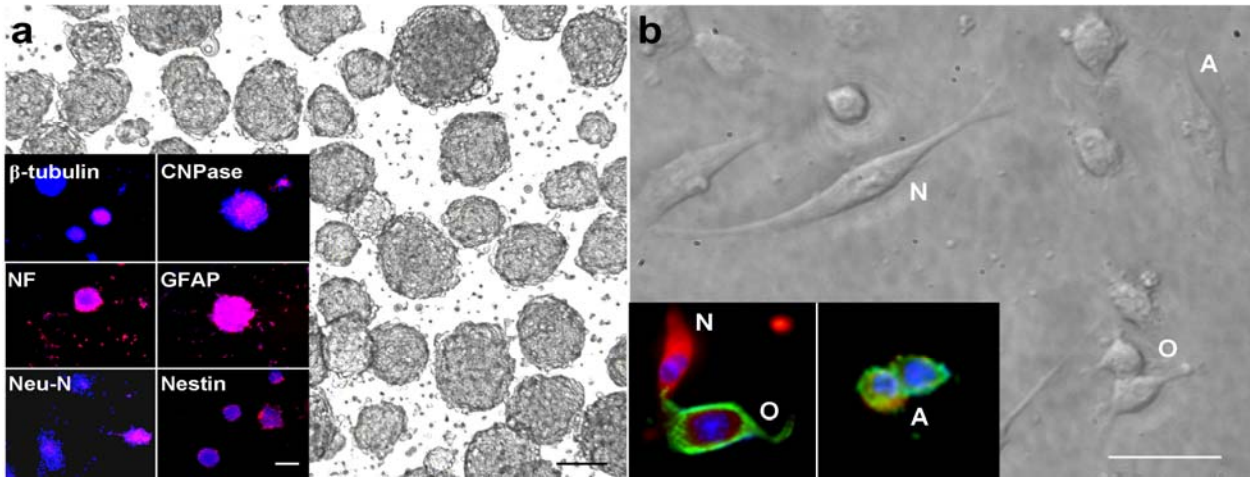

Figure 3.2: FNr-MDSCs display neurogenic and glial differentiation potential *in vitro*
(**a**) FNr-MDSCs were able to generate neurospheres (three-dimensional non-adherent clusters of cells) in neurogenic medium within 7 to 10 days in culture (bright-field image). FNr-derived neurospheres express the neuronal cell markers β-tubulin III, NF, Neu-N, the myelin producing oligodendrocytes marker CNPase, and the astrocytic marker GFAP, and retained their nestin (a neuroepithelial progenitor marker) expression (inset). For all immunofluoresence staining, antibodies used are visualized in red with the nuclear stain (DAPI) seen in blue. (**b**) The FNr-derived neurospheres can be further differentiated into neurons (β-tubulin [red], N), oligodendrocytes (NG2 [green], O), and astrocytes (GFAP [green], A) (inset). The above results represent at least three independent experiments and negative controls were sections similarly processed but without primary antibodies (not shown). Scale bars represent 100 μm (**a**) or 50 μm in (**b**).

In addition, we found β-gal-positive (red) cells that expressed markers associated with Schwann cells, including the S-100 protein (green, **Figure 3.3a**), CNPase (green, **Figure 3.3b**), GFAP (green, **Figure 3.3c**), the neurotrophin receptor p75 (green, **Figure 3.3d**) and the tyrosine kinase receptor TrkA (green, **Figure 3.3e**). Taken together these results indicate that FNr-MDSC-derived neurospheres can differentiate along all three neurogenic lineages, as well as into Schwann cells *in vitro*.

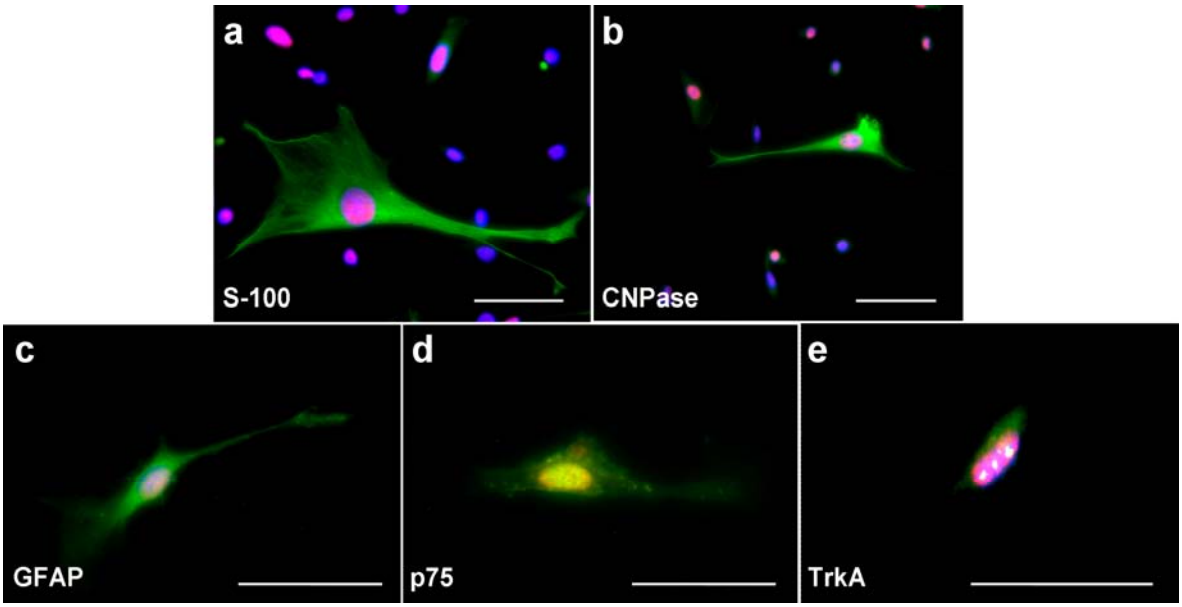

Figure 3.3: FNr-MDSCs can differentiate to Schwann cells *in vitro*
FNr-derived neurospheres were differentiated further into cells that expressed markers found on Schwann cells (green), including: (**a**) the Schwann cell protein S-100, (**b**) CNPase, (**c**) GFAP, (**d**) the neurotrophin receptor p75 and (**e**) the tyrosine kinase receptor TrkA. All cells were positive for β-gal (red). Note: for negative controls, sections were similarly processed but without primary antibodies. They demonstrated negligible levels of non-specific background (data not shown). Scale bars represent 50 μm**.**

3.2.2.2 FNr-MDSCs differentiate into Schwann cells and participate in the regeneration of the injured peripheral nerve

To test the ability of FNr-MDSCs to participate in the regeneration of the peripheral nerve following injury, the cells were implanted into a critical-sized sciatic nerve defect in mice. To generate the nerve defect, the sciatic nerve was exposed and a 4- to 5-mm segment of the

nerve was removed (**Figure 3.4a**), resulting in a ~6.5- to 7-mm critical-size defect (a defect preventing autonomous healing) due to retraction of the nerve ends (n = 48; three independent experiments, **Figure 3.4b**). Equal volumes of either FNr-MDSCs or phosphate buffered saline (PBS) were implanted in the proximal and distal nerve stumps, and the wound was closed. Complete sciatic nerve regeneration was observed 5 to 9 weeks following transplantation in all of the mice that received FNr-MDSCs (n = 24; three independent experiments; **Figure 3.4c**), while the control group exhibited no regeneration, though some nerve sprouting on the proximal side was observed (n = 24; three independent experiments). Notably, blood vessel networks were also present around all regenerated nerve (**Figure 3.4c,** arrows). The regenerated nerve contained many donor *nLacZ*-positive cells (**Figure 3.4d**) and exhibited both NF (green) and CNPase (red) immunoreactivities (**Figure 3.4e**). Furthermore, the regenerated nerve contained nodes of Ranvier-like-structures**,** the gaps (about 1 micrometer in diameter) formed between myelin sheath cells along axons or nerve fibers (**Figure 3.4f**).

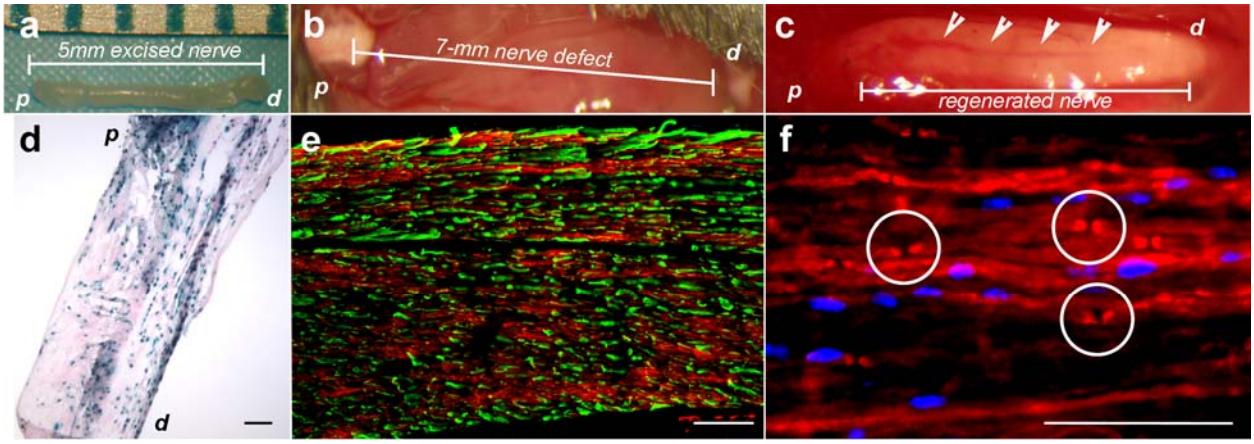

Figure 3.4: Transplanted FNr-MDSCs foster regrowth of critically-sized sciatic nerve defects
(**a**) A 4- to 5-mm segment of the sciatic nerve was removed at the hind limb of each mouse, (**b**) resulting in a 6.5- to 7-mm defect. (**c**) Following transplantation of FNr-MDSCs into the critical-size defect, complete regeneration from proximal to distal end was observed. (**d**) Many *nLacZ*-positive cells (blue) were observed between weeks 5 and 9 following injury. "*p*" corresponds to the proximal stump, and "*d*" to the distal stump. (**e**) The regenerated nerve exhibited both NF (green) and CNPase (red) immunoreactivity. (**f**) CNPase (red) staining of the regenerated sciatic nerve revealed nodes of Ranvier-like structures (white circles). Scale bars represent 100 μm (**d, e**) or 10 μm (**f**).

Cross sections of regenerated nerves exhibited many regenerated NF-positive axons (green) encompassing fluoromyelin-positive nuclei (red), indicating the presence of myelin-producing Schwann cells forming myelin sheaths surrounding the regenerated axons (**Figure 3.5a**). To confirm the differentiation of donor cells, we were able to detect ß-gal positive cells (red nucleated cells) expressing the glial and Schwann cell markers GFAP (green, **Figure 3.5b, 3.5c**) and CNPase (green, **Figure 3.5d**) on the regenerated sciatic nerve.

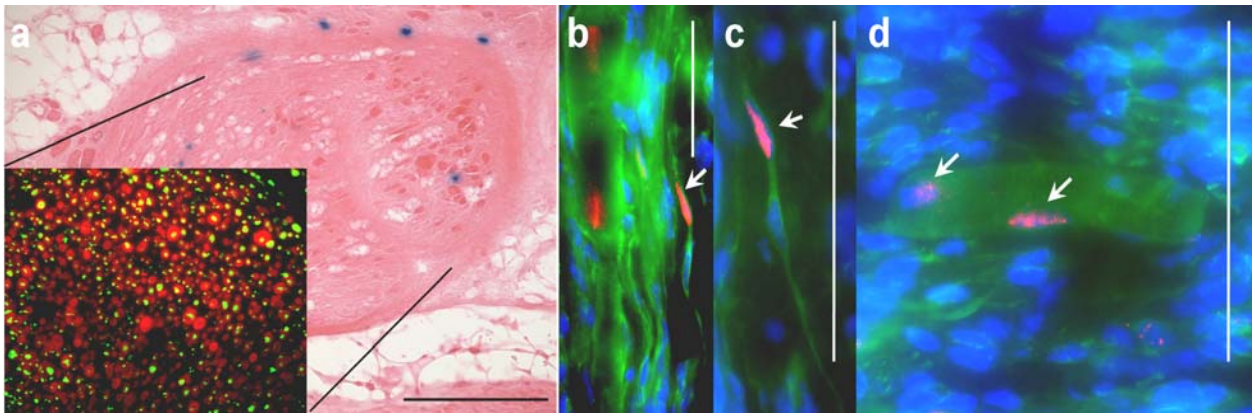

Figure 3.5: FNr-MDSCs differentiate toward Schwann cells *in vivo*
(a) Cross-section of regenerated nerve showed *nLacZ*-positive cells (blue) located at the epineurium, and exhibited NF-positive axons (green, inset) surrounded by fluoromyelin-positive cells (red, inset). (**b, c, d**) Colocalization of ß-gal (red) with (**b, c**) GFAP (green) or (**d**) CNPase (green) and DAPI stain (blue) suggests possible differentiation of the FNr-MDSCs into Schwann cells (several double-positive cells denoted by arrows). Scale bars represent 100 μm (**a**) or 10 μm (**b-d**).

Quantitative measurement of morphometric parameters, such as number of myelinated axons, myelin thickness, myelinated fiber area axonal cross-sectional area, and cross-sectional area of myelinated axons, and g-ratio (axon area : myelinated fiber area) [148] were compared between non-operated controls (uninjured) and FNr-MDSC-transplanted nerves on images taken with a transmission electron microscope (TEM) (**Figure 3.6a-c**). Ten weeks after implantation, the mid-section of the regenerated sciatic nerve contained an average number of 576 ± 33 myelinated axons, compared to 387 ± 12 in uninjured nerves ($P < 0.001$). Cross-sectional area of myelianted axons and myelin thickness were assessed as a measure of regenerated fiber maturation. Myelinated axons in the FNr-MDSC group showed a median thickness area of 5.07 μm^2 as compared to 7.1 μm^2 for the uninjured group ($P < 0.001$, **Figure 3.6d**) and cross-sectional area of 8.53 μm^2, versus 13.8 μm^2 for the uninjured group ($P < 0.001$, **Figure 3.6e**). The median and 25th to 75th percentiles of g-ratio in mid-sections of the regenerated nerves were 0.4 and 0.28 to 0.48%, respectively, versus the uninjured control group which was 0.5 and 0.42 to 0.56%, respectively, ($P < 0.001$, **Figure 3.6f**). The increase in the number of myelinated axons

following FNr-MDSCs transplantation may be the result of axonal branching leading to an increased muscle tissue reinnervation and thus less axonal dieback [149]. Although the regenerated peripheral nerves are significantly different from the uninjured nerves for all morphometric parameters mentioned, we believe the high number of myelin-producing Schwann cells (arrows, **Figure 3.6c**) and the low g-ratio (**Figure 3.6f**) indicates thick myelination of the regenerated axons highlighting the process of myelination exhibited by the FNr-MDSC-transplanted group.

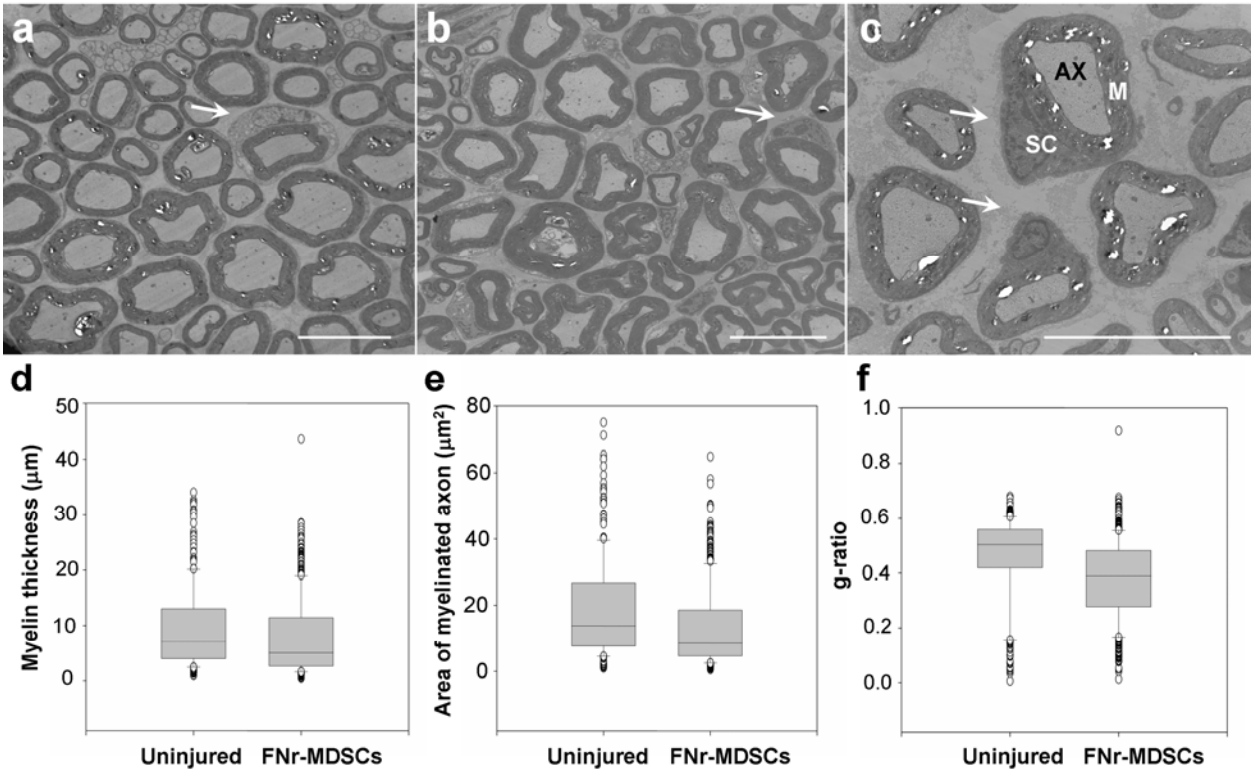

Figure 3.6: Regenerated nerve in FNr-MDSCs-treated mice show proper organization and remyelination

(a-c) Electron microscopy of semi-thin cross-sections of (**a**) non-operated (uninjured) control, and (**b, c**) FNr-MDSC-regenerated peripheral nerve, shows a high number of myelin-producing Schwann cells 10 weeks after implantation. Arrows indicate Schwann cells with surrounding myelinated axon. "Sc" corresponds to Schwann cells, "M" to myelin sheath, and "Ax" to axons, all of which are shown. (**d-f**) Graphical quantification of (**d**) myelin thickness, (**e**) area of myelinated axons, and (**f**) g-ratio (axon area: myelinated fiber area) represent the median values of both uninjured and FNr-MDSC-regenerated nerves to be significantly different ($P < 0.001$, Mann-Whitney Rank Sum Test). Sciatic nerve regeneration studies represent three independent experiments (n = 40 mice total). The morphometric parameters represent results from 5 mice (2 controls and 3 treated) and analysis of 1000 fibers. Scale bars represent 10 µm (**a-c**).

Functional recovery of regenerated sciatic nerves was determined by monitoring mice on a walking track. A detailed description of this method including the chosen parameters can be found in Appendix C. According to paw print analysis, FNr-MDSC-treated mice improved their walking pattern (**Figure 3.7a**). Further quantifications of paw prints revealed functional recovery determined by decrease in toe spread factor (**Figure 3.7b**), decrease in print length factor (**Figure 3.7c**), and increase in sciatic functional index (SFI) (**Figure 3.7d**), compared to PBS-

treated control mice. The first signs of motor nerve recovery could be observed at 6 weeks post-transplantation for the FNr-MDSCs (SFI: -52.4 ± 5.30) versus PBS-treated mice (SFI: -90 ± 2.51, $P < 0.001$). After 10 weeks, the SFI significantly increased in the FNr-MDSC groups (-45.2 ± 14.2, $P < 0.01$), demonstrating further improvement in comparison with to the PBS-treated control groups (-86.1 ± 4.28). Furthermore, stem cell transplantation significantly decreased the toe spread factor (0.326 ± 0.058 versus 0.604 ± 2.51 for PBS-treated mice, $P < 0.01$), and print length factor (0.132 ± 0.05 versus 0.24 ± 0.036 for PBS-treated mice, $P < 0.01$) at 6 weeks post-transplantation. These differences became even more evident at 10 weeks (toe spread 0.259 ± 0.097 versus 0.558 ± 0.026, $P < 0.01$ and print length 0.117 ± 0.054 versus 0.209 ± 0.052, $P < 0.01$). These results indicate that FNr-MDSCs facilitate functional nerve recovery possibly by improving muscle innervation.

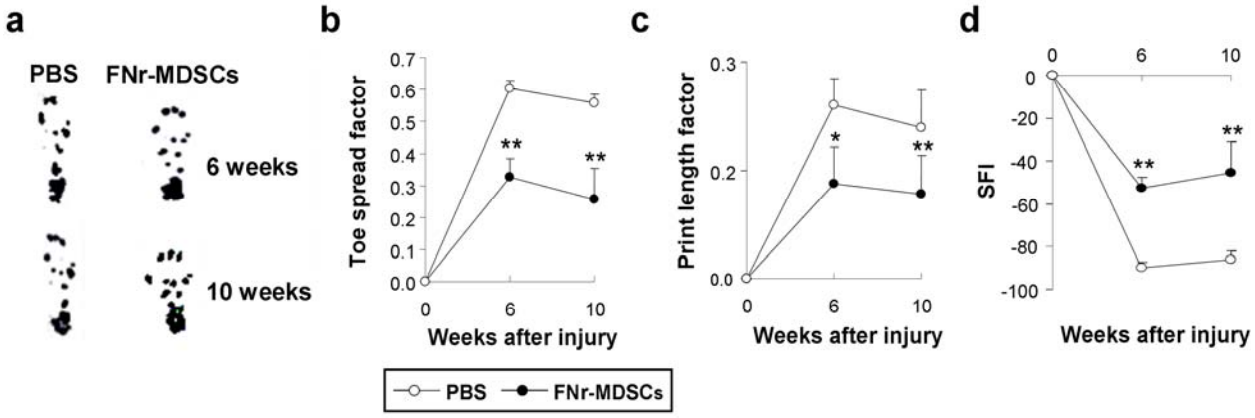

Figure 3.7: Transplanted FNr-MDSCs assist in functional recovery of critically sized sciatic nerve defects

(**a**) A depiction of representative paw prints from control- and FNr-MDSC-implanted mice at 6 and 10 weeks post-implantation. (**b-d**) Paw print analyses, indicating that FNr-MDSC transplantation increases the ability of the mice to walk normally, quantified by (**b**) decrease in toe spread factor, (**c**) decrease in print length factor, and (**d**) an increase in SFI (sciatic functional index) compared to PBS-treated mice. * indicates a $P < 0.05$, and ** denotes a $P < 0.001$, Mann-Whitney Rank Sum Test. A total of 35 paw prints were analyzed/group/time point.

3.2.3 Microenvironment transformation: A murine model of human malignant Triton tumors

3.2.3.1 FNr-MDSCs undergo transformation 11 weeks post-transplantation into a sciatic nerve defect

Although complete nerve regeneration was observed 6 weeks post-implantation, we were surprised to find that ~70% (7/10) of the mice formed large neoplastic growths between weeks 11 and 13 (**Figure 3.8a,b**). As these neoplasias were composed almost entirely of *nLacZ*-positive cells (data not shown), it was assumed that they originated from our donor cells. The neoplasias were highly invasive and positive for the myogenic cell markers α-smooth muscle actin (**Figure 3.5c, d**) and desmin (**Figure 3.8e, f**). The tumors were also positive for the neurogenic marker NF (**Figure 3.8g, h**), and contained focal areas positive for S-100 (**Figure 3.8i, j**), areas that are double-positive for both NF and S-100 (**Figure 3.8k, l**) and pockets of unorganized myelin deposition, as seen by fluoromyelin staining (**Figure 3.8m, n**). According to histological features, the resulting tumors were classified as malignant peripheral nerve sheath tumors with rhabdomyoblastic differentiation, otherwise known as "Triton tumors" [150]. Notably, while tumorigenesis was observed, nerve regeneration was still apparent (white arrow indicating regenerated nerve, **Figure 3.8n**), implying that tissue regeneration and cellular transformation may not be mutually exclusive events. Nevertheless, this phenomenon warrant future investigation.

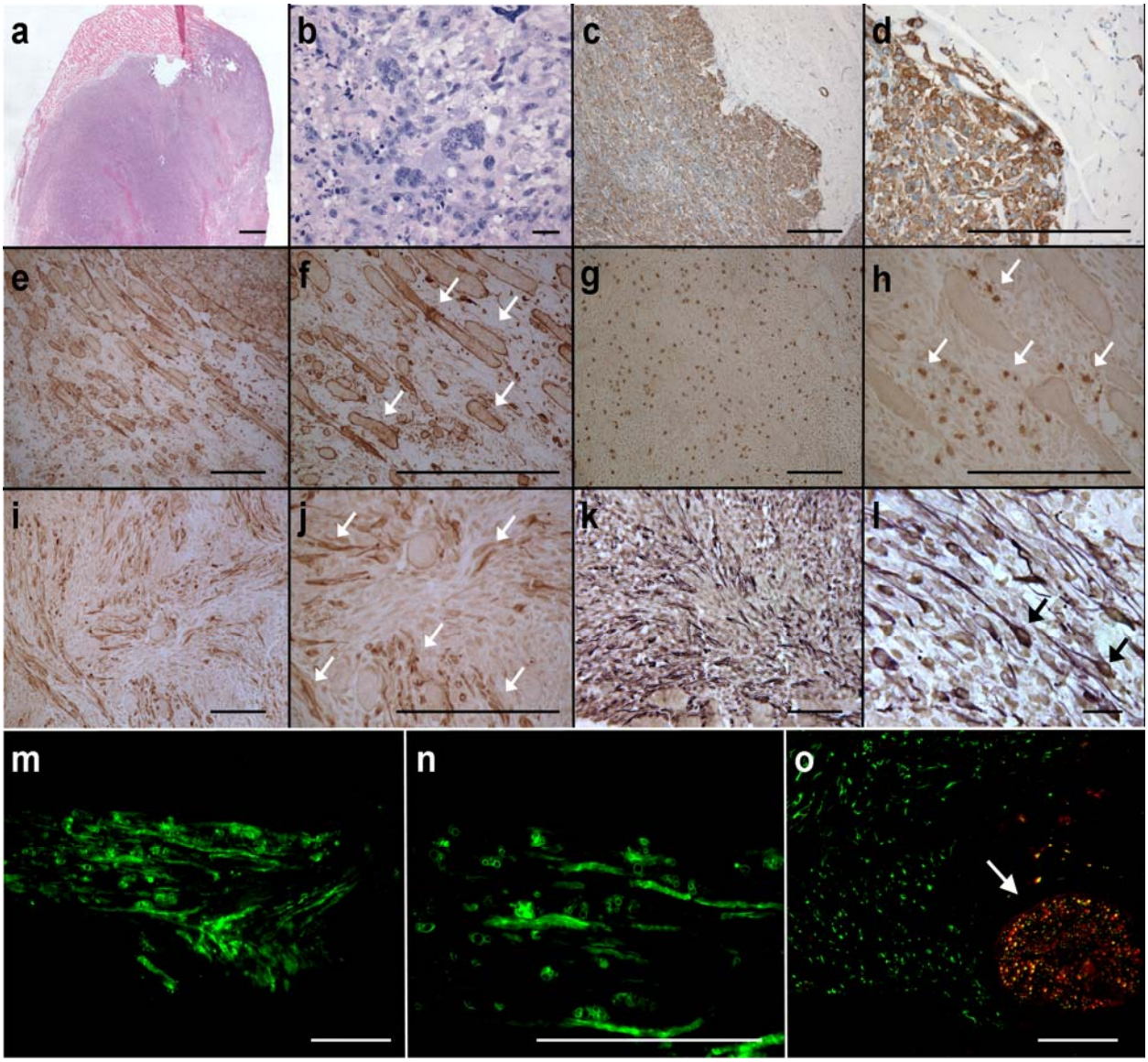

Figure 3.8: Between weeks 11 and 13, ~70% of mice implanted with FNr-MDSCs formed neoplastic growths

(**a, b**) Hematoxylin and eosin staining of a tumor that formed in mice implanted with FNr-MDSCs. (**c-l**) The resulting tumors were classified as malignant peripheral nerve sheath tumors with rhabdomyoblastic differentiation (Triton tumors) by showing positivity for (**c, d**) smooth muscle actin (brown) and (**e, f**) desmin (brown), (g, h) NF (brown), and pockets of (**i, j**) S-100 (brown), (**k, l**) as well as cells positive for both NF (brown) and S-100 (purple). Some positive cells (brown in f, h, and j) or double-positive cells (cells with a brown nucleus and purple cytoplasm in **k**, and **l**) are indicated by arrows. (**m, n**) The neoplasias were also positive for fluoromyelin (green), showing areas of unorganized myelin deposition. (**o**) Image depicting fluoromyelin (red) and NF (green) double-stained sections from a regenerated nerve (white arrow) in the area of tumor. Total of 40 mice (3 independent experiments) were used to generate tumors; negative controls sections were similarly processed but without primary antibodies (not shown). Scale bars represent 100 μm.

3.2.3.2 Cells isolated from FNr-MDSC-derived tumors grow as neurosphere-like structures

Cells were isolated from FNr-MDSC-derived tumors (TDCs) and cultured in regular proliferation medium (DMEM with 10% HS, 10% FBS, and 0.5% chick embryo extract). Although the cells were cultured in proliferation medium, they grew as neurosphere-like structures in the absence of neurogenic stimulation (**Figure 3.9a**) and were Lac-Z positive (**Figure 3.9b**). These spontaneously-occurring neurosphere-like structures were positive for ß-tubulin III (**Figure 3.9c**), CNPase (**Figure 3.9d**), GFAP (**Figure 3.9e**), nestin (**Figure 3.9f**), and NF (**Figure 3.9g**), but were negative for Neu-N (**Figure 3.9h**).

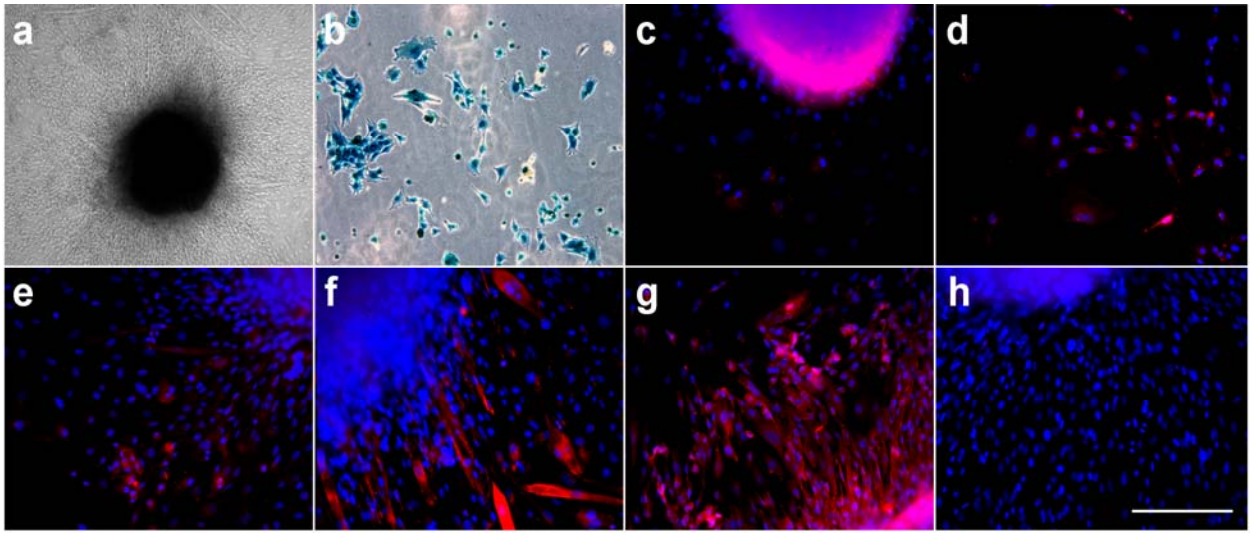

Figure 3.9: Cells isolated from FNr-MDSC-derived tumors (TDCs) maintain their neurogenic and myogenic differentiation potential *in vitro*
(**a**) TDCs grew as neurosphere-like structures in the absence of neurogenic medium, and (**b**) were *nLacZ*-positive (blue). (**c-h**) Immunofluorscent analysis of these spontaneously-occurring neurosphere-like structures demonstrated that they were positive for (**c**) β-tubulin III, (**d**) CNPase, (**e**) GFAP, (**f**) nestin, and (**g**) NF, but were negative for (**h**) Neu-N. For all immunofluoresence, the antibodies used are visualized in red, with the nuclear stain DAPI seen in blue. Scale bars represent 100 μm.

Furthermore, TDCs had gained the ability to grow independently of anchorage (as determined by soft agar assays) while their parental counterparts (FNr-MDSCs) were incapable of forming colonies (**Figure 3.10a and b**, respectively).

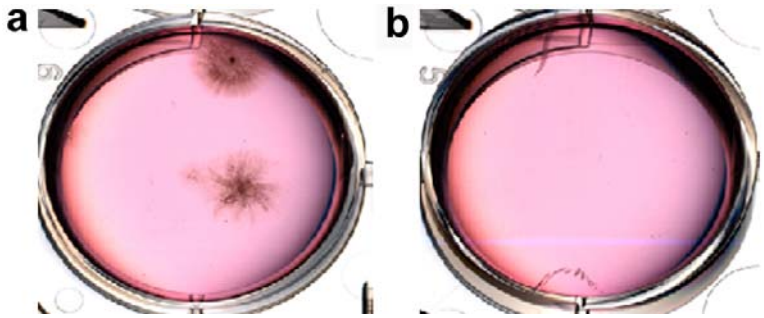

Figure 3.10: TDCs gained anchorage independent growth of colonies on soft agar
(**a**) TDCs showed sign of colony formation when grown on soft agar, while (**b**) FNr-MDSCs were incapable of forming colonies.

Cell cycle analysis of the parental FNr-MDSCs and TDCs revealed a shift of DNA content of the TDCs from the majority of cells being in the G_0 phase (parental 45.6% vs. TDCs 10.8%) to the G_1/M phase (parental 34.6% vs. TDCs 66.7%), with more than 50% of the TDCs possessing more than a diploid amount of DNA (**Figure 3.11a-d**). Cytogenetic analysis was conducted on both FNr-MDSC and TDC populations (**Figure 3.11e, f**). Analysis of the FNr-MDSC culture revealed murine chromosomes with near-diploid and near-tetraploid chromosome constitutions; no clonal structural abnormalities were observed. However, analysis of the TDCs revealed chromosome numbers ranging from 46-118 indicating their abnormal karyotype. None of the TDCs had a chromosome complement that would be considered normal diploid or tetraploid. Two of the structural abnormalities observed in the TDCs appear to be clonal, since they were each observed in more than one cell. Both of these were large, unidentifiable marker chromosomes, one of which appeared to be dicentric. Nonclonal chromosome abnormalities were seen in each of the TDCs. The karyotypic variability in these cells suggests the presence of chromosomal instability [151].

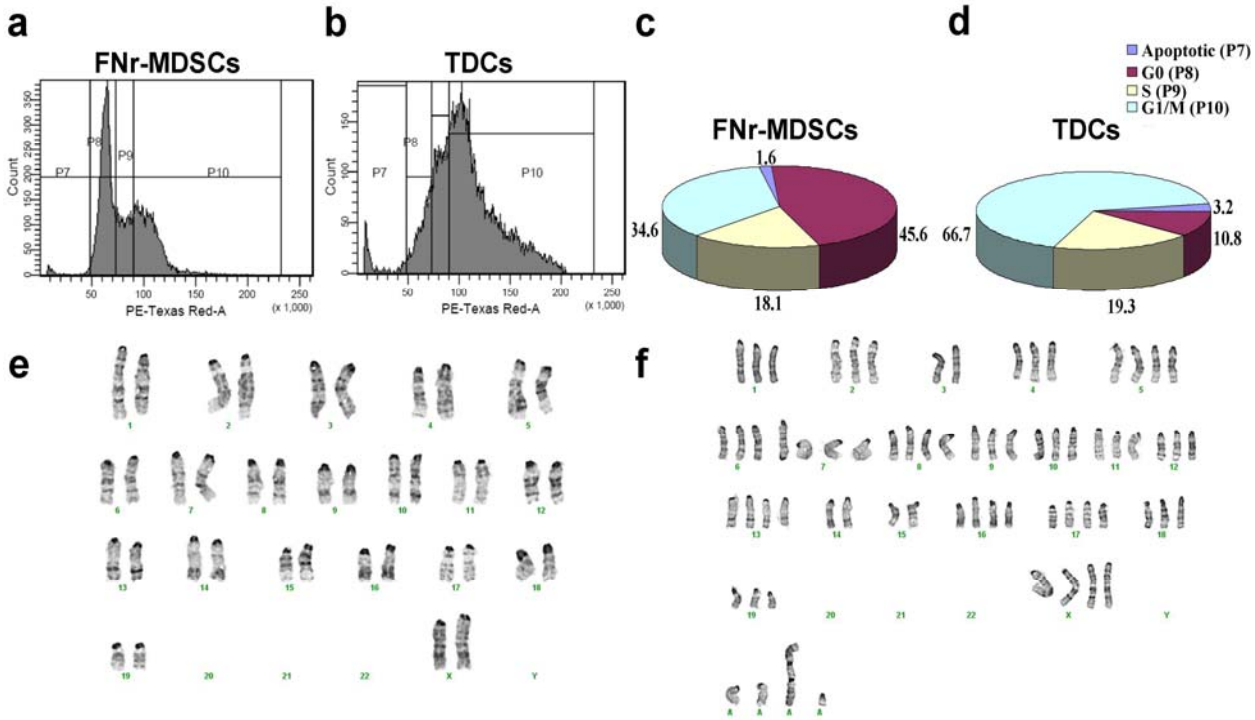

Figure 3.11: Cell cycle and cytogenetic analyses confirm FNr-MDSCs to be normal while TDCs exhibit abnormalities

(**a-d**) Cell cycle analysis of the parental FNr-MDSCs and TDCs was performed by FACS. Shown is the (**a, b**) DNA content and (**c, d**) graphical representation of the results, indicating the apoptotic, growth 0 (G_0), synthesis (S) and interphase/mitotic (G_1/M) fractions. These results indicate that majority of TDCs are constantly in mitotic phase. (**e, f**) Cytogenic analysis of FNr-MDSCs and TDCs. (**e**) Depicted is a representative karyotype from the FNr-MDSC population (40,XX). (**f**) Karyotype of one of the cells from the TDCs. This cell has 68 chromosomes, is hypertriploid, and expresses several unidentifiable marker chromosomes, the largest of which appears to be dicentric. The karyotypic variability in TDCs suggests chromosomal instability.

3.2.3.3 TDCs are serially transplantable, maintain their myogenic capacity *in vitro*, and tumorigenic *in vivo*

To determine whether the TDCs were able to regenerate tumors, the cells were implanted into a critical-size sciatic nerve defect in mice. Following implantation, neoplastic growths were observed between weeks 4 and 8 in all implanted mice. Furthermore, these tumors were highly aggressive and invaded all of the surrounding tissue of the leg, destroying muscle as well as bone (arrows) (**Figure 3.12a, b**), and were composed of poorly undifferentiated rhabdomyoblasts (small blue and pink cells) (**Figure 3.12a, b**).

Though TDCs appear to be spontaneously neurogenic, they express the myogenic marker desmin (red, 12%) (**Figure 3.12c**) and retain their ability to form f-MyHC-positive myotubes *in vitro* (red, **Figure 3.12d**). While the parental FNr-MDSCs regenerated muscle fibers and showed no sign of tumorgenesis (n = 10 representing two independent experiments, **Figure 3.12e**), the TDCs rapidly formed tumors when injected into the skeletal muscle of mice. These tumors formed rapidly, 4 weeks post-implantation, in 100% (4/4 mice) of the mice and were composed of donor *nLacZ*-positive cells (n = 8 representing two independent experiments, **Figure 3.12 f**). A schematic summary of methodology and results is provided in **Figure 3.13**.

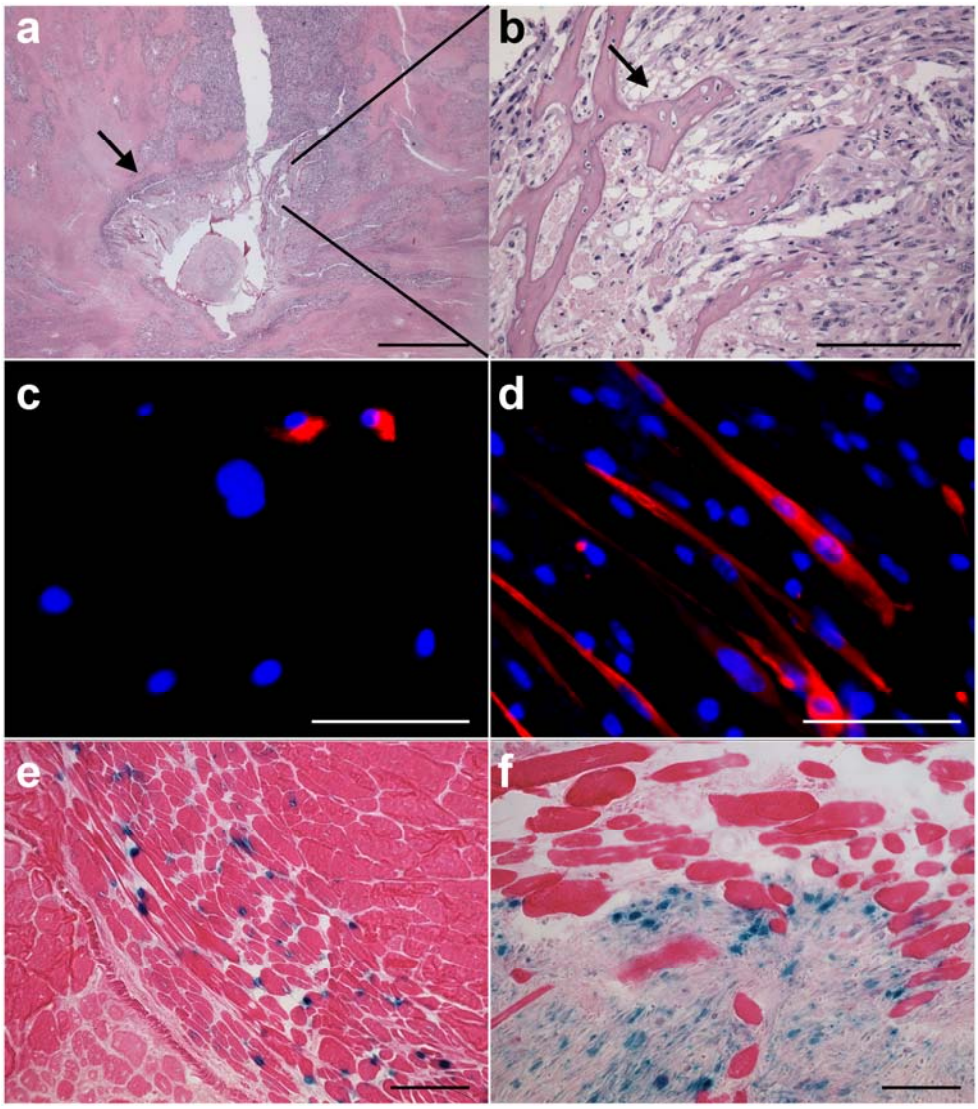

Figure 3.12: TDCs are serially transplantable
(**a, b**) Hematoxylin and eosin staining of a tumor generated from TDCs implanted into a sciatic nerve defect in mice, demonstrates the destruction of the bone, as seen by the pink, smooth stained portion (arrows). (**c, d**) *In vitro* myogenic analysis demonstrates that the TDCs possess expression of (**c**) the myogenic marker desmin (red, 12%) and have the ability to form myotubes *in vitro*, as seen by (**d**) f-MyHC staining (red). (**e, f**) *In vivo* myogenic analysis demonstrates that although (**e**) parental FNr-MDSCs showed myofiber regeneration after injection into the gastrocnemius muscles of *mdx* mice, and were detected up to 17 weeks without sign of tumor formation, the (f) TDCs implanted into the muscle formed tumor 100% of the time (10/10 mice), and as early as 4 weeks post-implantation. Note: the TDC reimplantation studies were performed in 2 separate experiments with a total of 16 mice; negative control sections were similarly processed without primary antibodies. They demonstrated negligible levels of non-specific background (data not shown). Scale bars represent 250 μm (**a**) or 100 μm (**b-f**).

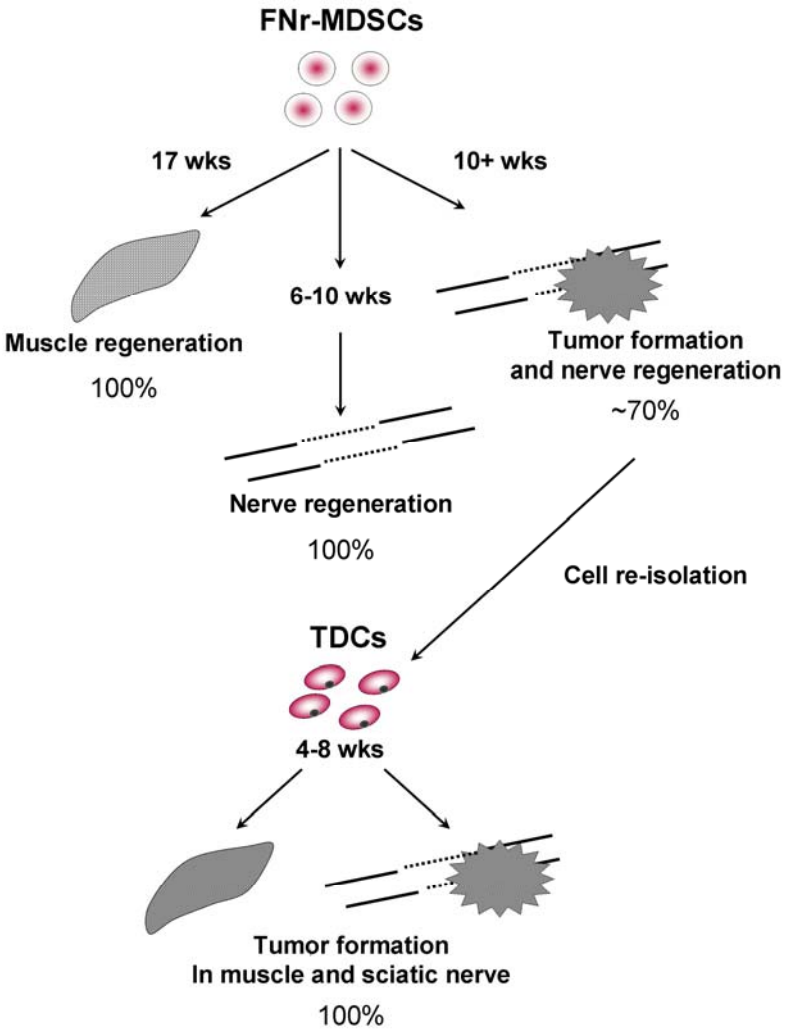

Figure 3.13: Schematic of experimental design and results for Figure 3.12

3.2.3.4 *In vitro* differentiation of FNr-MDSCs eliminates niche-specific transformation

To rule out the possibility that our perceived transformation was due to the presence of pre-transformed cells within our FNr-MDSC population, and was, in fact, due to an imbalance of intrinsic and extrinsic signaling, we altered the intrinsic predilection of the cells by differentiating them prior to implantation. FNr-MDSCs were cultured as neurospheres for 14 days, dissociated to a single cell suspension, and implanted into either the skeletal muscle of dystrophic mice or a critical-size sciatic nerve defect. If environmental cues were leading to the transformation of FNr-MDSCs, then altering the ability of cells to differentiate to a committed

lineage should abrogate transformation. When the dissociated neurospheres were injected into the skeletal muscle of *mdx* mice, poor muscle engraftment was observed (**Figure 3.14a, b**), as evident by a decrease in regeneration index (number of dystrophin positive myofibers per 100,000 injected cells) compared to parental FNr-MDSCs (36.7 ± 9.45 versus parental FNr-MDSCs 180.2 ± 49.1, $P < 0.001$, **Figure 3.14 c**). This suggests that *in vitro* differentiation of cells towards a neurogenic lineage reduced the ability of the cells to undergo myogenic differentiation. This was expected, since we postulated that differentiation of FNr-MDSCs prior to implantation would diminish their ability to respond to local environmental cues. More interestingly, when the dissociated FNr-MDSC-derived neurospheres were implanted into a critical-size nerve defect of mice, 80% (4/5 mice) of the mice formed fibrotic masses positive for Masson's trichrome 4 weeks post-implantation (as seen by intense collagen deposits [blue] **Figure 3.14d-e**). The remaining (20%) mice exhibited no signs of tumor formation, nerve regeneration, or fibrosis. Furthermore, the implanted parental FNr-MDSCs generated large neoplastic growths that contained almost no trichrome-positive areas (5.63 ± 1.6 versus neurosphere-implanted group 32.5 ± 16.1, $P < 0.001$, **Figure 3.14f**). These findings are summarized as a schematic representation in **Figure 3.15**.

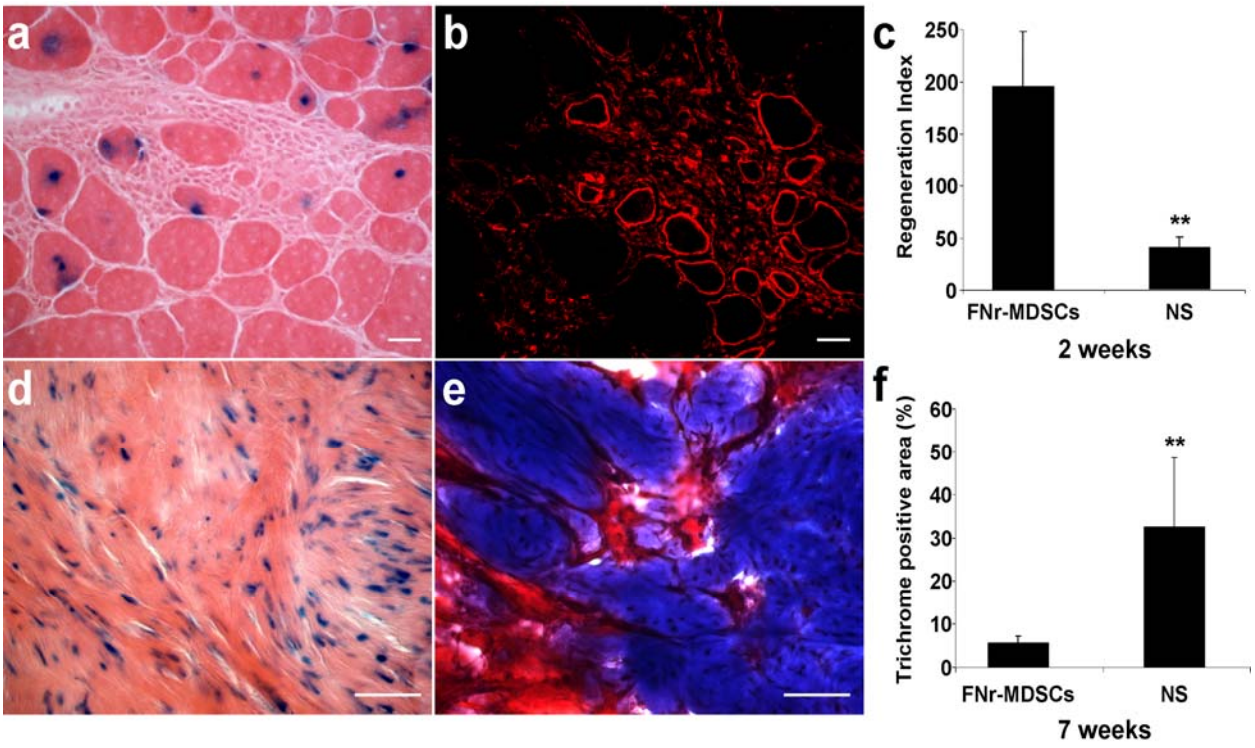

Figure 3.14: Neurogenic differentiation of FNr-MDSCs prior to implantation prevents transformation

(**a-c**) Two weeks post-implantation FNr-MDSC-derived neurospheres showed a reduction in muscle regeneration when compared to the parental FNr-MDSCs. (**a**) The *nLacZ* donor-derived FNr-MDSC-derived neurospheres (blue, n) could be detected in regenerated myofibers and (**b**) showed few regenerated dystrophin-positive myofibers (red) compared to undifferentiated FNr-MDSCs (not shown). (**c**) Graphical representation of the regeneration index (number of dystrophin positive fibers/100,000 injected cells) of parental FNr-MDSCs and FNr-MDSC-derived neurospheres (NS). NS-injected mice yield a lower regeneration index compared to the undifferentiated FNr-MDSCs. (**d-f**) Dissociated (**d**) FNr-MDSC-derived neurospheres were implanted into a sciatic nerve defect, and tumor formation was abrogated. Furthermore, (**e**) 4/5 mice formed large fibrotic masses, as seen by hematoxylin and eosin staining with intense collagen deposits identified by Masson's trichrome staining (blue, labeled c). (**f**) Graphical representation of the trichrome-positive area of parental FNr-MDSCs and NS. Parental FNr-MDSCs show minimal signs of fibrosis (evident by a lower percentage of collagen-positive area). Scale bars represent 10 μm. Note: negative control sections were similarly processed without primary antibodies (not shown).

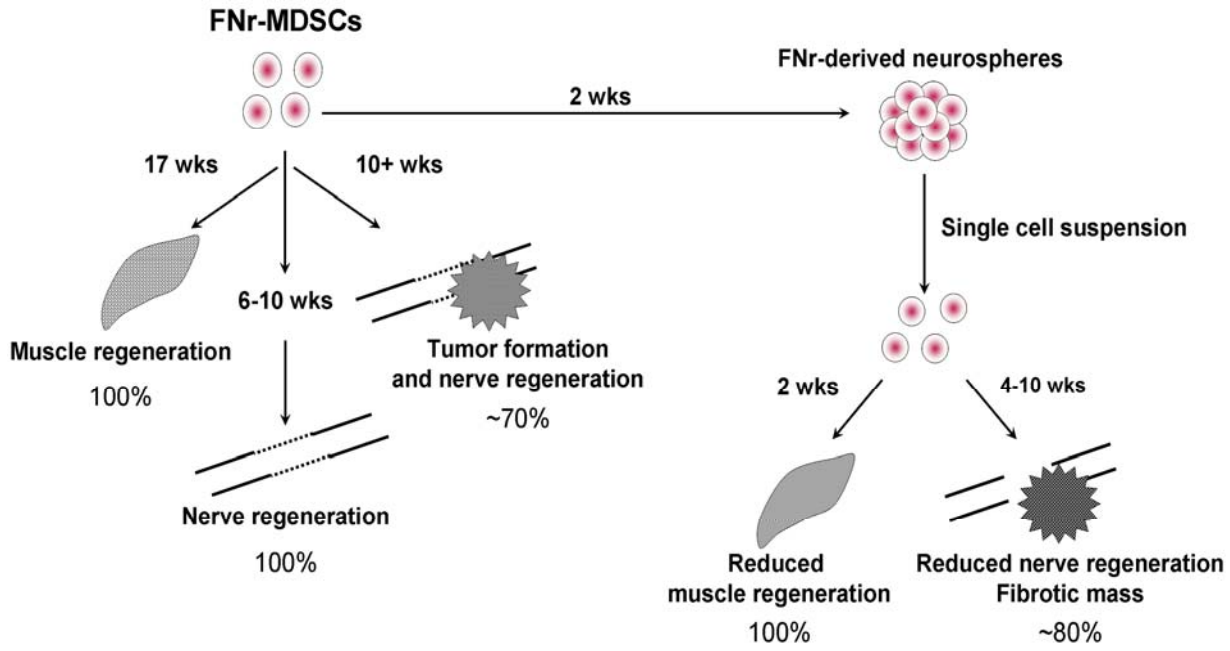

Figure 3.15: Combine scheme of experimental design and results for Figures 3.12 and 3.14

3.3 DISCUSSION

In this chapter, we have shown that a unique population of female neonatal MDSCs (FNr-MDSCs) can be induced to express biochemical markers and morphological features consistent with differentiation toward myogenic and neurogenic phenotypes depending on the environmental cues that they received. In addition to their ability to undergo myogenesis, undifferentiated FNr-MDSCs express both neuronal and glial cell markers, can generate neurospheres, and can be further differentiated to all three neural cell lineages, as well as Schwann cells. The cells engrafted effectively into the gastrocnemius muscles of *mdx* (dystrophic) mice, and can be detected in regenerated myofibers 17 weeks post-implantation. FNr-MDSCs, when implanted into a critical-size sciatic nerve defect, functionally regenerated the nerve 5 weeks post-surgery. Furthermore, active differentiation of FNr-MDSCs into glial

cells, especially Schwann cells *in vivo* and the presence of *LacZ*+ donor cells suggest that these cells surround the regenerating axons, and promote direct axonal regeneration. We posit that this regeneration improves the probability of target organ innervation, thus facilitating functional recovery after transplantation. Although the number of donor-derived supportive cells was too small to conclude that regeneration was mediated only by donor cell differentiation, other mechanisms, such as recruitment of host cells at the site of injury, and release of cytokines that exert neuroprotective effects independent of neurogenesis [152-155] are likely to be also involved in nerve regeneration. Further evaluation is needed to determine the fate of grafted cells and clarify the mechanism of nerve regeneration.

In addition to tremendous regenerative potential of MDSCs for both muscle and nerve, neoplastic growths classified as malignant Triton tumors (MTTs) were formed in ~70% (10/16) of mice between 11 and 13 weeks post-transplantation into sciatic nerve defect. MTTs, a type of malignant peripheral nerve sheath tumor (MPNST) with rhabdomyoblastic differentiation [156], comprise approximately 5 to 10% of all soft tissue sarcomas [150, 157] with crude two- and five-year survival rates of 33 and 12%, respectively [158, 159]. Histopathologic and immunohistochemical results of our tumor samples demonstrated them to be positive for S-100, desmin and muscle-specific actin, similar to human MTTs [157, 160]. The cell cycle and chromosomal analyses demonstrate that the tumors generated from our FNr-MDSCs appear to be genetically unstable consistent with reported cases of MTTs in human [157, 160]. Hence, it appears that the tumors generated may be the murine equivalent of human MTTs that, to the best of our knowledge, have never been reported by previous investigators.

The name triton was first used by Woodruff *et al.* [161] in reference to work done by Locatelli [162] supernumerary limbs containing bone and muscle were induced to grow on the

back of triton salamanders via the implantation of the sciatic nerve into the soft tissues of the back. The traditional view to the origin of these tumors in humans suggest that either Schwann cells induce muscular differentiation of other cells, or malignant Schwann cells transform directly into skeletal muscle cells [156]. Recent studies on peripheral nervous system (PNS) tumors conclude that more differentiated cells, such as Schwann cells (or perhaps their closely related progenitors), rather than the stem cells may give rise to or facilitate the transformation [135, 163]. Our observed transformation could be explained by various hypotheses, one of which is of our particular interest. We introduce the idea that the stem/progenitor cells may become transformed when their intrinsic predilection (genotype) and extrinsic (environmental cues) signaling pathways become conflicted due to multiple differentiation signals. Our recent publication demonstrates how a lack of regulation of these signals is involved in the initiation of the oncogenic potential [164]. In this model, we have shown that progenitor cells isolated from the skeletal muscle of mice can undergo spontaneous microenvironment-specific transformation when expressing the osteogenic factor BMP4 [164]. The tumors generated were osteorhabdomyosarcomas, and formed only when a specific population of MDSCs was transduced with BMP4 and implanted into a myogenic environment [164]. Here we show another case of transformation that may attribute to concomitant signal-induced oncogenesis. Hence, if the progenitor cells used here receive both myogenic and neurogenic stimulation from the environment, as we suspect they do, this dual-signaling pathway may induces a state of continuous transient amplification. The fact that there is a time delay in our observed transformation may explain the time necessary for our murine cells to differentiate to the appropriate post-mitotic differentiated state to undergo transformation.

Cytogenetic analysis was carried out to exclude the possibility of culture-induced transformation. The cells used in this study possessed a normal karyotype, and did not show any signs of colony formation when grown in soft agar. They remained untransformed with no sign of tumorigenesis after subcutaneous implantation or intravenous injection over 1 year. We also did not observe any tumor formation when FNr-MDSCs were implanted into skeletal muscle of *mdx* mice for a period lasting over 17 weeks, or when differentiated towards a neurogenic lineage prior to injection. It is noteworthy that we have screened other cell populations isolated in our lab but didn't find any other population to regenerate nerve. Our distinct cell population, FNr-MDSCs, has tremendous potential for nerve regeneration but also show susceptibility for transformation. High tendency of FNr-MDSCs towards Schwann cell (glial) differentiation may account for their receptiveness toward MTTs. Recent report by Joseph *et al.* 2008 [163] shows that benign tumors and cancers of the PNS such as neurofibromatosis is caused by the loss of *neurofibromin* (*Nf1*) appeared to arise from differentiated glial and not neural crest stem cells and only in region of the PNS.

To eliminate the possibility that the process of long term culturing or the *nLacZ* transduction may explain the underlying transformation phenomenon, we implanted early passage and control (non-transduced at later passage) parental cells and tumor formation was still observed in ~30% (2/6) and ~70% (4/6) respectively starting at 11-12 weeks post-transplantation. The tumorigenesis and nerve regeneration observed here, though reproducible, were not mutually exclusive events. Mice that developed Triton tumors simultaneously displayed complete sciatic nerve repair and regeneration within the skeletal muscle. Our collected data present the possibility that our transformation may be related to the microenvironment. Microenvironment dictating the fate of adult stem cells is not a new concept and the finding that

stem cells may undergo spontaneous transformation is not unique to MDSCs. Stem cell and cancer biologists have known for many years that the microenvironment plays a role in maintaining and determining the fate of both normal and cancer stem cells. As mentioned by Kuica *et al.* [165], accumulating evidence start to recognize that if circulating normal stem cells or cancer stem cells exposed to a damaged environment may undergo malignant transformation over time. Mesenchymal stem cells (MSCs) have been shown to become tumorigenic [166-168] and have been implicated in childhood leukemia [169], epithelial cancers [170], and osteosarcomas [171-173]. Additionally, Leukemic stem cells express antigens similar to those expressed by hematopoietic stem cells (HSCs) [174]. The basis for observed transformations is not clear and origin of MTT remains unknown. Nevertheless, future experiments to explain the mechanism behind the origin of these rare tumors and the role of the stem/differentiated cells in that origin are required.

In our effort to stop the FNr-MDSC transformation, we observed that differentiating the cells toward the neurogenic lineage prior to implantation abrogated tumorigenesis, but induced fibrotic-like tissue formation. The theory of halting the transformation of stem cells by differentiating them prior to implantation has been a long and established protocol for researchers using embryonic stem (ES) cells. In 2006, a publication demonstrated that co-culturing human ES cells with immortalized human astrocytes from fetal midbrain tissue cells (making them more similar to adult progenitor cells prior to implantation), not only halt the transformation of the ES cells, but resulted in substantial and long-lasting restitution of motor function when transplanted into a Parkinsonian model [175]. We believe that the ability to immobilize transformation, at least in part, by removing the cells' ability to respond to environmental cues (by differentiating our cells prior to implantation) is important. Potentially

by using a synthetic "nerve guide" [176], the FNr-MDSCs may be protected from non-neuronal environmental signals and "forced" to only undergo neurogenic differentiation, while avoiding an oncogenic phenotype. This may explain the reason for lack of reports on tumor formation in most studies performed by scientist using nerve guides for peripheral nerve regeneration [177].

Since the population of the MDSCs study here is a mixed population of many cells types including the myogenic and neurogenic cells, we can not disregard the possibility that under neurospheres conditions, myogenic cells are selected against. These cells may be the ones that underwent our perceived microenvironment-specific oncogenesis *in vivo*, and this may explain the lower regeneration index and lose of transformation potential by the FN-MDSC-derived neurospheres. If the myogenic cells are tumorigenic, then it may explain why the neural sphere cells lose their transformation potential and reduced muscle regeneration capacity *in vivo*.

It should be emphasized that at this point the underlying mechanisms of our observed malignant transformation can not be fully explained; therefore, future studies are essential to find the responsible environmental cues. Also, the hypothesis of concomitant and conflicting differentiation signals inducing transformation mentioned here needs to be validated. We have isolated clones from the FNr-MDSCs and the titration studies on these clones are underway in order to determine their specific profiles individually. The results obtained here and future studies using our model display the potential to provide both a novel therapeutic approach to the treatment of peripheral neuropathies, and provides a potential paradigm shift in understanding of the cellular events responsible for the initiation events leading toward the development of MPNTs and MTTs.

3.4 CONCLUSIONS

In conclusion, the data presented here demonstrate several key findings: female newborn muscle-derived stem cells isolated via preplate technique (i) adopt neuronal and glial differentiation under controlled culture conditions, (ii) functionally regenerate peripheral nerve; (iii) undergo spontaneous transformation when implanted *in vivo*; and, (iv) this transformation may occur in an environment and time-dependent fashion; and, (v) differentiating the cells prior to implantation appears to eliminate transformation. Collectively, these findings provide evidence of myogenic and neurogenic differentiation potential of a unique population of MDSCs, and a useful murine model system to explore the relationship between effective tissue regeneration and microenvironment specific transformation.

3.5 MATERIALS AND METHODS

3.5.1 Cell isolation and culturing

The Institutional Animal Care and Use Committee of Children's Hospital of Pittsburgh approved all animal procedures. The MDSCs were isolated from the hind limbs of female neonatal mice (C57BL/6J; Jackson Laboratory) via the preplate technique previously described [122, 124]. Briefly, the muscle tissue was minced and processed through a series of enzymatic dissociations: 0.2% of collagenase type XI (Sigma-Aldrich) at 37^{o}C for 1 hr, 2.4 units/ml of dispase (Invitrogen) for 45 min, and 0.1% of trypsin-EDTA (Invitrogen) for 30 min. After enzymatic dissociation, the muscle cells were centrifuged and resuspended. The cells were then maintained

in proliferation medium (DMEM [Invitrogen] with 10% HS [Invitrogen], 10% FBS [Invitrogen], 1% penicillin-streptomycin [Invitrogen] and 0.5% chick embryo extract [Accurate Chemical and Scientific Corporation]). Different populations of muscle-derived cells were isolated based on their adhesion characteristics. Small, round cells, appeared late in the preplate process (pp6) during isolation. These cells were allowed to adhere for approximately 2 weeks, at which point they began to proliferate to become long-term proliferating (LTP) cultures. LTP cultures were sub-plated at 100 cells/well in 12-well tissue culture plates to obtain MDSCs [122, 124]. The resulting MDSCs were then transduced with a retroviral vector encoding a *LacZ* reporter gene containing a nuclear localization sequence (*nLacZ*, kindly provided by Dr. Paul Robbins, University of Pittsburgh, Pittsburgh, PA) to enable donor cell tracking [178]. Limiting dilution was then used to sub-clone the transduced cells such that a population >90% *nLacZ*-positive was obtained.

3.5.2 Flow cytometry analysis

Fluorescence activated cell sorting (FACS) was used to analyze the expression of CD34, Sca-1, and CD45 (FACSAria cytometer using FACSDiva software; Becton Dickson). Cultured cells were trypsinized, centrifuged, washed with PBS containing 0.5% BSA (Sigma-Aldrich) and 0.1% sodium azide (Sigma-Aldrich), and counted. The cell suspension was then divided into equal aliquots and centrifuged. The cells were placed on ice and resuspended in a 1:10 dilution of mouse serum (MS; Sigma-Aldrich) in PBS that was supplemented with 10% MS, and incubated for 10 min. Fluorescein isothiocyanate (FITC)- and Phycoerythrin (PE)-conjugated rat anti-mouse monoclonal antibodies (CD34, Sca-1, and CD45) were added to each tube for an additional 30 min. Separate cell portions received an equivalent amount of isotype control

antibodies. After several rinses, all fractions (including the controls) were labeled with strepavidin-allophcocyanin (APC) for 20 min. Just before analysis, 7-amino-actinomycinD (7-AAD) was added to each tube for dead cell exclusion. All antibodies, as well as APC and 7-AAD, were purchased from BD Bioscience Pharmingen. On average, 10,000 live single cell events were collected and analyzed.

3.5.3 Myogenic Differentiation

To induce differentiation, MDSCs were plated on collagen type-I-coated (Sigma-Aldrich) 24-well plates in proliferation medium at a density of 1000 cells/cm^2, and then shifted to differentiation medium (low serum: DMEM supplemented with 2% FBS and 1% penicillin-streptomycin) 3 days after seeding. *In vitro* myogenic differentiation was evaluated after 5 days by immunocytochemical staining for f-MyHC, a marker of late myogenic differentiation, using the protocol described below.

3.5.4 Neurosphere formation and differentiation

To form neurospheres, FNr-MDSCs were plated as a suspension on 12-well plates at a concentration of 4x10^4 cells/ml in a medium consisting of Neurobasal™ A (Invitrogen), 100 U/ml penicillin-streptomycin, L-glutamine (2 mM; Invitrogen), 1X B27 supplement (Invitrogen), bFGF (40 ng/ml; Invitrogen), and EGF (20 ng/ml; Sigma-Aldrich) using a similar protocol to that used by Romero-Ramos *et al*. [125]. Cells were maintained in this medium for 7 to 14 days, and the growth factors replaced every 3 to 4 days. The FNr-derived neurospheres were passaged before the diameter exceed 100 μm by enzymatic (using TrypLE [Gibco™]) and mechanical

(with P200 plastic micropipettor) dissociation, and supplemented with Neurobasal™ A, 1X B27, bFGF (20 ng/ml), and EGF (10 ng/ml). To induce differentiation, the FNr-derived neurospheres were collected, centrifuged, and gently triturated in a "differentiation medium" containing 10% FBS, and Neurobasal™ A supplemented with 1X B27 without the presence of mitogens. Single cell suspensions were plated on poly-D-lysine (Sigma-Aldrich, MW 70,000-150,000)-coated 8-well CultureSlides (BD Falcon™) at an initial density of $5x10^4$ cells/0.7 cm^2. Plates were checked daily to determine the state of differentiation, and 50% of the medium was replaced with fresh differentiation medium when necessary (when the medium became acidic by turning yellow). Cells were incubated at 37°C in 5% CO_2 in a fully humidified atmosphere for 7 to 14 days and then fixed for immunocytochemical detection of neuronal/glial-specific antigens (see below).

3.5.5 Immunocytochemistry

The FNr-MDSCs (pre- and post-differentiation) were screened for several lineage-specific markers. Briefly, cells were fixed for 30 min in 4% paraformaldehyde (PFA; Fisher Scientific) in PBS (pH 7.4; Invitrogen), washed, and incubated for 10 min at room temperature with PBS plus 0.3% Triton X-100 to permeabilize the cell membrane. They were incubated with 10% normal donkey serum (DS; Jackson ImmunoResearch Laboratories) or goat serum (GS; Vector), to block non-specific binding, for 60 min. Cells were incubated at 4°C overnight with the following primary antibodies (in 2.5% DS or GS): goat anti-Nestin (1:1000; Santa Cruz Biotechnology Inc.), mouse anti-β-tubulin III (TU-20, 1:500; Chemicon), mouse anti-CNPase (1:200; Sigma-Aldrich), rabbit anti-S-100 (1:500; Sigma-Aldrich), goat anti-NGFR p75 (c-20, 1:200; Santa Cruz Biotechnology Inc.), rabbit anti-TrkA (763, 1:500; Santa Cruz Biotechnology Inc.), rabbit

anti-GFAP (1:500; Chemicon), rabbit anti-NF (neurofilament 150 kD, 1:500; Chemicon), mouse anti-Neu-N (neuronal nuclei, 1:100; Chemicon), mouse anti-O4 (1:200; Chemicon), rabbit anti-NG2 (1:200; Chemicon). The secondary antibodies to the appropriate species used were as follows: donkey anti-mouse IgG-AlexaFluor® 594- or 488-conjugated (1:500; Molecular Probes), donkey anti-rabbit IgG-AlexaFluor® 594- or 488-conjugated (1:500; Molecular Probes) for 30 min, and Cy3-conjugated anti-goat IgG (1:1000; Sigma-Aldrich) against nestin antibody for 60 min. For desmin and f-MyHC immunocytochemical staining, the cells were fixed with cold methanol for 2 min and blocked with 10% HS (Vector) for 1 hour and incubated with the primary antibody (1:200, mouse; Sigma-Aldrich) in 2.5% HS at 4°C overnight. After thorough washing, the cultures were incubated at room temperature for 45 min with the secondary antibody biotinylated anti-mouse IgG (1:250; Vector) and subsequently reacted with streptavidin-conjugated Cy3 (1:500; Sigma-Aldrich) at room temperature for 20 min. To visualize the nuclei, the cultures were then incubated with DAPI (4′, 6′ diamidino-2-phyenylindole, 100 ng/ml; Sigma-Aldrich) for 10 minutes. Culture slides (BD Falcon™) were mounted with Vectashield® medium (Vector). Bright-field and fluorescent images were taken using a Nikon Eclipse E800 microscope equipped with a Spot digital camera and software system (v. 3.0.4; Diagnostic Instruments) or a Leica DMIRB microscope equipped with a Retiga 1300 digital camera (Q imaging) and Northern Eclipse software system (v. 6.0; Empix Imaging, Inc.). Cells were systematically quantified in at least 15 fields across the slides, or wells of culture dishes from four to six independent experiments. Controls included omitting the primary or secondary antibodies during the procedure.

3.5.6 Neurosphere and stem cell transplantation

To examine myogenic differentiation, $2x10^5$ viable FNr-MDSCs or single cell suspension from FNr-derived neurospheres (14 days in culture) were suspended in 20 μL of PBS and injected into the gastrocnemius muscle of 6- to 8-week-old *mdx* mice (C57BL/10ScSn DMD*mdx*/J; Jackson Laboratories) via an Ultra-Fine II syringe (BD BioSciences). At 2 and 17 weeks post-transplantation, mice were sacrificed and the gastrocnemius muscles were harvested and flash frozen in liquid nitrogen-cooled 2-methybutane. Serial cryosections 10 μm in thickness were prepared from frozen muscles for immunohistochemical analysis. Muscle regeneration was quantified by manually counting the number of dystrophin-positive myofibers in an area containing the largest graft and calculating the regeneration index. Neurogenic differentiation was examined by creating a 7-mm sciatic nerve defect in 6- to 8-week-old SCID mice. Immediately thereafter, a viable single cell suspension of $3x10^5$ FNr-MDSCs, FNr-derived neurospheres, or an equal volume of PBS (15 μL), was injected into proximal and distal nerve stumps. Some of the mice from each group were sacrificed 6 weeks after transplantation, and the hind limbs, including the sciatic nerve, were harvested, frozen, and cryosectioned for further analysis. The rest of the mice were maintained until later time-points (up to 15 weeks) to check for possible tumor formation.

3.5.7 Histochemistry

Sections were fixed in 1% glutaraldehyde (Sigma-Aldrich), and stained for *nLacZ* expression (using X-Gal solution 3 hours at 37°C) for donor cell tracking, and then counterstained with eosin [179]. Masson's modified protocol was used to determine the amount of collagen content

in the fibrotic tissue using Masson's trichrome staining. Slides were processed and stained as detailed in the manufacturer's protocol (Masson's trichrome stain kit, K7228; IMEB Inc.), which stains collagen blue, muscle fibers red, and nuclei black.

3.5.8 Immunohistochemistry

To colocalize the donor cells with neurogenic and/or glial cell markers, the tissue sections were incubated with mouse anti-ß-galactosidase (1:200; Chemicon) and rabbit anti-GFAP (1:1000; Chemicon) overnight at 4°C. Sections were rinsed with PBS and incubated with Cy3-conjugated anti-rabbit IgG (1:250; Sigma-Aldrich) for 30 min. To detect the donor cells, biotinylated anti-mouse IgG (1:200; Vector) was added to the slides for 90 min, and subsequently reacted with streptavidin-conjugated FITC (1:500; Sigma-Aldrich) at room temperature for 20 min. ***Muscle sections:*** Cryosections were fixed with 5% formalin (Sigma-Aldrich) and blocked with 10% HS in PBS for 1 hour at room temperature or 4ºC overnight, and then incubated with rabbit anti-dystrophin (1:300; Abcam). The sections were washed in PBS and incubated with Cy3-conjugated anti-rabbit IgG (1:500; Sigma-Aldrich) in PBS for 30 min. For desmin staining, fixed sections were incubated with mouse anti-desmin (1:200; Sigma-Aldrich); the following steps were performed in accordance with the MOM kit (FMK-220; Vector) manufacturer's instructions, except that streptavidin-conjugated Cy3 was used to replace fluorescence-conjugated avidin. Nuclei were revealed by DAPI. ***Sciatic nerve sections:*** Cryosections of the hind limb were first immunostained for FluoroMyelin red (Molecular Probes) according to the protocol provided by the manufacturer, and then fixed in 4% PFA blocked with 5% DS for 1 hour, and incubated with rabbit anti-NF (1:300, Chemicon) for 2 hours at room temperature. The tissues were then rinsed with PBS and stained with donkey anti-mouse IgG-AlexaFluor® 488-

conjugated for 20 min. In addition, the regenerated sciatic nerves were cryo-sectioned longitudinally, fixed with 5% formalin, blocked with 10% HS, and incubated overnight at 4°C with both rabbit anti-NF (1:300; Chemicon) and mouse anti-CNPase (1:200; Sigma-Aldrich) antibodies. The next day, the sections were rinsed with PBS and incubated with biotinylated anti-mouse IgG (1:200; Vector) for 1 hour, and subsequently stained with streptavidin-conjugated Cy3 (1:500; for CNPase immunostaining) at room temperature for 20 min. Sections were then exposed to donkey anti-rabbit IgG-AlexaFluor® 488-conjugated (1:500; Molecular Probes) for 30 min to immunostain for NF-positive axons. Controls included omitting the primary or the secondary antibodies during the procedure. ***Tumor sections:*** Slides were processed and stained as detailed in the manufacturer's protocol (Vectastain® *Elite* ABC kit; Vector Laboratories) with anti-mouse or rabbit IgG appropriate to primary antibody including: rabbit anti-NF (1:500; Chemicon), rabbit anti-S-100 (1:500; Sigma-Aldrich), and mouse anti-desmin (1:200; Sigma-Aldrich). Slides were developed using the peroxidase 3,3′-diaminobenzidine (DAB) substrate kit (Vector Laboratories). For the purpose of double labeling, a sequential staining of each primary antibody was performed using anti-rabbit IgG Vectastain ABC kit (Vector Laboratories). The slides were developed using DAB Substrate Kit (brown) for NF and Vector VIP Substrate Kit (purple) for S-100 (both from Vector Laboratories).

3.5.9 Morphometric analysis of the regenerated nerve

Some of the regenerated nerves 10 weeks post-operation were fixed in 2.5% glutaraldehyde (EM grade, Taab Chemical) in 0.1M phosphate buffer (pH 7.3; Fisher Scientific) overnight at 4°C for light and transmission electron microscopy studies. The contralateral sciatic nerve harvested at the same level served as a “normal” control. The nerves were then rinsed in PBS, post-fixed in

1% osmium tetroxide (Electron Microscopy Sciences) with 0.1% potassium ferricyanide (Fisher Scientific), dehydrated in a series of ethanol solutions (30% - 90%; Fisher, and 100% [Ethanol 200 Proof]; Pharmco), exposed to propylene oxide twice for 10 min each and embedded in Epon (Dodecenyl Succinic Anhydride, Nadic Methyl Anhydride, Scipoxy 812 Resin and Dimethylaminomethyl; Energy Beam Sciences). All grafted segments were carefully oriented in order to obtain sections perpendicular to their long axis. Semi-thin (300 nm) sections were cut using a Lecia Ultracut and stained with 0.5% toluidine blue (Fisher Scientific) and examined under light microscope (Olympus BX51) with Magnafire 2.1A image capture software, and quantified for the number of the myelinated axons. Ultrathin sections (65 nm) at distal, mid, and proximal ends were obtained using a Leica Ultracut Microtome (Leica) and stained with 2% uranyl acetate (Electron Microscopy Sciences) and Reynold's lead citrate (Fisher Scientific), and examined on a JEOL JEM-1011 transmission electron microscope in collaboration with Dr. Simon Watkins (University of Pittsburgh, Pittsburgh, PA). The number of myelinated axons in ~10,000 μm^2 of the cross-sectional area of the nerve was counted, and median area of myelin thickness, median cross-sectional area of myelinated axons, and g-ratio (axon area/myelinated fiber area) were examined in mid-sections of the regenerated nerves. Each section was divided into four quarters. Each quarter of the nerve was analyzed individually, and morphometric parameters of 300-500 fibers were calculated using the Northern Eclipse software system (v. 6.0; Empix Imaging, Inc.) following image capture, background subtraction, image enhancement, automatic thresholding, and final editing.

3.5.10 Functional assessment

Functional recovery was analyzed using a walking track assessment, and quantified by measuring two factors including toe spread (TS, distance from the first to the fifth toe), paw length (PL, distance from the third to the heel) taken from the mouse footprints of uninjured (normal) and experimental sides. Paw prints were collected on white paper with the hind paws painted with black ink and evaluated based on published model for recovery of sciatic nerve motor function [180, 181]. Footprint parameters were scanned and analyzed with imaging Northern Eclipsed Software system. The sciatic functional index (SFI) was calculated using previously described protocol [180, 181] at 6 and 10 weeks after injury. A more detailed description of the model, schematics, and calculations including the formulas can be found in Appendix C.

3.5.11 Soft agar analysis

Cells were suspended in DMEM over a 0.6% agar (Sigma) underlay at concentrations of 100, 500, and 1000 cells/well. The cultures were allowed to grow for 2 weeks and then scored for colonies as a % (number of colonies/100 cells).

3.5.12 Cytogenetic analysis

Cytogenetic analysis was carried out by the University of Pittsburgh Cancer Institute Cytogenetics Facility. The cells from both the FNr-MDSC (passage 36) and TDC (passage 12) populations were harvested following mitotic arrest with a 2 h treatment with Colcemid^{TM}

(0.1µg/ml, Irvine Scientific). The cells were then incubated in hypotonic KCl (0.075M) for 30 min at 37^{o}C, and fixed in 3:1 methanol: glacial acetic acid for 20 minutes, followed by two washes in fixative. Slides were prepared from the cell suspensions and aged overnight at 60°C. Chromosomes were trypsin-Giemsa banded and 20 cells were counted and analyzed from each cell culture.

3.5.13 Statistical analysis

Statistical analysis was carried out using SigmaStat (Jandel Scientific v2.0) software package. Morphometric parameters are expressed as the median values, 25th-75th percentiles. Direct comparisons between treatment and control groups for myelianted fiber counts data was analyzed using Student's *t*-test. However, the data for the myelin thickness, myelinated fibers area, axon area, and g ratio violated the assumptions of normality and variance and these were compared using Mann-Whitney Rank Sum test. The Student's *t*-test or the Mann-Whitney Rank Sum test (where appropriate) were used for paw prints analysis. Significant was placed at $P < 0.05$.

4.0 HUMAN MUSCLE-DERIVED PROGNITOR CELLS: POTENTIAL FOR CELL-MEDIATED THERAY FOR PERIPHERAL NERVE INJURY

4.1 INTRODUCTION

The identification of cell populations capable of neural differentiation has generated great interest [182, 183] due to limited capacity of neural tissue for intrinsic repair and regeneration. Stem cells from embryonic tissue are able to expand and differentiate into multiple lineages including neural lineage *in vitro* and *in vivo*. However, there are still some limitations on the practical use of embryonic stem cells because of ethical questions [184, 185].

Until recently, myogenic cells have primarily been used for muscle fiber regeneration [124, 186, 187]. These cells are normally mitotically quiescent but become activated and start to divide in response to injury [188]. However, studies in the past few years have shown that adult skeletal muscle tissue contains progenitor cells able to differentiate into several phenotypes of mesodermal and ectodermal origin such as astrocytes and neurons [125, 189-191]. This suggest that reservoirs of stem cells may reside in skeletal muscle that can retain the potential to transdifferentiate from one phenotype to another, presenting exciting possibilities for cellular therapies. In fact, studies have reported using these cells for experimental treatment of a variety of diseases and disorders, including clinical trials for urological dysfunction [192] and cardiac repair [193-200]. The rationale behind using skeletal-derived cells (myoblasts, satellite cells,

and skeletal muscle-derived stem cells [MDSCs]) is that it can be easily isolated from a simple muscle biopsy of adult tissue in a relatively noninvasive method, readily be expanded *in vitro*, and transplanted in an autologous manner. This approach can also eliminate the ethical issues raised by using of embryonic or fetal tissues as a source.

Though recently, it has been demonstrated that adult human skeletal muscle includes progenitor cells that can generate cells with neurogenic properties *in vitro* [125, 201, 202], their engraftment potential *in vivo* needs further investigation. Obtaining encouraging results in our sciatic nerve regeneration model using mMDSCs, led us to utilize the same isolation technique [124, 142] to isolate MDSCs-like cells from human muscle biopsies. We sought to determine if a fraction of slowly adhering cells (SACs) containing human muscle-derived progenitor cells (hMDPCs) could (i) adopt neuronal/glial phenotype in culture; (ii) help to restore severed sciatic nerve defect; (iii) survive and engraft in the sciatic nerve defect area post-implantation; and, (iv) acquire Schwann cell-specific phenotype after transplantation. We hypothesized that hMDPCs can adopt neuronal and glial phenotypes under controlled culture conditions, and transplantation of hMDPCs improves the regeneration and functional recovery of critically sized sciatic nerve defects in mice following injury.

hMDPCs were screened for a series of neurogenic and glial cell markers pre- and post-differentiation using immunocytochemistry and real time PCR (RT-PCR). The efficacy of sciatic nerve regeneration and remyelination were evaluated quantitatively by immunohistochemistry and electron microscopy. Recovery of motor function was assessed by monitoring mice on a walking track in our murine model as discussed in Chapter 1.

4.2 RESULTS

4.2.1 hMDPCs differentiate into phenotypically mature neuronal and glial under controlled culture conditions

hMDPCs generate neurospheres, starting as early as after 2 days in neurogenic culture medium (**Figure 4.1a**) that are successfully passaged and expanded. hMDPCs-derived neurospheres express the astrocyte marker, GFAP (**Figure 4.1b**) and the neuron marker, β-tubulin III (**Figure 4.1c**). Neurospheres also contain cells co-expressing β-tubulin (red) and Schwann cell protein, S-100 (green) (**Figure 4.1d,** arrow), while others only express β-tubulin (**Figure 4.1d,** arrowhead). The hMDPCs-derived neurospheres can be further differentiated into glial and Schwann cells positive for p75 (**Figure 4.1e**) and GFAP (**Figure 4.1f**) and mature neurons positive for β-tubulin (**Figure 4.1g**) and MAP2ab (Microtubule associated protein 2ab, **Figure 4.1h**). Nuclei stained with DAPI (blue) or human lamin A/C (green). Data represent three to six independent experiments.

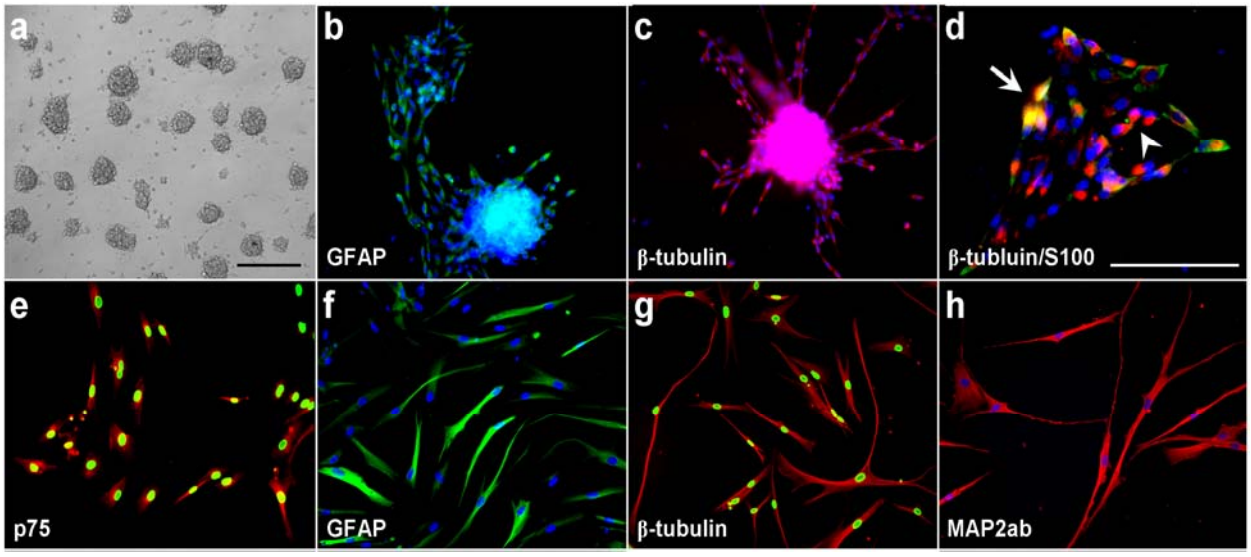

Figure 4.1: Differentiated hMDPCs under controlled culture conditions express mature phenotype of neuronal and glial lineage including Schwann cells
(**a**) hMDPCs are able to generate neurospheres. These hMDPCs-derived neurospheres expressed the (**b**) astrocytic and Schwann cell marker, GFAP, (**c**) the mature neuronal marker, β-tubulin III. (**d**) Single suspended neurospheres exhibited co-expression (yellow, arrow) of both markers β-tubulin III (red) and S-100 (green) while some cells only showed β-tubulin III expression (red, arrowhead). The hMDPCs-derived neurospheres can be further differentiated into glial and Schwann cells positive for (**e**) p75 and (**f**) GFAP and mature neurons positive for (**g**) β-tubulin and (**h**) MAP2ab (the nuclear stain DAPI, seen in blue and human lamin A/C seen in green). (**i**) Above data represent three to six independent experiments. Scale bar in (**a**) applies to all other panels except for (**d**). Scale bars represent 100 μm.

4.2.2 Differentiated hMDPCs show upregulation in both neuronal and glial cell marker expression when compared to undifferentiated counterparts.

Three distinct undifferentiated (UN) cell populations of hMDPCs underwent neurosphere (NS) formation and terminal differentiation (TD). Real-time PCR analysis was carried out to further analyze the expression level of several neuronal and glial cell markers prior and post-differentiation. Differentiation of hMDPCs toward neurospheres increased the expression of neuroectodermal marker, Pax6 (4-fold), a gene expressed in neural stem cells and in neurospheres [203] when compared to undifferentiated counterpart (**Figure 4.2**). The expression of mature neuronal marker MAP2ab increased (2-fold) after terminal differentiation when

compared to undifferentiated hMDPCs. In particular, differentiation of hMDPCs highly up-regulate the expression of the Schwann cell marker, S-100 (10-fold NS; 3-fold TD) and the astroglial and Schwann cell marker, GFAP (20-fold NS; 10-fold TD) at neurospheres and terminal stages of differentiation respectively, compared to undifferentiated controls (**Figure 4.2**). Furthermore, terminal differentiation of hMDPCs revealed 25-fold increase in the expression of oligodendrocytes marker, OSP. These results further confirm hMDPCs potential to differentiate into myelin producing glial cells.

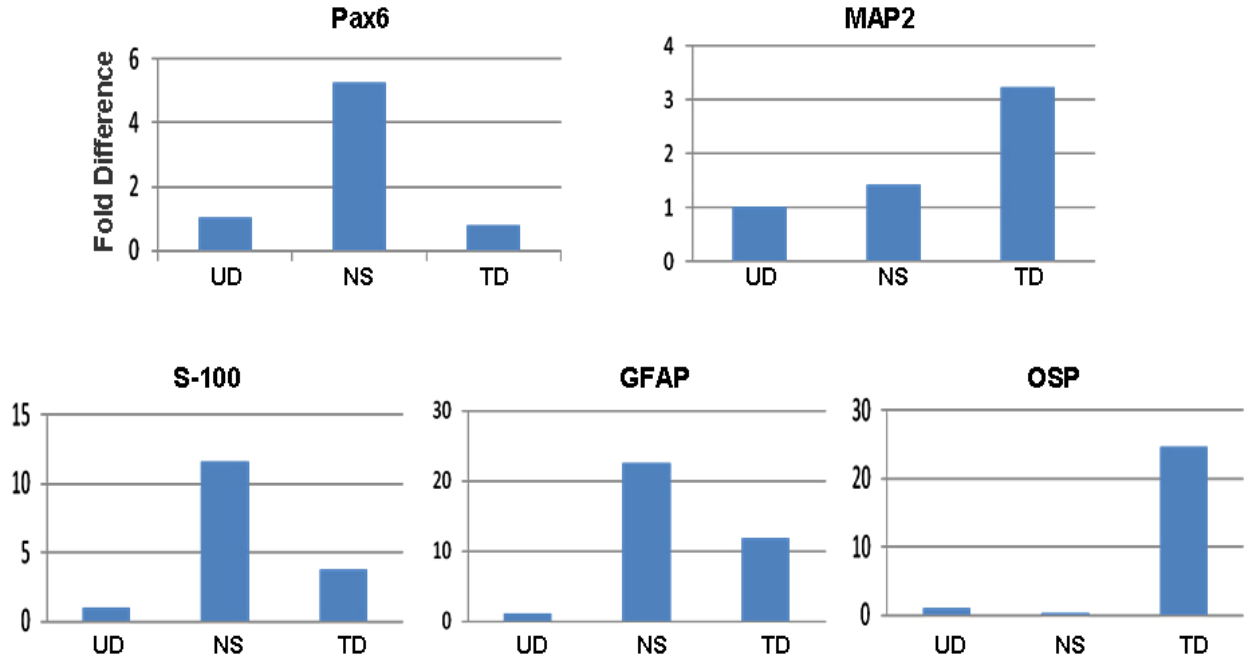

Figure 4.2: The expression level of all markers up-regulated after differentiation of hMDPCs when compared to initial undifferentiated hMDPCs.
Quantitative transcription profile of neurospheres (NS), terminal differentiation (TD) into glial and neuronal cell types compared to undifferentiated (UN) hMDPCs counterparts. Data are pooled from three independent experiments obtained from hMDPCs isolated from three distinct skeletal muscle biopsies. Expression levels are expressed relative to the housekeeping gene Cyclophlin.

4.2.3 hMDPCs promote functional regeneration of severe sciatic nerve defects after injury

hMDPCs from four separate isolations were transplanted into critical-size sciatic nerve defects in SCID mice (n = 96 mice; three independent experiments). Complete regeneration from proximal (*p*) to distal (*d*) stump was observed as early as 6 weeks after injury (**Figure 4.3a**), whereas nerve gaps in which PBS was injected (n = 20 mice) exhibited minimal regeneration (Gap, **Figure 4.3b**) at the same time post-injury.

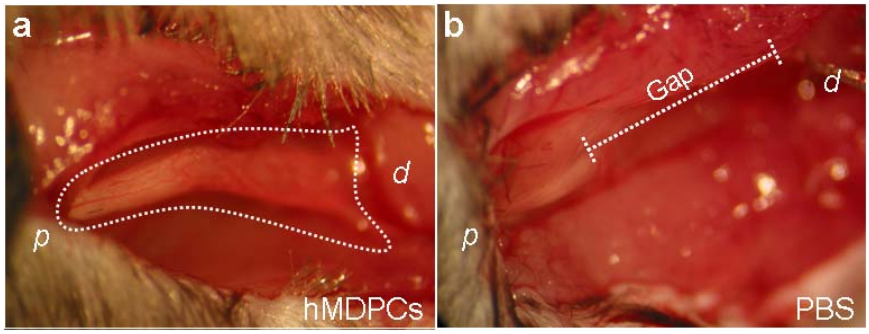

Figure 4.3: hMDPCs regenerate severe sciatic nerve defect
(**a**) Following transplantation of hMDPCs into critical-size (7-mm) sciatic nerve defects of SCID mice, complete regeneration from proximal (*p*) to distal (*d*) stump was observed as early as 6 weeks after injury. (**b**) The nerve gap injected with PBS exhibit minimal regeneration (Gap).

Cross-sections of regenerated nerves exhibited NF-positive axons (green) enclosed by fluoromyelin-positive cells (data not shown). Longitudinal sections of regenerated nerves exhibited both NF (green) and CNPase (red) immunoreactivity (**Figure 4.4a)**. CNPase (red) staining of the regenerated sciatic nerve revealed node of Ranvier-like structures (white circles) similar to FNr-MDSCs regenerated nerves (**Figure 4.4b)**. Regenerated nerves positive for Schwann cell marker GFAP (green) contained many donor PCNA positive cells (red) that particularly situated themselves in front and along the growth cones of the nerves (**Figure 4.4c**).

Detecting PCNA+ donor cells (red) positive for GFAP (green) and CNPase (data not shown) suggests differentiation of hMDPCs into glial cells particularly Schwann cells (**Figure 4.4d, e**; double-positive cells denoted by arrows).

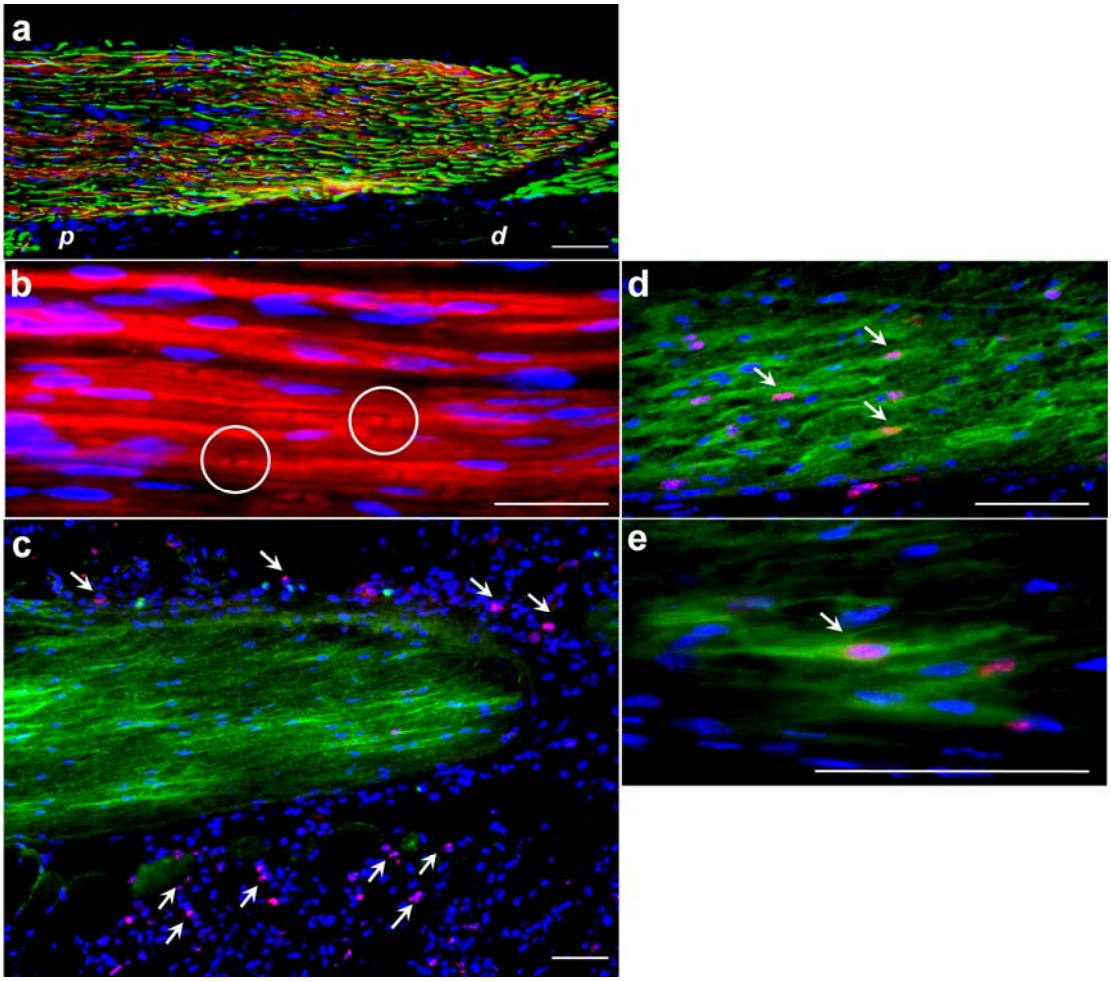

Figure 4.4: hMDPCs undergo glial differentiation particularly Schwann cells *in vivo*
(**a**) Longitudinal sections of the regenerated nerve exhibited both NF (green) and CNPase (red) immunoreactivity. (**b**) CNPase (red) staining of regenerated sciatic nerve revealed nodes of Ranvier-like structures (white circled) at higher magnification. (**c**) Close association and distribution of human donor cells positive for proliferating nuclear antigen specific, PCNA (red), were observed with growing cone of regenerated sciatic nerve stained with GFAP (green). (**d, e**) Colocalization of PCNA positive donor cells (red) with GFAP (green) and DAPI stain (blue) suggests possible differentiation of the hMDPCs into glial cells (several double-positive cells denoted by arrows). Scale bars represent 100 μm (**a, d, and d**) or 10 μm (**b, e**).

Ten weeks post-transplantation, regenerated nerves contain many nerve fibers with organized fascicles (F) surrounded with perineurium (P, arrows) (**Figure 4.5a**). The mid-sections of the regenerated sciatic nerves contained an average 450 ± 21 myelinated axons, compared to 356 ± 17 in non-operated (uninjured) control nerves, this differences was statistically significant ($P = 0.002$, ANOVA). Pairwise Multiple Comparison showed a significant difference ($P < 0.05$, Tukey Test) between uninjured control and hMDPCs-treated nerves, while no significant difference was observed among the hMDPCs isolated from different donors. Electron microscopy at proximal and mid-sections of regenerated nerves revealed proper regeneration, absence of connective tissue fibrosis, and many myelinated Schwann cells (arrows, **Figure 4.5b** and **c** respectively). The myelinated axons in the hMDPCs group showed a median cross-sectional area of 8.6 μm^2, versus 15.5 μm^2 for uninjured control nerves ($P < 0.001$, **Figure 4.5d**), and median myelin thickness of 5.2 μm^2 versus 8.1 μm^2 ($P < 0.001$, **Figure 4.5e**. The median and 25^{th} to 75^{th} percentiles of g-ratio in mid-sections of the regenerated nerves were 0.48 and 0.41 to 0.54%, respectively, as compared to 0.49 and 0.4 to 0.56% for uninjured control group (**Figure 4.5f**), indicating a close resemblance between the regenerated nerves by means of hMDPCs transplantation and uninjured nerves.

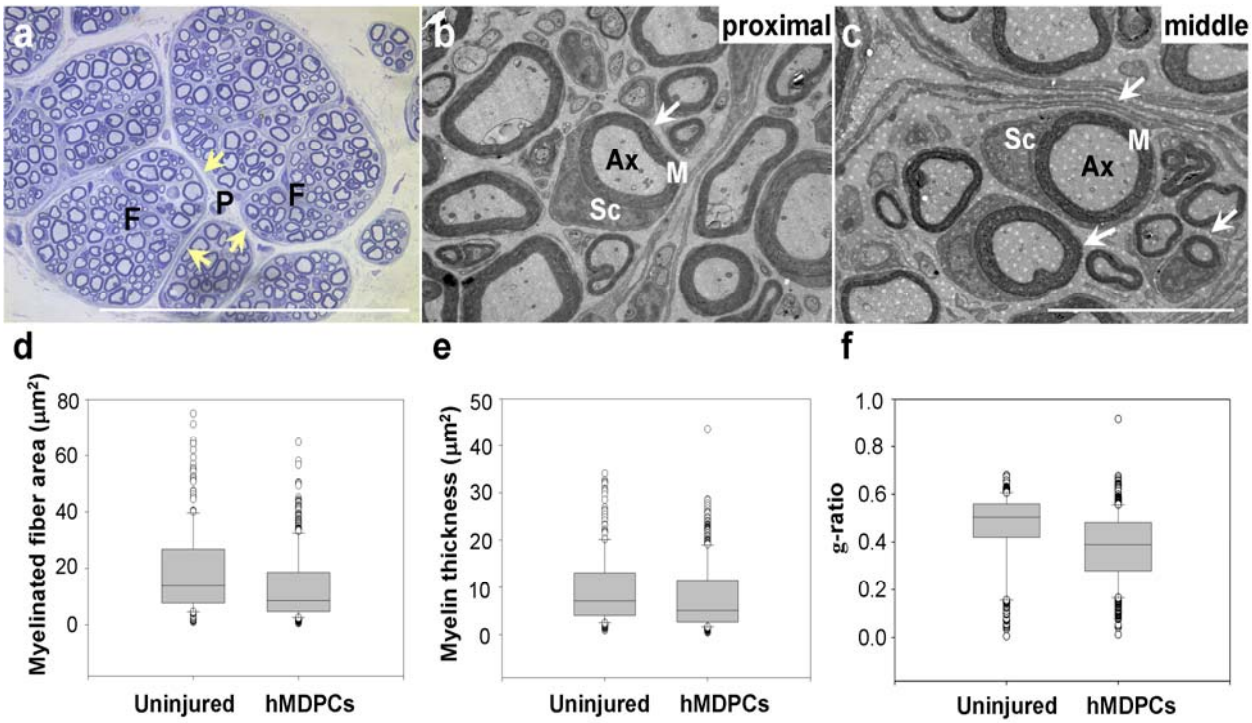

Figure 4.5: Regenerated nerves in hMDPCs-treated mice show proper organization and remyelination

(**a**) Eight to ten weeks post-transplantation, light microscopy image of regenerate nerve stain with toluidine blue show organized nerve regeneration with perineurium (P, arrows) surrounding the nerve fascicles (F). (**b, c**) Electron microscopy at proximal and mid-sections of the regenerated nerves revealed proper regeneration, absence of connective tissue fibrosis, and many myelinated Schwann cells in proximal and mid-sections (arrows, **b** and **c** respectively). "Sc" corresponds to Schwann cells, "M" to myelin sheath, and "Ax" to axon. (**d-f**) Graphical quantification of the morphometric parameters display the median values for (**d**) area of the myelinated fiber, (**e**) myelin thickness, and (**f**) g-ratio (axon area : myelinated fiber area) of the regenerated nerve to the non-operated (uninjured) control nerves. A total of 35 mice were transplanted. The morphometric parameters represent results from 5 mice (2 controls and 3 treated) and analysis of at least 600 fibers/group. Scale bars represent 10 μm.

Paw print analyses revealed an enhanced gait recovery of hMDPCs-treated mice in comparison with PBS-treated mice (**Figure 4.6**). This improvement is quantitatively supported by significant decrease in both toe spread factor (**Figure 4.7a)** and print length factor (**Figure 4.7b)**, and significant increase in SFI (**Figure 4.7c)** for hMDPCs-treated versus PBS-treated mice in each consecutive weeks after injury**.** These differences started at week two and became highly evident at week fourteen (toe spread: 0.18 ± 0.091 versus 0.514 ± 0.021, $P < 0.01$, print length: 0.161 ± 0.037 versus 0.338 ± 0.052, $P < 0.01$, and SFI: -37.2 ± 1.17 versus -86.1 ± 2.55,

$P < 0.001$). It is noteworthy that both hMDPCs isolated from different donors showed close association at each time point indicating a possible consistency in the isolation technique.

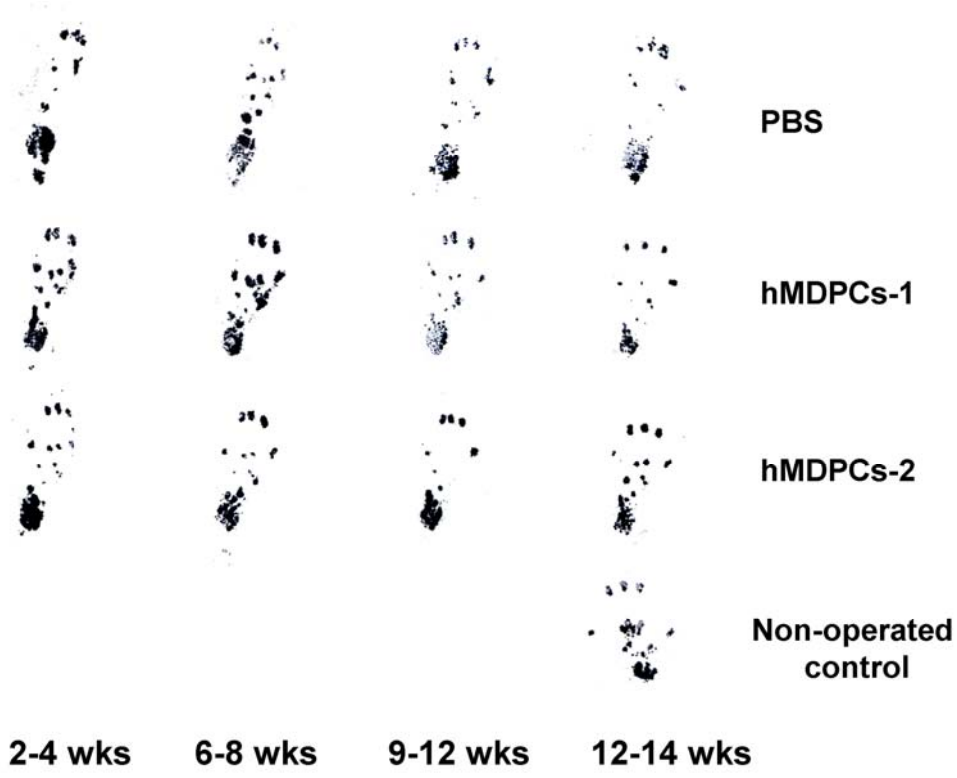

Figure 4.6: Representation of paw prints from PBS and hMDPCs-treated mice
A depiction of representative paw prints from PBS (control) and hMDPCs-treated mice are shown for 14 consecutive weeks post-implantation. Paw print analyses indicate that transplantation of hMDPCs isolated from two different patient (hMDPCs 1 and 2) increases the ability of the mice to walk normally in comparison to PBS-treated mice. These differences become highly apparent at 12-14 weeks post-implantation.

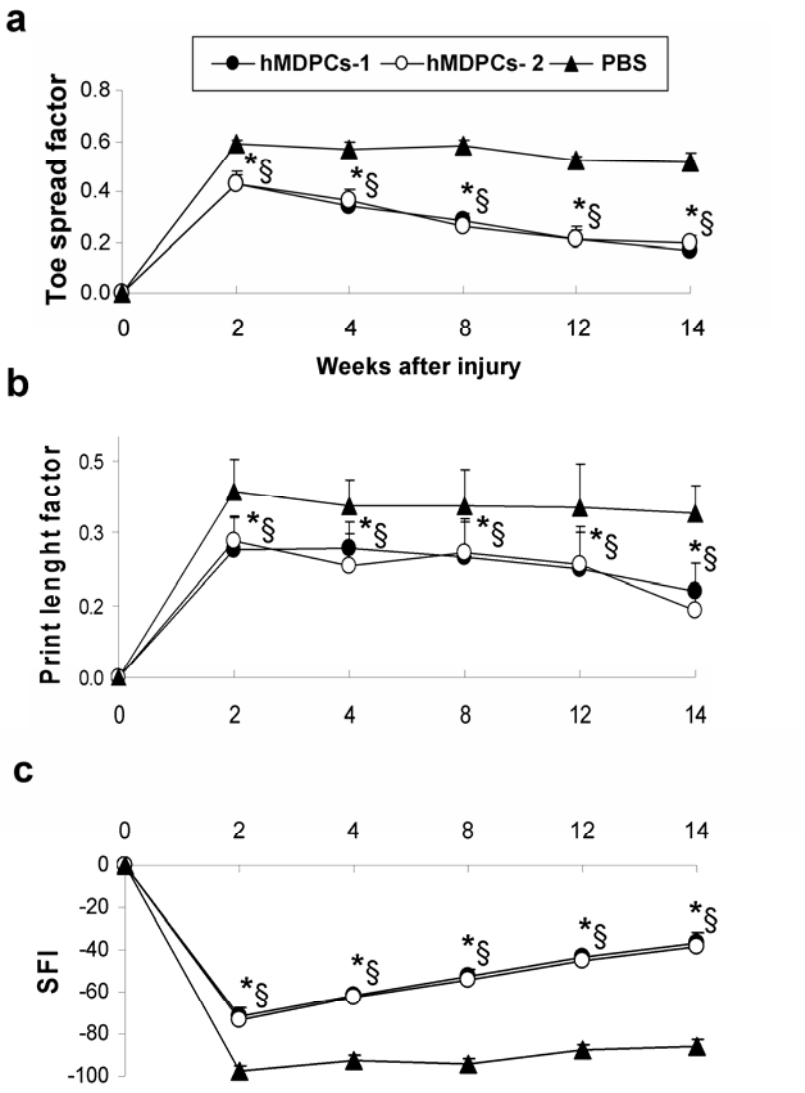

Figure 4.7: hMDPCs improve functional recovery after injury

(**a-c**) Further quantification of data obtained by measuring the paw print factors revealed functional recovery determined by (**a**) a significant decrease in both toe spread factor and (**b**) print length factor, and (**c**) significant increase in SFI for hMDPCs-treated versus PBS-treated mice in each consecutive weeks after injury. (*$P < 0.05$ indicates PBS vs. hMDPCs isolated from patient 1, ANOVA, Kruskal-Wallis on Ranks; § $P < 0.05$ indicates PBS vs. hMDPCs isolated from patient 2, ANOVA, Kruskal-Wallis on Ranks). Data present three independent experiments. A total of 30-90 paw prints were analyzed/group/time point.

4.3 DISCUSSION

Skeletal muscle is not commonly used as a source of neurogenic cells. However, adult human skeletal muscle was recently shown to include progenitor cells with neurogenic properties *in vitro* [201, 202], but regeneration capacity of these cells has not been demonstrated yet. Our findings suggest that progenitor cells isolated from the skeletal muscle of humans via modified preplate technique express neuronal and glial cell markers and undergo myogenic and neurogenic differentiation *in vitro*. These cells formed neurospheres and further differentiated to all neuronal and glial cell lineages including the most important cells involved in peripheral nerve, the Schwann cells. These findings reinforce that skeletal muscle contains a progenitor/stem cell population with a high capacity for neurogenesis. Furthermore, these cells survived and grafted in the area of sciatic nerve defect post-transplantation and greatly enhanced the restoration of critically sized sciatic nerve defect with induction of nerve fiber regeneration through myelin-producing Schwann cell-like cells. We posit that regeneration of motor axons in cell transplanted animals improved the probability of muscle tissue reinnervation resulting to a functional recovery. Together these data provide evidence, at both the anatomical and functional levels, that implantation of hMDPCs are capable of significantly accelerating the regeneration of peripheral nerve damage.

It is important to mention that transplantation of hMDPCs in our sciatic nerve model of mice did not lead to development of abnormal growth. While nerve regeneration and functional recovery was observed, no sign of tumorigenesis was detected up to one year following implantation. From a theoretical perspective, hMDPCs perhaps more differentiated/committed cells compared to undifferentiated murine MDSCs counterparts. As previously stated, differentiated cells seems to be less prone to microenvironment related transformations. Also,

due to some differences in mouse and human growth factors and their receptors, hMDPCs may show a lower specific activity to the corresponding mouse cytokines. This makes hMDPCs less influenced by exogenous murine growth factors and their environmental cues and lowers the chance of transformation. These possibilities remain to be confirmed.

Although a limited number of donor cells underwent Schwann cell differentiation, other mechanisms are most likely responsible for our observe nerve regeneration. These mechanisms may include recruitment of host Schwann cells at injury site, production and/or release of growth factors by the donor/host cells. These growth factors play an important role in survival, recruitment, and differentiation of the host/donor cells toward supporting cells, the Schwann cells, to enhance continuity of the axonal regeneration at the site of injury. Previous studies have proposed the expression of certain growth factors by implanted cells as a possible mechanism for functional improvement [196, 197, 204]. In addition, differentiation of host cells toward Schwann cell may be activated by transplantation of the donor cells stimulating the body to heal itself more effective manner. Further evaluation is needed to determine the fate of grafted cells, and clarify the mechanism behind our observed regeneration.

4.4 CONCLUSIONS

Here we report that cells isolated from adult human skeletal muscle using a modified preplate technique can form neurospheres and be further differentiated into all three main cell lineages of central nervous system, neurons, oligodendrocytes and astrocytes, as well as peripheral nerve supporting cells, the Schwann cells. Following transplantation of these cells into a peripheral nerve injury model, complete functional regeneration was observed after injury. In addition,

regeneration improved the ability of mice to walk normally. These results help to further validate the multipotentcy of progenitor cells isolated from human skeletal muscle via modified preplate technique and facilitate their usage as a valuable source for cell-mediated therapies.

In addition, this work represents one of the first attempts to have used isolated muscle cells by the modified preplate technique for the purpose of neuronal tissue engineering. The ability of the preplate technique to generate highly purified, although heterogeneous population of cells, in a large quantity from human muscle biopsies with minimal manipulations is extremely important since this will greatly facilitate clinical trials using autologous muscle biopsies for regenerative medicine.

4.5 MATERIALS AND METHODS

4.5.1 Cell isolation and culturing

Using the modified preplate technique as previously described for mMDSCs (detailed in 3.5.1, and Appendix A), early and late preplate cell fractions human muscle-derived progenitor cells (hMDPCs) were isolated from four human skeletal muscle biopsies (mean age 27.3 years; range, 21 to 72 years) obtained from the National Disease Research Interchange (NDRI). The fraction of the slowly adhering cells (SACs) containing hMDPCs was considered as human counterparts to mouse PP6 and was used throughout the study.

4.5.2 Real-Time PCR analysis

Total RNA was extracted from $1x10^5$ cells using Nucleospin RNA kit (Clontech Laboratories). cDNA was synthesized with SuperScript™ II reverse transcriptase (Invitrogen), according to manufacturer's instructions. PCR was performed with Taq polymerase (Invitrogen) per manufacturer's instructions for 35 cycles at 58°C annealing temperature and PCR products were electrophoresed on 1% agarose gels. The cDNA and primers, listed in Appendix B under Table B.1, were added to SYBR green PCR master mix (Applied Biosystems) according to manufacturer's instructions. Each set of oligonucleotides was designed to spam two different exons to avoid genomic DNA contamination. Results are expressed relatives the housekeeping gene Cyclophlin. The assays were carried out in triplicates. All target genes were normalized to *18S* used as an internal control. The data were normalized to values obtained from undifferentiated cells.

4.5.3 Immunocytochemistry

Fraction of SACs containing the hMDPCs (pre- and post-differentiation) isolated from four individual donors were screened according to the detailed methodology in Chapter1 (section 3.5.5) for several neuronal (Nestin, NeuN, NF, β-tubulin III, and MAP2ab), glial and Schwann cell-specific markers (CNPase, GFAP, p75, S-100), immature oligodendrocyte marker (NG2), mature oligodendrocyte marker-O4 [O4]), and a high affinity receptor for nerve growth factor (TrkA) by immunocytochemical staining.

hMDPCs were detected using human specific marker lamin A/C. Cells were incubated with mouse anti lamin A/C (1:200; Vector) combined with all the antibodies listed above except

for the ones developed in mouse to avoid cross reactivity at 4°C overnight. The next day, the cells were rinsed with PBS and incubated with biotinylated anti-mouse IgG (1:200; Vector) for 1 h at room temperature, and subsequently stained with streptavidin-conjugated 488 (for lamin A/C immunostaining, 1:500; Vector) for 20 min. hMDPCs were then exposed to the following secondary antibodies to the appropriate species: donkey anti-mouse IgG-AlexaFluor® 594- or 488-conjugated (1:500; Molecular Probes), donkey anti-rabbit IgG-AlexaFluor® 594- or 488-conjugated (1:500; Molecular Probes) for 30 min, and Cy3-conjugated anti-goat IgG (1:1000; Sigma-Aldrich) against nestin antibody for 1 h. To visualize the nuclei, the cultures were then incubated with DAPI (4′, 6′ diamidino-2-phyenylindole, 100 ng/ml; Sigma-Aldrich) for 10 minutes. Culture slides (BD Falcon™) were mounted with Vectashield® medium (Vector). Bright-field and fluorescent images were taken using a Nikon Eclipse E800 microscope equipped with a Q imaging Retiga Exi digital camera or Leica DMIRB microscope equipped with a Q imaging Retiga digital camera both running with the Northern Eclipse software system (v. 6.0; Empix Imaging, Inc.). Cells were systematically quantified in at least 15 fields across the slides, or wells of culture dishes from four to six independent experiments and the ratio of positive nuclei to the total nuclei defined the percent positive cells. Negative control culture wells were similarly processed but without primary antibodies. To control for nonspecific binding, some wells were processed with normal mouse or rabbit IgG and followed by the same secondary antibodies.

4.5.4 Cell transplantation

All procedures were performed according to the University of Pittsburgh Institutional Animal Care and Ethics Committee with approved protocol (13-03). Four to five-millimeter segment of

sciatic nerve from 6- to 8-week-old SCID mice (C57BL/6J-*Prkdc*^{scid}/SzJ; Jackson Laboratory) was removed resulting in a ~6.5- to 7-mm defect due to retraction of the nerve ends. Immediately thereafter, a viable single cell suspension of $3x10^5$ SAC containing hMDPCs isolated from human donors, or an equal volume (15 μL) of PBS (control), was injected into proximal and distal nerve stumps. Mice from each group were sacrificed 6 and 12 weeks after transplantation, and the hind limbs, including the sciatic nerve, were harvested, flash frozen in 2-methylbutane pre-cooled in liquid nitrogen, serially sectioned in 6 μm thickness, and stored at -80 °C for further analysis.

4.5.5 Immunohistochemistry

Cryosections of the hind limb were first immunostained for FluoroMyelin red (Molecular Probes) according to the protocol provided by the manufacturer, and then fixed in 4% PFA blocked with 5% DS for 1 h, and incubated with rabbit anti-NF (1:300, Chemicon) for 2 h at room temperature. The tissues were then rinsed with PBS and stained with donkey anti-mouse IgG-AlexaFluor® 488-conjugated for 20 min. In addition, the regenerated sciatic nerves were cryo-sectioned longitudinally, fixed with 5% formalin, blocked with 10% GS, and incubated overnight at 4°C with both rabbit anti-NF (1:300; Chemicon) and mouse anti-CNPase (1:200; Sigma-Aldrich) antibodies. The next day, the sections were rinsed with PBS and incubated with biotinylated anti-mouse IgG (1:200; Vector) for 1 h, and subsequently stained with streptavidin-conjugated Cy3 (for CNPase immunostaining, 1:500; Sigma-Aldrich) at room temperature for 20 min. Sections were then exposed to donkey anti-rabbit IgG-AlexaFluor® 488-conjugated (1:500; Molecular Probes) for 20 min to immunostain for NF-positive axons.

For human cell survival and colocalization study, the fixed sections were blocked with 5% GS and incubated with human anti-human PCNA (Proliferating Cell Nuclear Antigen, 1:500; US Biological) for 45 min. Sections were rinsed with PBS and exposed to goat anti-human IgG-AlexaFluor® 555-conjugated (1:500; Molecular Probes) for 15 min. Sections were then incubated with rabbit anti-GFAP (1:500; Chemicon) for 3 h at room temperature, rinsed with PBS, and exposed to donkey anti-rabbit IgG-AlexaFluor® 488-conjugated (1:500; Molecular Probes) for 20 min. Nuclei were revealed with DAPI. For all the above procedures, negative control sections were similarly processed but without primary antibodies or with normal mouse or rabbit IgG in replacement for secondary antibodies to control for nonspecific bindings.

4.5.6 Morphometric analysis of the regenerated nerve

Morphometric characteristics of 300-500 fibers in mid-sections of regenerated nerve were evaluated using toluidine blue and electron microscopy images. Number of myelianted axons, myelin thickness, cross-sectional area of myelianted axons, and g-ratio were measured and analyzed following the same protocols as previously described in methodology section of Chapter 1 (3.5.9).

4.5.7 Functional assessment

We used our previously established walking track model to evaluate functional recovery of mice implanted with hMDPCs versus PBS during 14 weeks interval (2,4,8,12, and 14weeks) post-operation. Measuring factors were quantified from mice foot prints and used to calculate SFI following same methodology as previously described in Chapter 1 (3.5.10) and Appendix C.

4.5.8 Statistical analysis

Statistical analysis was carried out using SigmaStat (Jandel Scientific v2.0) software package. Morphometric parameters are expressed as the median values, 25^{th}-75^{th} percentiles. Direct comparisons between treatment and control groups for myelianted fiber counts data was analyzed using One-way ANOVA. However, the data for the myelin thickness, myelinated fibers area, axon area, and g ratio violated the assumptions of normality and variance and these were compared using Kruskal-Wallis One-way ANOVA on ranks. If statistical difference was observed, Tukey Test was performed using All Pairwise Multiple Comparison Procedures to isolate the group or groups that differ from the others. One-way ANOVA or the Kruskal-Wallis One-way ANOVA on ranks (where appropriate) were used for paw prints analysis. Significant was placed at $P < 0.05$.

5.0 DIRECT CONTRIBUTION OF VASCULAR-ENDOTHELIAL CELLS FROM VENOUS GRAFTS SUPPORTS PERIPHERAL NERVE REGENERATION

5.1 INTRODUCTION

Vein wrapping and vein grafts, as non-nervous conduits, have been effective alternative treatments of peripheral neuropathy in both experimental and clinical settings [40, 205-210]. The results of these studies and others have also shown improvement of the nerve function and the symptoms associated with recurrent compressive peripheral neuropathy [207-214], carpal tunnel syndrome [207, 215], tarsal tunnel syndrome [212], prevention of scar formation [213, 216, 217], and alleviation of painful neuroma [218, 219] in clinical settings. However, little is known at present about the mechanisms that mediate the observed improvement. Recently, a vascular niche for adult hippocampal neurogenesis was identified [220]. Endothelial cells are recognized as a critical component of the neural stem cell niche, as they secrete factors that maintain the self-renewal and multipotency of neural stem cells [134]. Our group has recently isolated a vascular-endothelial cell population form human biopsies, which express both myogenic and endothelial cell markers and possess superior multipotency, regenerative abilities and resistance to oxidative stress when compared with myogenic or endothelial fractions [135]. The description of multipotent myoendothelial cells in human skeletal muscle and pericytes throughout the organism [135, 136] supported our hypothesis that the healing of peripheral nerves is mediated by vascular cells from venous grafts.

To test our hypothesis, we used femoral veins obtained from donor (male) rats as conduits to bridge peripheral nerve defects created in the femoral nerves of host (female) rats. The possibility that vascular cells residing in the blood vessel can contribute in the process of nerve regeneration was assessed using fluorescence in situ hybridization **(**FISH) to detect donor-derived Y chromosomes co-localized with Schwann cells nuclei of host regenerated nerve in our sex-mismatch model. To further verify our hypothesis, we altered the course of cell contribution from donor venous grafts by decellularization (complete cell removal) and irradiation (preventing cell proliferation and migration). A sustained decrease in nerve regeneration in decellularized or irradiated groups would be an appropriate indicator if active participation of migrated cells is essential. Proper organization and remyelination of axons and level of scar formation was assessed by histology and immunohistochemistry. Morphometric parameters were quantitatively measured in the mid-section of the regenerated nerves using toluidine blue and electron microscopy images. Results from this study may uncover valuable information to explain the cellular basis for success of using vein wrapping as an effective clinical treatment for peripheral nerve injuries.

5.2 RESULTS

5.2.1 Migration and proliferation in vein grafts are inhibited following irradiation

To determine the effect of decellularization or irradiation on venous grafts before transplantation, pieces (~1–2 mm) from intact (control), decellularized, and irradiated veins were placed in fibronectin-coated 24-well plates in endothelial cell growth medium (EGM-2, n = 3). While

many cells had migrated out of the vein at 7 days in culture (**Figure 5.1a)**, no migrating cells were detected out of the irradiated veins (**Figure 5.1a**) in parallel cultures. Cells were still visible at the edges of the intact and irradiated veins after 14 days of culture (**Figure 5.1b**, arrows), and continuously outgrew from the explants (**Figure 5.1b**, arrowheads) as a mixture of endothelial cells, vascular smooth muscle cells, and pericyte progenitors (**Figure 5.1c**). Human endothelial cells fail to replicate after a 1000-rad irradiation [221]. We have assessed doses of 1000, 2000, 5000, and 10,000 rad. The 1000-rad was chosen because it limits the cell damage while preserving the integrity of vein grafts. The viability of clustered cells attached to the irradiated veins was verified using the MTT assay. Presence of purple cells suggests that mitochondrial dehydrogenase enzyme from these viable cells cleaved the tetrazolium ring, resulting in accumulation of impermeable purple formazan crystals. Though the cells appeared to be viable (**Figure 5.1c**, purple), the cells could not migrate out of the vein even after 25 days, proving that irradiation inhibited cell proliferation and migration.

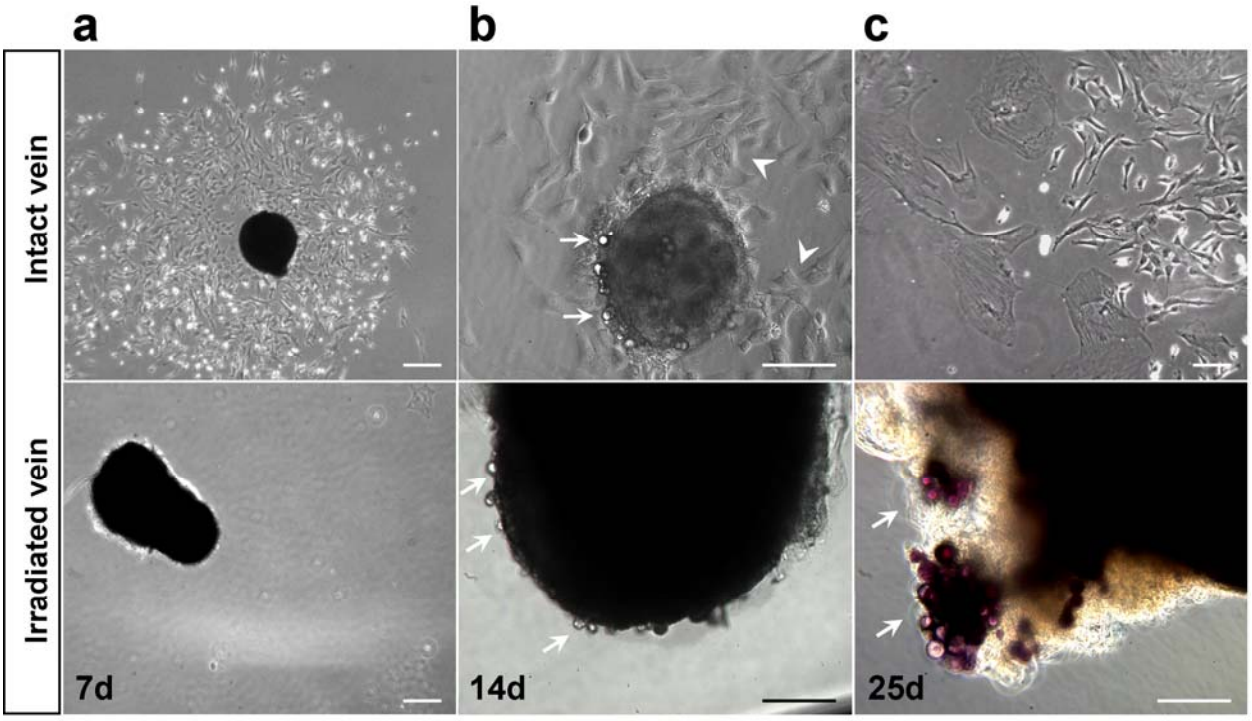

Figure 5.1: Migration and proliferation of the cells are inhibited following irradiation
The pieces (1-2 mm) from intact and irradiate veins were separately cultured in wells of 24 well plate coated with fibronectin in EGM2, an endothelial growth medium. (**a**) Many cells were outgrown from the intact vein at 7 days in culture, while no cells were visible in the irradiated vein. (**b**) Fourteen days post-culture, cells were still visible at the edges of the intact and irradiated veins (arrows), and continuously outgrown only from the intact vein (arrowheads). (**c**) Cells outgrown from the intact vein were showed a diverse morphology, while cells in the irradiated vein stayed as clusters and could not migrate out of the even after 25 days of being in the culture dish but were viable verified by using the MTT assay (purple). Data represent at least three independent experiments. Scale bars represent 200 μm (**a**) or 100 μm (**b** and **c**).

Similar to previous work reported by Schaner *et al*. [222], treating the venous grafts with SDS resulted in cell disappearance throughout the tissue while preserving matrix integrity. We did not observe cells on the dish containing the decellularized vein (**Figure 5.2**).

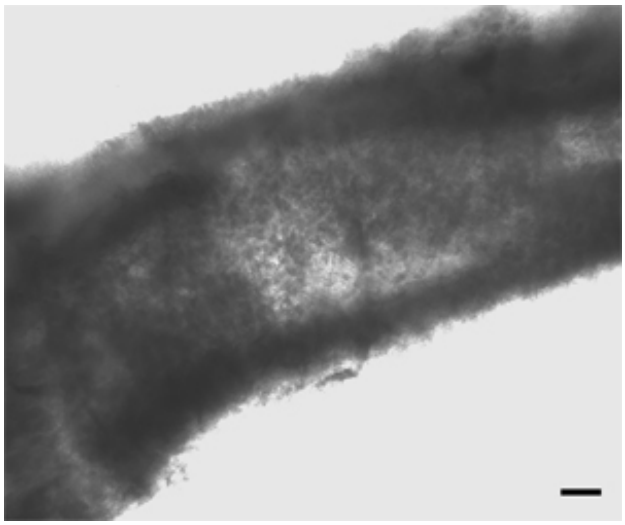

Figure 5.2: Vein rendered acellular with SDS has well-preserved matrix for grafting
Light microscopy of venous graft after treatment with 0.075% SDS revealing preservation of extracellular matrix but disappearance of cells throughout the treated tissue. Scale bar represent 100 μm.

5.2.2 Cells from venous grafts contribute in nerve regeneration

Peripheral nerve lesions were bridged using venous conduits in a rat sex-mismatch model, and fluorescence in situ hybridization **(**FISH) was used for detecting donor-derived Y chromosomes in regenerated nerves. A segment of the femoral vein separated from artery and nerve compartment of a male rat was used as a conduit to bridge femoral nerve defect made in female rat (**Figure 5.3**).

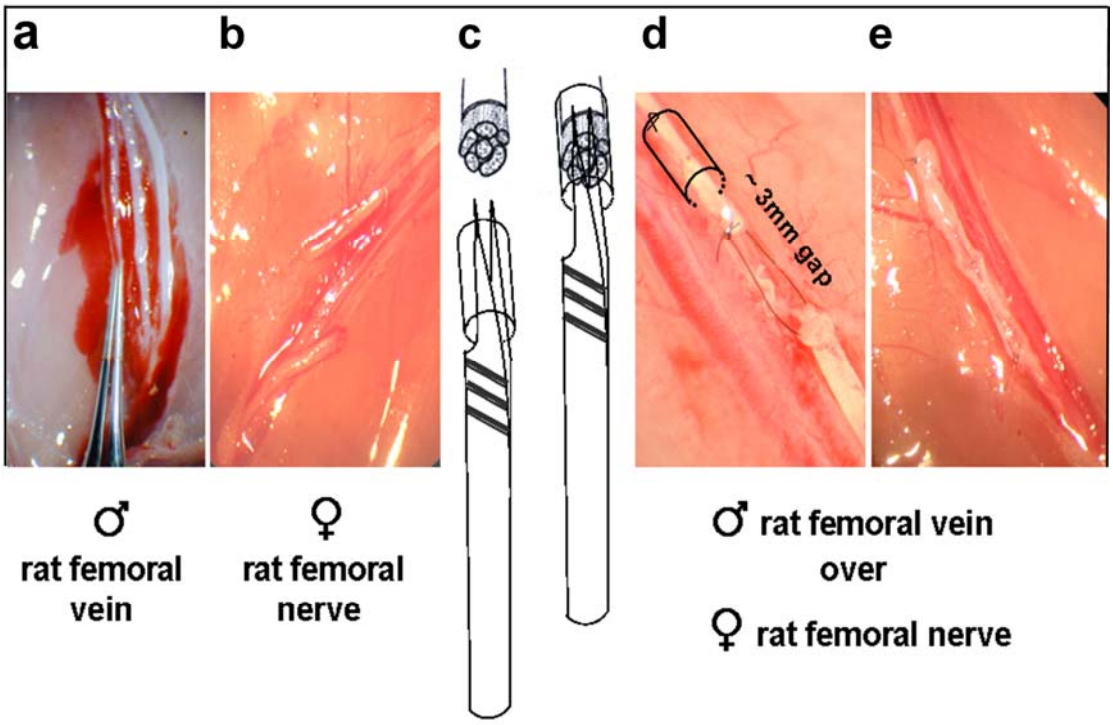

Figure 5.3: Surgical procedure for isolation and implantation of venous graft
(**a**) Five to six millimeters segment of pure femoral vein from a male Fisher rat was isolated, pulled over a 0.2-mm forceps (vessel dilator) and placed in sterile PBS for later use. (**b**) The right femoral nerve from a female rat was exposed, and a 5-mm segment of peripheral nerve was carefully separated so as not to disturb the attached artery and vein compartment. Using surgical scissors, a cut was made in the middle of the femoral nerve of a female Fisher rat to create two ends. (**c**) The distal end of the femoral nerve was grabbed by the forceps carrying the previously removed male-derived vein. One millimeter of the distal end was cut later to have a fresh end. (**d**) Using 10/0 monofilament nylon, the proximal and distal stumps was drawn together and tied to form a loop while keeping a gap of ~3-mm. Every effort was made to avoid tension and correct rotational alignment throughout. (**e**) Using the forceps, the femoral vein was pulled over the gap toward the proximal end of the nerve like a glove. The vein graft was interposed between ends of the femoral nerve with 10/0 monofilament nylon, using 2–3 epineurial stitching for each stump.

Proper nerve regeneration four–six weeks after implantation was assessed using histochemistry, immunohistochemistry, and electron microscopy. At the time of harvesting, the vein grafts could be identified under the operating microscope in all the groups without any sign of absorption or degeneration. Minimal scar or adhesions were noticed between the nerve and the vein graft, although some scarring was evident in recipient of irradiated veins. Complete femoral nerve regeneration was observed in all of the rats that received intact control vein grafts, while

the recipient of decellularized and irradiated veins exhibited only minimal regeneration. Four–six weeks after transplantation, Masson's trichrome stain of regenerated nerves in decellularized and irradiated grafts (**Figure 5.4a**) showed lower myelinated axons regeneration (no traces of pink stain) and more collagen deposition (intense blue stain), as compared to nerves in intact grafts. The regenerated nerve in intact venous grafts showed a well-organized architecture of myelinated nerve fibers, including less fibrotic tissue (collagen, blue) between fascicles (epineurium) and within individual axons (endoneurium) (**Figure 5.4a**). Regenerated nerves in intact grafts exhibited many neurofilament-positive axons (green) surrounded with myelin sheets positive for fluoromyelin (red), as compared to other experimental groups (**Figure 5.4b**), suggesting proper formation of mature myelinated axons at the site of nerve regeneration. This pattern of maturation is not apparent in recipient of decellularized or irradiated veins **(Figure 5.4b**).

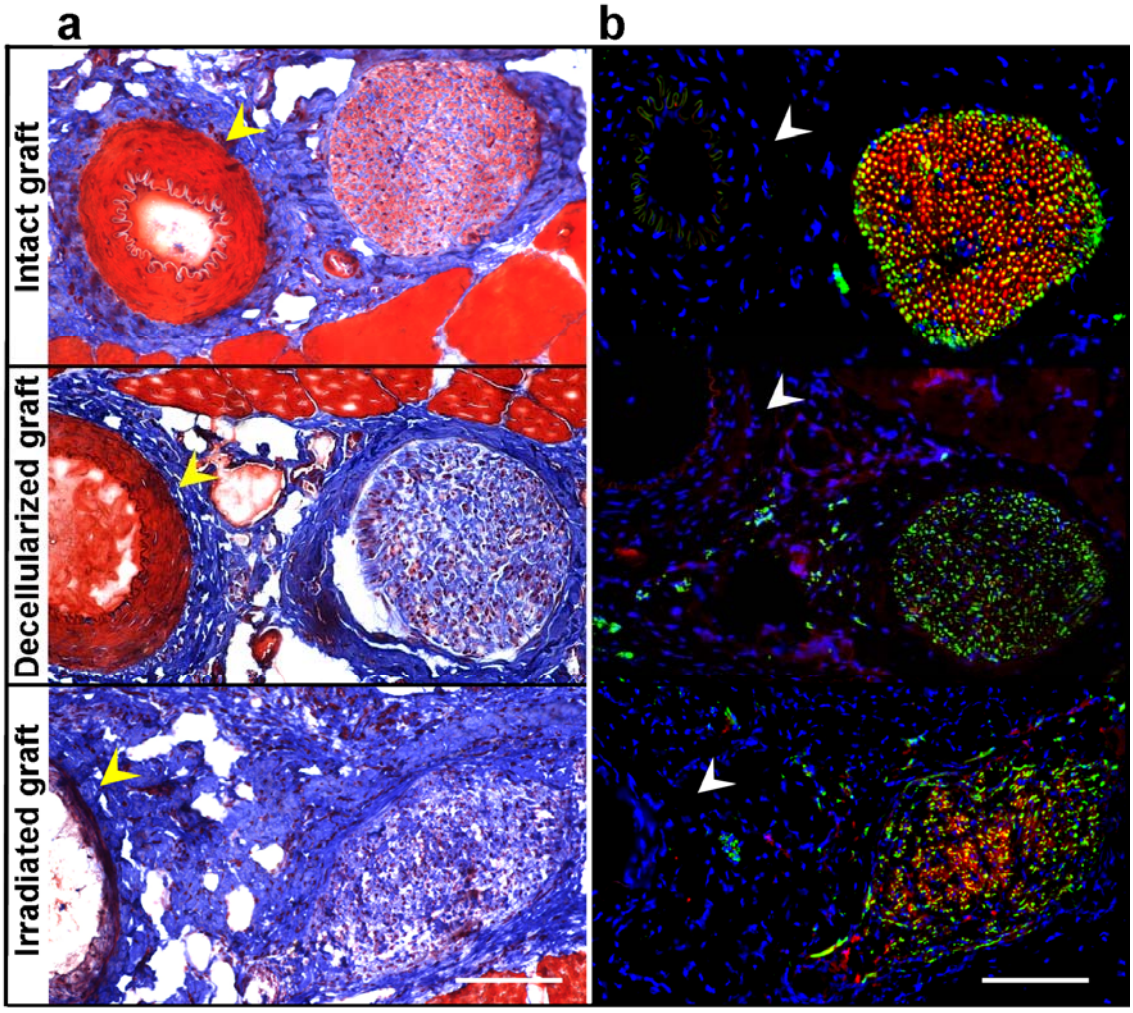

Figure 5.4: Intact venous grafts exhibit more effective nerve regeneration
(**a**) Eight weeks post-transplantation, Masson's trichrome staining revealed absence of collagen matrix and adventitia of the grafted vein (blue) and defined nerve regeneration with perineurium surrounding the nerve bundles (pink) in intact graft, while thickening of the extracellular matrix and disorganized perineurium was obvious in decellularized and irradiated grafted groups. Undamaged host artery shown with arrowheads is used as reference point. (**b**) the cross-section of the regenerated nerve exhibited regenerated NF-positive axons (green) encompassed by fluoromyelin-positive Schwann cells (red) suggesting proper regeneration of the femoral nerve in intact control grafts compare to treatment groups. Scale bars represent 100 μm.

Toluidine blue staining (**Figure 5.5a**), and transmission electron microscopy (TEM) images of the same sections **(Figure 5.5b**) revealed that the decellularized and irradiated veins induced only scattered regeneration in form of small axons with thin myelin sheets and more

prominent thickening of the extracellular matrix when compared to intact venous grafts (**Figure 5.5a, b**).

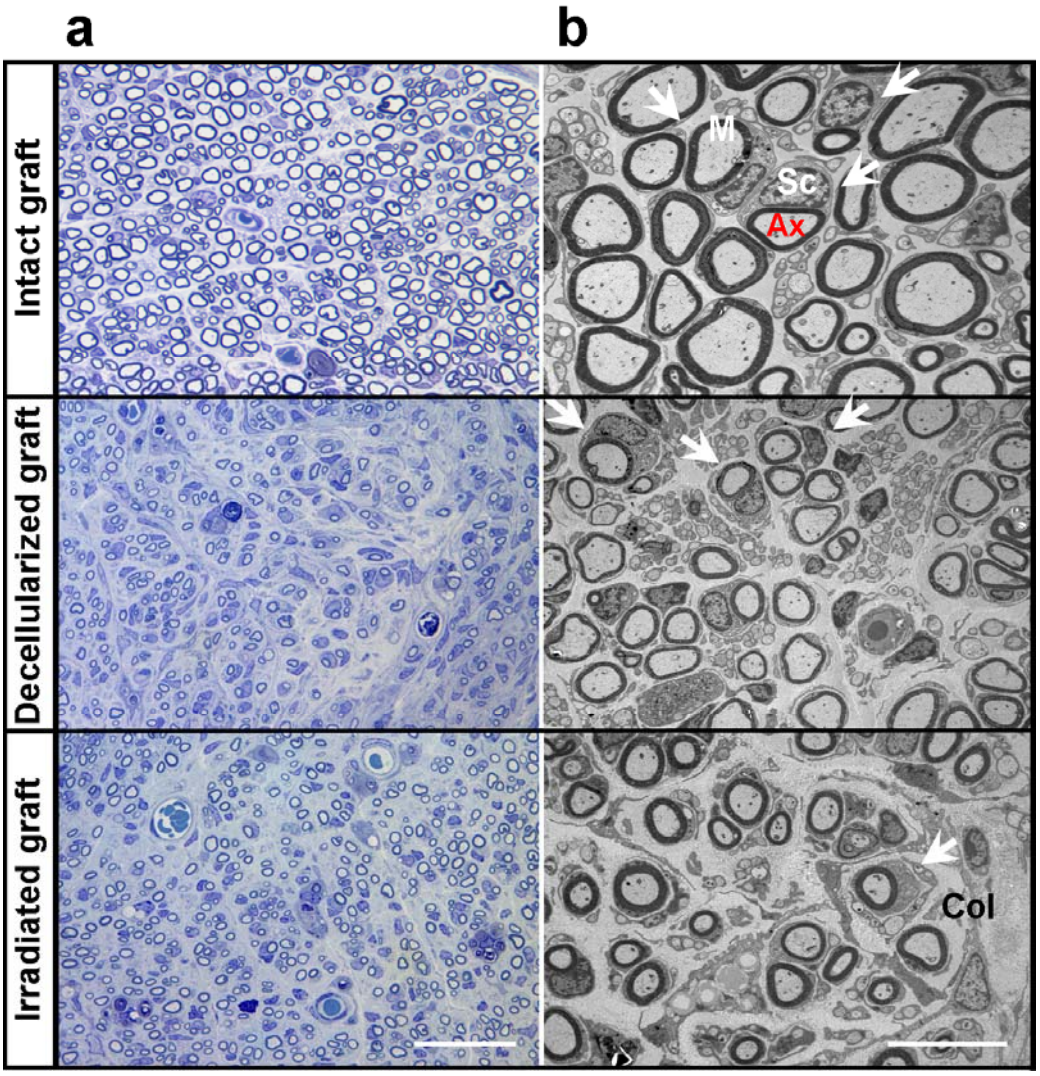

Figure 5.5: Intact venous grafts show proper regeneration and myelination
(**a**) Toluidine blue staining and (**b**) transmission electron microscopy at the mid-proximal sections confirm superior regeneration with larger myelianted axons including presence of myelin-producing Schwann cells (arrows) surrounding the regenerated axons and absence of connective tissue fibrosis in transplanted intact grafts while both treated grafts showed poor level of nerve regeneration evident with small myelinated Schwann cells and high level of connective tissue fibrosis indicated by collagen. "Sc" corresponds to Schwann cells, "M" to myelin sheath, "Ax" to axon, and "Col" to collagen. Scale bars represent 100 μm (**a**) or 10 μm (**b**).

Morphometric parameters such as number of myelinated axons, myelin thickness, myelinated fiber area, axon area, and g-ratio (axon area : myelinated fiber area) [148] were

quantitatively measured in the mid-section of the regenerated nerves using toluidine blue and TEM images (**Table 1**). Eight–ten weeks after transplantation, number of the regenerated myelinated axons were not significantly different between the treatment groups and when compared to the intact femoral nerve. Although, there were clearly larger and thicker myelinated axons in uninjured control nerves and nerves treated with intact vein grafts, compared to nerves associated with decellularized and irradiated vein grafts. Therefore, axonal cross-sectional area and myelin thickness were assessed as a measure of regenerating fiber maturation. Median values for myelinated fiber area and myelin thickness in decellularized and irradiated graft groups were significantly smaller than in the intact grafts. Although, intact grafts showed better myelination, the values did not reach the level of the uninjured control nerves. The median axonal area and the g-ratio, which describes the relationship between axon caliber and myelinated fiber caliber, were significantly smaller in decellularized or irradiated vein compared to intact grafts and control femoral nerves. The low g-ratio in nerves decellularized or irradiated veins is due in part to the shrinkage of axons and their failure to regain their normal diameter [223], and the presence of more regenerated fibers with thin myelin sheaths compared to nerves treated with intact veins and uninjured control nerves. In contrast, no significant difference was seen in the median axonal area and g-ratio between the intact grafts and uninjured control nerves, suggesting that intact venous grafts contributed considerably to nerve regeneration.

Table 5.1: Morphometric analysis of regenerated myelianted axons
Median values for the number of the myelinated axons (per 10,000 μm^2) at the mid-proximal portion of the regenerated nerve stained with toluidine blue showed no significant difference between the groups (P = 0.760; ANOVA, Kruskal-Wallis on Ranks). Parametric analyses of transmission electron microscopy images of the proximal-mid cross-sections of the regenerated femoral nerves show that median (25^{th}–75^{th}) values of the myelianted fiber area and myelin thickness were statistically differ between the groups (*P < 0.05; ANOVA, Kruskal-Wallis on Ranks) when compared to control femoral nerves (§ P < 0.05; ANOVA, Kruskal-Wallis on Ranks). The quantitative measurement of axon area and g-ratio (axon area : myelinated fiber area) showed no difference between the intact graft and control femoral nerves. The decellularized and irradiated groups showed significantly lower g-ratio associated with thinner axonal remyelination when compared to intact grafts (*P < 0.05, ANOVA, Kruskal-Wallis on Ranks) and control femoral nerve (§ P < 0.05; ANOVA, Kruskal-Wallis on Ranks).

	Control femoral nerve	Untreated graft	Decellularized graft	Irradiated graft
Number of myelinated axons	400	375	440	435
Myelinated fiber area (μm)	21.9 (11.1–28.1)	13.0 §(6.25–21.9)	3.81 §*(1.50–6.26)	5.25 §*(1.50–6.26)
Myelin thickness (μm)	9.72 (6.0–14.4)	5.86 §(3.35–8.89)	2.05 §*(0.97–3.32)	2.87 § (1.84–4.57)
Axon area (μm)	10.1 (5.93–13.3)	7.64 (2.08–12.2)	1.43 §*(0.24–2.85)	2.19 §*(0.77–4.26)
g-ratio	0.54 (0.40–0.61)	0.50 (0.42–0.57)	0.36 §*(0.14–0.51)	0.44 §*(0.14–0.54)

Supporting the hypothesis that cells residing in the blood vessel wall participate in the process of myelination, colocalization of Y chromosomes-Cy3 (red) with Schwann cell nuclei of the host (DAPI, blue) revealed the possible fusion of donor cells with host glial cells (**Figure 5.6a,** arrows). FISH analysis on positive control section of male rat confirmed high level of probe sensitivity, specificity, and hybridization efficiency (**Figure 5.6b**, arrows). Hence, to further examine if the direct contribution of cells play a major role in the regeneration process, decellularized and irradiated vessels were used simultaneously with intact venous grafts. Four–six weeks after injury, FISH against Y chromosome verified the contribution of male-derived donor blood vessel progenitor cells with female host Schwann cells nuclei in regenerated nerves of intact venous grafts, but not in decellularized or irradiated grafts. Thus cells residing in the blood vessel walls support axonal growth and restoration after nerve injury.

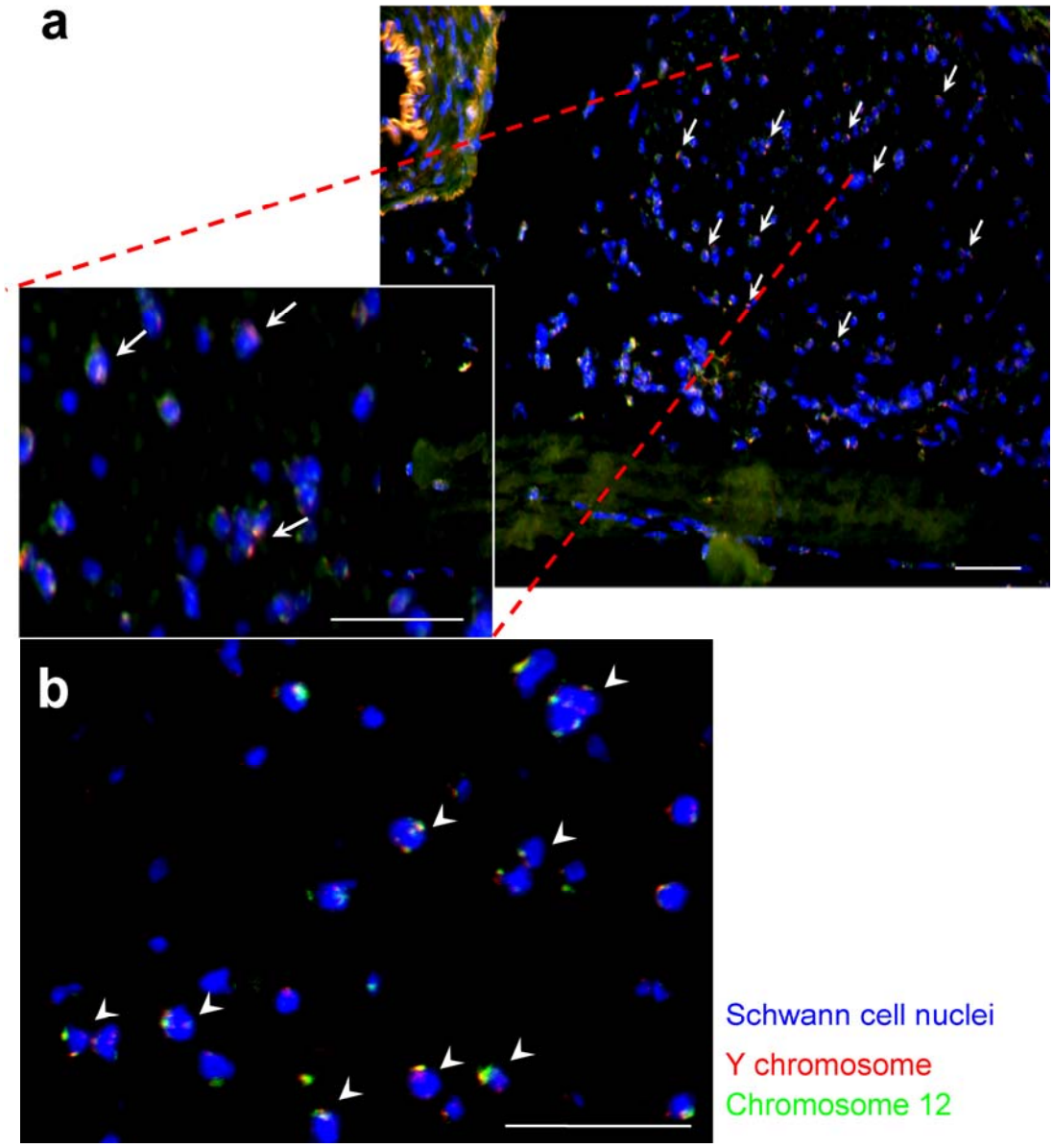

Figure 5.6: Donor blood vessel cells from venous grafts actively participate in nerve regeneration
(**a**) Four-six weeks after injury, FISH against Y chromosome verified the active contribution of male-derived donor blood vessel progenitor cells (Y chromosome-Cy3 positive nuclei) in the regenerated female femoral nerve (host Schwann cells nuclei counterstained with DAPI are shown by arrows, n = 6). (**b**) detection of Y chromosome signals in almost all of the nuclei of positive control tissues obtained from male rat revealed high specificity of the chosen probe. Chromosome 12-FITC probe is used as a reference chromosome to check for the hybridization efficiency. Scale bars represent 100 μm.

5.3 DISCUSSION

Our sex-mismatch venous graft model reveals active contribution of stem/progenitor cells that migrate from the venous nerve guide to the site of nerve injury and accelerate the process of remyelination and regeneration. This was evidenced by the presence of donor-derived Y chromosomes in regions of regenerated nerve that were co-localized with Schwann cell nuclei of the host. The proper nerve regeneration and reduced endoneurial scarring shown by intact venous grafts may be due on the one hand to Schwann cell motility, that facilitate graft invasion [67], but also to decrease in fibroblast infiltration [224], prevention of uncontrolled fiber outgrowth [225] and neuroma formation [218, 219], improved gliding on the smooth inner surface of the vein [208, 216], and scarring prevention [213]. Neovascularization [212, 215] and growth factor secretion [225] are suggested to be involved in facilitating the process of nerve regeneration using venous conduits. Notably, vein decellularization, which destroys the residing cells while the mechanical properties of the vessel are not impaired [226], and irradiation, that causes cell depletion and prevents cell replication and migration [221, 227] severely compromised nerve regeneration. Collectively these experiments provide evidence that without direct involvement of cells, the nerve regeneration mediated by vein wrapping is limited.

The efficacy of a venous nerve conduit for reconstruction of a peripheral nerve likely relies on many factors, for instance the secretion of cytokines by donor and/or host cells, recruitment of host Schwann cells to promote regeneration, and improvement of angiogenesis. Here we provide evidence that blood vessel wall derived cells migrate and contribute to myelination by way of fusion or differentiation into Schwann cells. As almost all issues are vascularized, the walls of blood vessels are emerged as a possible reservoir of ubiquitous multi-lineage cells that could be recruited in emergency situations or when tissue-specific progenitors

have been exhausted. This concept has been largely emerged by description of mesoangioblasts and hematopoietic stem cells [228, 229]. More recently, adipose vasculature has been identified as a niche where white fat progenitor cells reside [230]. The notion that myoendothelial cells and/or pericytes are likely at the origin of muscle derived stem cells was the conclusion of our previous study and is further supported by the current study [135, 136], indicating that venous nerve conduits may promote nerve repair through similar populations of cells. Future experimentation will be needed to distinguish which types of blood vessel-derived cells are the key players in such a process. It is noteworthy that combine muscle-vein nerve guides have shown promising results for larger nerve defects regeneration [38, 231-233]. Clinical application of muscle-vein-combined grafting led to efficient nerve repair, both for motor and sensory nerves, with satisfactory functional recovery in 85% of the patients [38]. Muscle tissues used to fill up the vein graft, contain satellite cells, myoendothelial cells, and pericytes that may migrate, proliferate, and differentiate toward the glial lineage thus promoting axonal growth and nerve regeneration.

5.4 CONCLUSIONS

In conclusion, this study establishes that blood-vessel-derived cells residing in the wall of venous grafts contribute in the process of peripheral nerve repair by way of migration, and cell fusion and/or differentiation. Presences of donor-derived Y chromosomes in the region of host regenerated nerve prove migration of vascular cells to the area of injury. This finding is validated by showing a sustained decrease in nerve regeneration by decellularization or irradiation of the venous grafts. Co-localization of Y chromosomes with host Schwann cells' nuclei indicate that

nerve repair through vein grafting is mediated at least in part by vascular cells. Here, we uncovered valuable information to understand mechanisms underlying therapeutic benefits of using venous grafts as a nerve guide in clinic. We believe these results provide a cornerstone for future work intended to explore the relationship between stem/progenitor cells, cell fusion and/or differentiation, and nerve regeneration.

5.5 MATERIALS AND METHODS

5.5.1 Vein decellularization, and irradiation procedure

With the aid of an operating microscope (WILD M690, WILD HEERBRUGG, Switzerland), segment of pure femoral veins were isolated and decellularized according to a protocol previously reported by Shaner *et al*. [222]. Briefly, isolated femoral veins were placed into 0.075% sodium dodecyl sulfate (SDS; Bio-Rad Laboratories) in PBS for 15 h at 37°C in a shaking water bath. Subsequently, they were rinsed by agitation in PBS at 37°C for 15 min repeatedly for five times. This method of decellularization has been confirmed to remove >94% of cells from the treated vein. For irradiation study, the grafts were irradiated at 1000-rad (4.4 min) dose.

5.5.2 MTT assay

MTT [3-(4,5-Dimethylthiazol-2-yl)-2,5-diphenyltetrazolium bromide] assay, was carried out to evaluate the cell viability [234]. Sterile solution of MTT (5 mg/ml stock, Sigma) was added to

the culture dishes (0.1 ml/ml media) containing control and experimental venous grafts and incubated for 60 min at 37°C. Mitochondrial dehydrogenase enzyme from viable cells cleaves the tetrazolium rings of the pale yellow MTT and form purple formazan crystals which is impermeable to cell membranes, thus resulting in its accumulation within healthy cells. Presence of purple color was detected and captured using a Leica DMIRB microscope equipped with a Retiga 1300 digital camera (Q imaging) and Northern Eclipse software system (v. 6.0; Empix Imaging, Inc.).

5.5.3 Isolation and transplantation of venous nerve guide

Surgical procedures were carried out according to protocol (13-03) approved by the University of Pittsburgh Animal Care and Use Committee. Female Fischer 344 rats weighing 100-125 grams and male Fischer 344 rats weighing 200-225 grams were obtained from Harlan (Indianapolis, IN). With the aid of an operating microscope (WILD M690, WILD HEERBRUGG, Switzerland), 5- to 6-mm segment of pure femoral vein from a male Fisher rat was isolated, pulled over a 0.2-mm forceps (vessel dilator), and placed in sterile saline solution for later use. The right femoral nerve from a female rat was exposed, and a 5-mm segment of peripheral nerve was carefully separated so as not to disturb the attached artery and vein compartment. Using surgical scissors, a cut was made in the middle of the femoral nerve of a female Fisher rat to create two ends. The distal end of the femoral nerve was grabbed by the forceps carrying the previously removed male-derived vein. Note that 1-mm of the distal end was cut later to have a fresh end. Using 10/0 monofilament nylon, the proximal and distal stumps was drawn together and tied to form a loop while keeping a gap of ~3–4 mm. Every effort was made to avoid tension and correct rotational alignment throughout. Using the forceps, the

femoral vein was pulled over the gap toward the proximal end of the nerve like a glove. The vein graft was interposed between ends of the femoral nerve with 10/0 monofilament nylon, using 2–3 epineurial stitching for each stump. A small knot with a silk suture was left on the muscle above the construct at the proximal and distal end to allow easy identification at the time of harvest and cryosectioning. A total of 35 rats were transplanted with vein grafts for sex-mismatched study (24 intact grafts, 4 decellularized grafts, and 4 irradiated grafts) and 3 sex-matched (used as negative control for FISH analysis).

5.5.4 Fluorescence in Situ Hybridization (FISH)

Venous graft cryosections (6 μm) were fixed in methanol : acetic acid (3:1), dehydrated by 70, 80, 95, and 100% ethanol for 3 min each and then denatured in 70% formamide-2 × saline sodium citrate (SSC) at 69 ± 1 °C. Slides were then dehydrated as above and air dried. Following manufacture's protocol, directly-labeled fluorescence rat-specific Y-chromosome-Cy3 and chromosome 12-FITC probes (Cambio) was applied to the target areas (sections marked with diamond scriber), covered with plastic coverslips, glued with rubber cement and incubated in a humidity chamber for 18–24 h at 37 °C. The next day, coverslips were pilled off from the sections and slides were washed with 2 × SSC for 5 min, followed by washes in 50% formamide-2 × SSC (12-13 min), 2 × SSC (three times for 7 min) and 2 × SSC-Tween (2 min). All washes were done in 45 °C. Slides were subsequently counterstained with DAPI and were mounted with Vectashield® medium (Vector). The hybridized Y-chromosome-specific probe was detected under Nikon Eclipse E800 microscope equipped with a Retiga Exi digital camera and Northern Eclipse software system (v. 6.0; Diagnostic Instruments). Sections of hind limb from male rats

served as positive control and were similarly processed to check for probe specificity and hybridization efficiency for Y chromosomes. Negative control tissues consisted of sex-matched venous grafts (female femoral vein transplanted over the female femoral nerve) to check for absence of the Y-chromosomes signals.

5.5.5 Morphometric analysis of the regenerated nerve

To evaluate the degree of myelination, reconstructed femoral nerves including all tissue surrounding them, were processed for light and transmission electron microscopy studies. The tissues were fixed in 2.5% glutaraldehyde (EM grade, Taab Chemical) in 0.1M phosphate buffer (pH 7.3; Fisher Scientific) overnight at 4°C. The contralateral sciatic nerve harvested at the same level served as a "normal" control. The nerves were then rinsed in PBS, post-fixed in 1% osmium tetroxide (Electron Microscopy Sciences) with 0.1% potassium ferricyanide (Fisher Scientific), dehydrated in a series of ethanol solutions (30% - 90%; Fisher, and 100% [Ethanol 200 Proof]; Pharmco), exposed to propylene oxide twice for 10 min each and embedded in Epon (Dodecenyl Succinic Anhydride, Nadic Methyl Anhydride, Scipoxy 812 Resin and Dimethylaminomethyl; Energy Beam Sciences). All grafted segments were carefully oriented in order to obtain sections perpendicular to their long axis. Semi-thin (300 nm) sections were cut using a Lecia Ultracut and stained with 0.5% toluidine blue (Fisher Scientific) and examined under light microscope (Olympus BX51) with Magnafire 2.1A image capture software, and quantified for the number of the myelinated axons. Ultrathin sections (65 nm) at distal, mid, and proximal ends were obtained using a Leica Ultracut Microtome (Leica) and stained with 2% uranyl acetate (Electron Microscopy Sciences) and Reynold's lead citrate (Fisher Scientific), and examined on a JEOL JEM-1011 transmission electron microscope in collaboration with Dr.

Simon Watkins (University of Pittsburgh, Pittsburgh, PA). The number of myelinated axons in ~10,000 μm^2 of the cross-sectional area of the nerve was counted, and median area of myelin thickness, median cross-sectional area of myelinated axons, and g-ratio (axon area/myelinated fiber area) were examined in mid-sections. Each section was divided into four quarters. Each quarter of the nerve was analyzed individually, and morphometric parameters of 300-600 fibers were calculated using the Northern Eclipse software system (v. 6.0; Empix Imaging, Inc.) following image capture, background subtraction, image enhancement, automatic thresholding, and final editing.

5.5.6 Statistical analysis

Statistical analysis was carried out using SigmaStat (Jandel Scientific v2.0) software package. Morphometric parameters are expressed as the median values, 25^{th}-75^{th} percentiles. Direct comparisons between treatment and control groups for myelianted fiber counts data was analyzed using One-way ANOVA. However, the data for the myelin thickness, myelinated fibers area, axon area, and g ratio violated the assumptions of normality and variance and these were compared using Kruskal-Wallis one-way ANOVA on ranks. If statistical difference was observed, Dunn's Method was performed using All Pairwise Multiple Comparison Procedures to isolate the group or groups that differ from the others. Significant was placed at $P < 0.05$.

6.0 DISSERTATION SYNOPSIS

Here we described a population of stem cells isolated from post-natal skeletal muscle that can differentiate into muscle, neuron, and glial cells *in vitro*. Transplantation of these cells into a critical-size sciatic nerve defect in mice greatly enhanced the rate of nerve regeneration, showing full restoration of sciatic nerve by promoting axonal regeneration via myelin-producing Schwann-like cells. Functional recovery was evident by improved walking pattern of cell-transplanted mice after sciatic nerve injury indicating an enhancement in target organ reinnervation. Several weeks after complete regeneration of the sciatic nerve, neoplastic growths were observed. The resulting tumors were classified as malignant peripheral nerve sheath tumors with rhabdomyoblastic differentiation, expressing myogenic, neurogenic, and glial cell markers, common markers of human malignant Triton tumors. We observed that the neoplasias were composed almost entirely of donor cells, and cells isolated from the tumors were serially transplantable. We provide evidence that the stem cells used in this study were not oncogenic in nature, and displayed no sign of tumorigenesis 17 weeks post-implantation into the gastrocnemius muscles of *mdx* mice or 1 year following subcutaneous or intravenous injection. We postulate that the time- and microenvironment-dependent transformation observed here was due to donor cells receiving concomitant neurogenic and myogenic signals. Interestingly, further differentiation of the cells toward the neurogenic lineage prior to implantation abrogated the transformation.

The studies presented in Chapter 1 provide evidence that experiments in tissue engineering and regenerative medicine should be evaluated over a prolonged period of time, as the transformation observed here occurs only after 11 weeks post-implantation. We believe that an effective cell-based intervention therapy will rely on the better understanding of the interaction of transplanted cells with their environmental cues and critical aspects of risk versus benefit of using stem cells need to be further addressed. We consider our findings intriguing and anticipate that our results obtained using the murine cells in the process of peripheral nerve regeneration will constitute proof of concept, and will provide the foundation for future studies. In addition, our murine model of MTT may open new areas of investigation to elucidate underlying mechanism of transformation and can provide an opportunity for contribution from other investigators in several fields, including stem and cancer cell biology, regenerative medicine, and cancer therapeutics.

Our aim in objective 2 was to determine whether progenitor cells isolated from human adult skeletal muscle using modified prelate technique differentiate toward neural/glial cell lineages *in vitro*, and, ultimately be applied in our sciatic nerve defect model in mice. As expected, hMDPCs were able to undergo myogenic differentiation and form multinucleated myotubes expressing f-MyHC under low-serum conditions. These cells were able to form neurospheres and terminally differentiated into all three ectodermal lineages, neuronal, astroglial and oligodendroglial, as well as peripheral nerve supporting cells, the Schwann cells. hMDPCs showed remarkable capacity to regenerate nerve and improved functional deficits upon transplantation into critical-size sciatic nerve defect model of mice. Histological and immunological analysis revealed that regenerated nerves contained many PCNA+ donor cells predominantly located in front and along the growing cone of the proximal end. Colocalization of

hMDPCs with GFAP and CNPase suggested possible differentiation of donor cells into glial lineage especially the Schwann cells. We believe these cells may present to be the counterpart to our murine MDSCs suggesting that human muscle tissue contain multipotent progenitor cells that could be directed to express or differentiate toward neuronal and glial phenotypes.

The mechanism by which the MDSCs promoted the repair of the injured sciatic nerves remains unclear; however, the ability of the injected MDSCs to differentiate into Schwann cells may have contributed to these events. Schwann cells release various neurotrophic substances that are key regulatory proteins in the modulation of neuronal survival, axonal elongation, synaptic plasticity, and neurotransmission [71]. The fact that a large number of Schwann cells in the regenerated nerves were belong to the host suggests that the hMDPCs may have released factors that induced endogenous axonal growth and host Schwann cells proliferation. Much work remains to be done before applications based on these cells progress from bench to bedside, but the preliminary data reviewed above strongly suggest that the future use of the preplate technique to isolate cells for cell-based therapies for peripheral nerve is promising.

Multi-lineage progenitor cells have been recently identified in blood vessel walls, notably in skeletal muscle, and venous grafts have been used effectively to bridge nerve defects experimentally and clinically, through unknown cellular mechanisms. According to the results in chapter 3, we introduced and provided evidence of another important factor that may explain the mechanism (s) underlying therapeutic benefits of vein wrapping in clinic. Previously we have touched up on few ideas that have been introduced to explain the reason behind the usefulness of this technique in clinic including: (i) the venous graft can be easily obtained from sites near the injury so that closer to it is not necessary to perform any new incisions at other sites, and secondary damage created by the withdrawal of healthy nerve is also avoided; (ii) the venous

graft walls, which appear to act as a barrier prevent ingrowths of fibrous scar tissue and dispersion of the regenerating nerve fibers, (iii) vein may also be a source of growth factors; and, (iv) capping the nerve stump with vein seems to be one of the most effective methods of neuroma prevention in clinical settings. Using a sex-mismatch model, we identified donor-derived Y chromosomes co-localized with host Schwann cells' nuclei, indicating that nerve repair through vein grafting is mediated by vascular cells. Migration of these cells to the site of injury helped to facilitate the process of remyelination and regeneration. Furthermore, a sustained decrease in nerve regeneration by decellularized or irradiated venous grafts also highlights the contribution of blood vessel-derived cells to nerve repair

Collectively, the above findings encourages a new look at nerve repair by vein wrapping whereby cell migration from the vessel walls improve axonal in-growth. Also, neuronal and glial differentiation of progenitor cells isolated from mouse and human skeletal muscle further elucidate their multipotentiality and lays the foundation for future clinical experimentation of peripheral neuropathies.

APPENDIX A

THE MODIFIED PREPLATE TECHNIQUE

All stem/progenitor cells used throughout this study were isolated from mouse or human skeletal muscle using a modified preplate technique developed in the laboratory of Dr. Johnny Huard, reported in Qu-Peterson *et al*. [124], and revisited by Burhan *et al*. [142]. Biopsies were obtained from hind limbs of female neonatal C57BL/6J mice (Jackson Laboratory) or human skeletal muscle of 4 human donors obtained from the National Disease Research Interchange (NDRI). The muscle tissues were was minced and enzymatically digested in 0.2% collagenase-type XI (Sigma) for 1 h. After centrifugation, the cells were incubated in 0.3% dispase (2.4 units/ml of HBSS [Invitrogen]) for 30-45 min. They were then transferred to 0.1% trypsin-EDTA (Invirogen) for 30 min, centrifuged, re-suspended in proliferation medium (DMEM [Invitrogen] with 10% horse serum (HS [Invitrogen]), 10% fetal bovine serum (FBS [Invitrogen]), 1% penicillin-streptomycin [Invitrogen] and 0.5% chick embryo extract [Accurate Chemical and Scientific Corporation] and put into a dish coated with collagen Type I (Sigma). As seen in Figure A.1, some cells attach to first dish and those that do not are transferred to a new dish 2 hours later. The cells found in the first dish are known as preplate 1 or PP1 and contain mostly fibroblastic cells. PP2 to PP6 are obtained by transferring the supernatant to new flasks every 24

hours. PP2 to PP5 are known as “early preplate” (EP) cells. Cells in the PP6 cell population took an additional 24–72 h to attach to collagen-coated dishes after transfer from PP5 and were termed “late preplate” (LP) cells. The LP cell culture was then sub-plated in a 12-well tissue culture dish. Most of the LTP cells died during the first 1–2 wks of the cultivation period, with very few of the adherent surviving cells proliferating and forming colonies that are called “long-term proliferating” (LTP) cells. These cells were then called muscle-derived stem cells (MDSCs) based on their superior capacity for survival, self-renewal, and multilineage differentiation [124]. In case of human muscle-derived progenitor cells (hMDPCs), the fraction of the rapidly adhering cells (RACs) are considered as human counterparts to PP2–PP5 and slowly adhering cells (SACs) to PP6 in mouse MDSCs (mMDSCs).

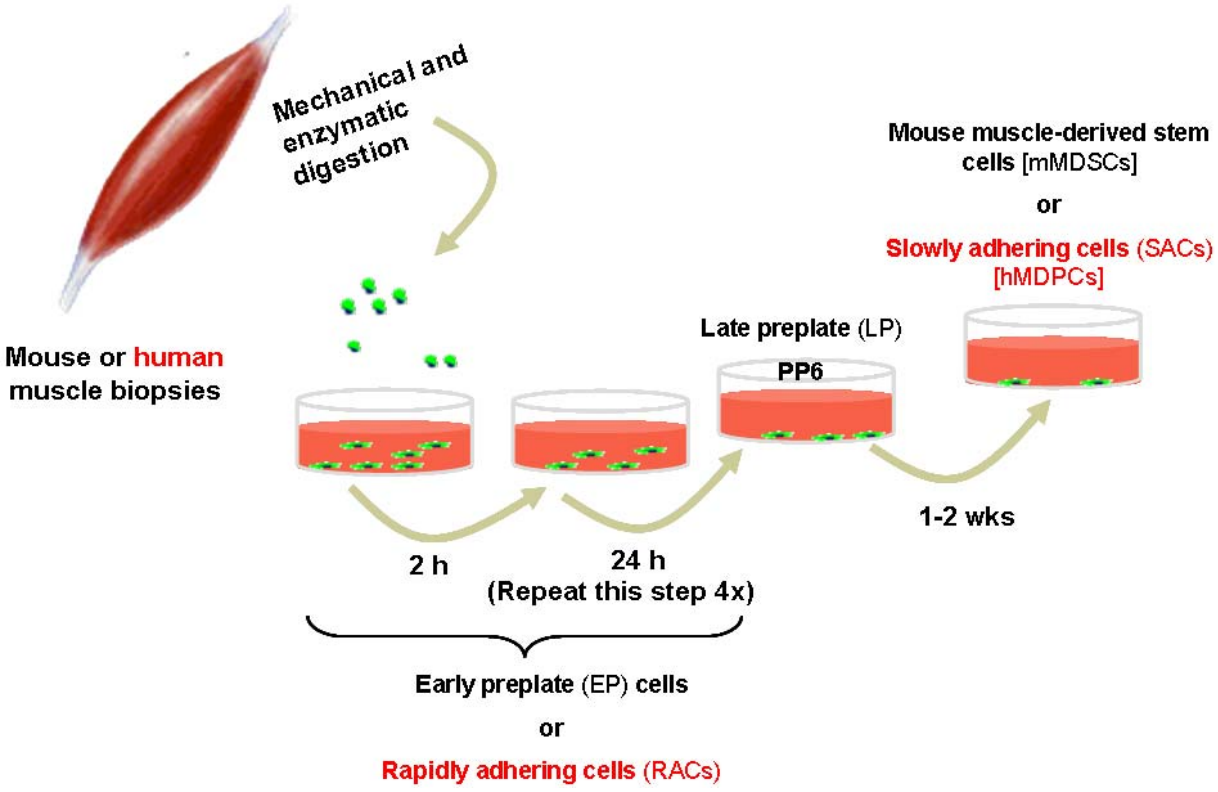

Figure A. 1: Schematic diagram of the preplate technique used to isolate muscle-derived cell populations

APPENDIX B

SUPPLEMENTAL DATA FOR REAL-TIME PCR ANALYSIS

All the primers used in study presented in Chapter 2 have been designed using the program found at http://**frodo**.**wi**.**mit**.edu/cgi-bin/primer3/ primer3_www.cgi and ordered from Integrated DNA Technologies. All the primers were designed specifically against human genes. The name, sequences, and aplicon position of the target gene primers are listed below in Table B.1.

Table B.1: Sequences for primers and probes used in RT-PCR

Primer name	Gene access number	Sequence (forward, reverse)	Aplicon position (start–end)
Pax6	NM_0061604	CCGGCAGAAGATTGTAGAGCT CCGTTGGACACGTTTTGATTG	510–630
Nestin	NM_006617	GACTTCCCTCAGCTTTCAGG GTCTTGGATCTTTGCTCC	1096–1179
MAP2	NM_001039538	CCAATGGATTCCCATACAGGG CTCTCCGTTGATCCCATTCTC	585–686
GFAP	NM_002055	CTGGAGGTTGAGAGGGACAAT CAGCCTCAGGTTGGTTTCATC	423–504
OSP	NM_005602	CTGGTGTTTTGCTCATTCTGC AGCCTGCATACAGGGAGTAG	558–675

APPENDIX C

WALKING TRACK ANALYSIS

Although the best method to evaluate the improvement of nerve function remains undiscovered, sciatic functional index (SFI) has shown to be a quantitative, non-invasive, and reliable method of tracking the regeneration capability, visible by the gait of the animal over time. SFI has been shown to have the highest correlation to nerve function [235], and is considered an assessment of overall nerve function because "walking requires complex motor-unit reinnervation coordination by cortically integrated sensory feedback" [236]. To calculate the SFI, walking tracks were first obtained using a 6 × 46 cm corridor (straight maze) lined with white paper (Benchkote; Cardinal) illuminated with a 50W lamp with an open end to a darkened compartment. The hind paws of the animals were pressed into the surface of a black waterproof inkpad. The animals were then walked multiple times to obtain measurable footprints over 14 weeks time period. The animals' feet were immediately washed in lukewarm water at the end of the tests. The collected paw prints were scanned with a Microtek 9800XL scanner (**Figure C.1**). The investigators were blinded to the animal treatment groups and during walking-track analysis.

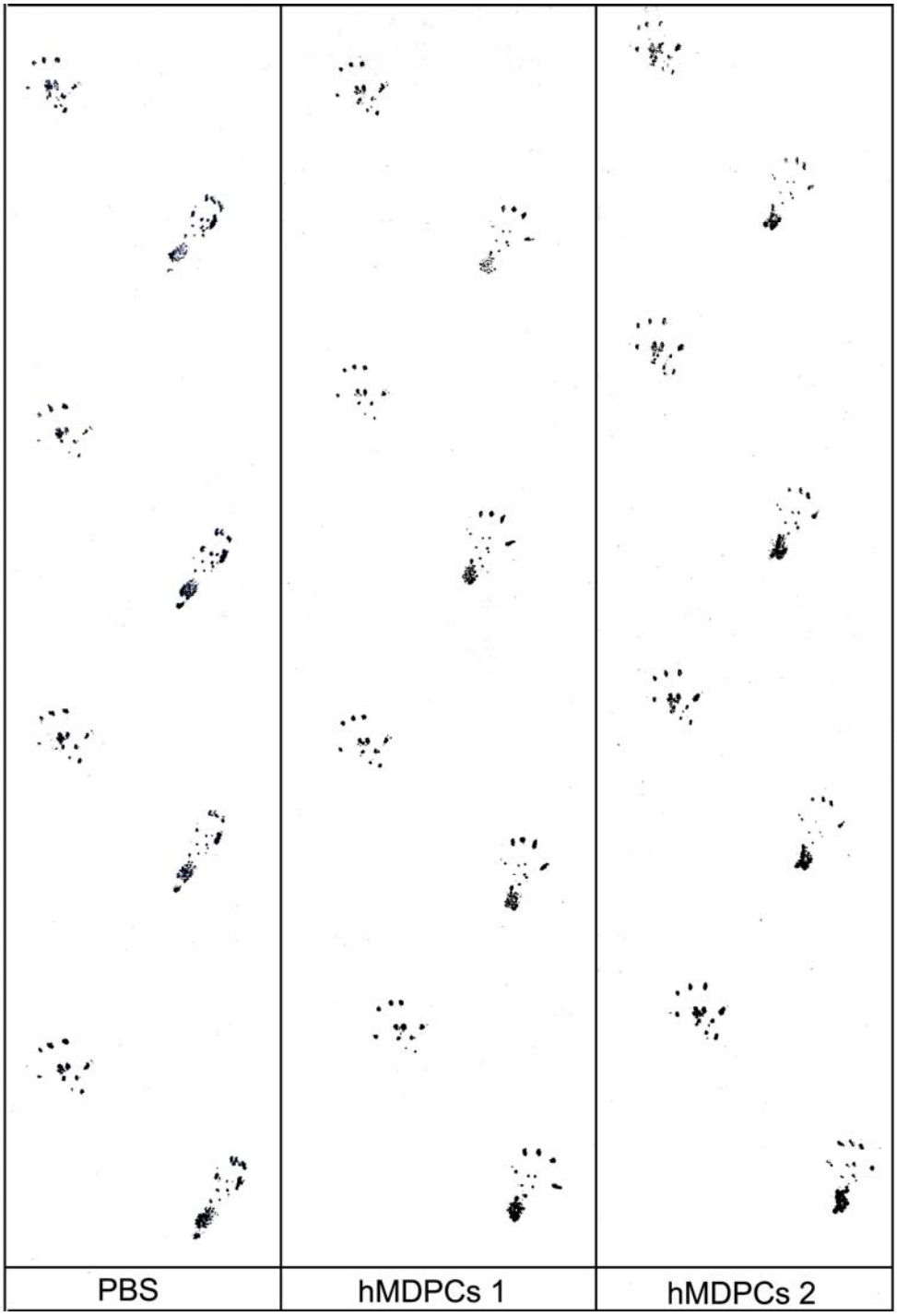

Figure C.1: Pattern of postoperative mouse paw prints 12 weeks following transaction of the right sciatic nerve

The narrowing of the toe spread and the elongation of the print length are greatly evident in PBS versus hMDPCs (isolate from patient 1 and 2) injected mice and when compared to left uninjured (normal) paw prints.

The tracks from FNr-MDSCs-treated, hMDPCs-treated, and PBS-treated groups were then evaluated for toe spread (TS, the distance between the first and the fifth toe) and print length (PL, the distance between the third toe and the heel) using the Northern Eclipse software system (**Figure C.2**). Factors were derived for each parameter by subtracting the values of post-operative contralateral non-operated footprint (normal) from the right operated footprint (experimental) values and dividing by the normal values as previously described [237].

Formula 1 $$TS \text{ factor} = \frac{ETS - NTS}{NTS} \qquad PL \text{ factor} = \frac{EPL - NPL}{NPL}$$

In the above equations, ETS is the experimental toe spread (distance between 1st and 5th toes), NTS is the normal toe spread, EPL is the experimental print length (distance from the heel to the third toe), and NPL is the normal print length. These factors were incorporated into the equation derived by Bain *et al.* [237] for rats, and modified and validated by Inserra *et al.* [180, 181] for mice, to calculate the sciatic functional index (SFI):

Formula 2 $$SFI = 118.9\left[\frac{ETS - NTS}{NTS}\right] - 51.2\left[\frac{EPL - NPL}{NPL}\right] - 7.5$$

A SFI of 0 reflects normal function, and a SFI of -100 indicates total loss of function.

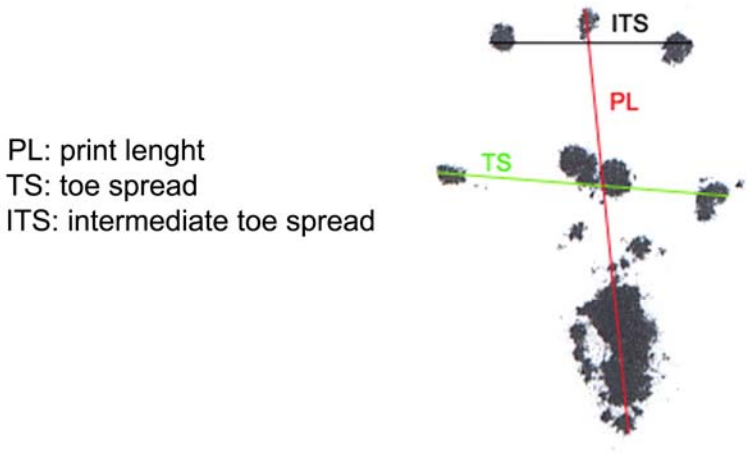

Figure C.2: Representation of normal mouse footprint

Of note, only TS and PL factors with their corresponding weighted coefficients, contributed to the mouse SFI formula (Formula 2). The values for the ITS factor were not statistically significant ($P = 0.30$) in our model, therefore, it was eliminated in our calculations. In fact, stepwise multiple linear regression by Inserr *et al.* [180] has also revealed very low correlation for ITS in their sciatic nerve transaction model, while changes in TS and PL were significant with high correlation ($R^2 = 0.88$).

BIBLIOGRAPHY

1. Ganong WF, Review of Medical Physiology. 17 ed. Physiology. 1995, Norwalk, Connecticut: APPLETON & LANGE.

2. Guyton AC and Hall JE, TextBook of Medical Physiology. 9 ed. 1996, Philadelphia, Pennsylvania: W.B. Saunders Company.

3. Goldstein B. Anatomy of the peripheral nervous system. *Phys Med Rehabil Clin N Am* 2001. **12**(2):207-36.

4. Stoll G, Griffin JW, Li CY, and Trapp BD. Wallerian degeneration in the peripheral nervous system: participation of both Schwann cells and macrophages in myelin degradation. *J Neurocytol* 1989. **18**(5):671-83.

5. Chaudhry V, Glass JD, and Griffin JW. Wallerian degeneration in peripheral nerve disease. *Neurol Clin* 1992. **10**(3):613-27.

6. Pellegrino RG and Spencer PS. Schwann cell mitosis in response to regenerating peripheral axons in vivo. *Brain Res* 1985. **341**(1):16-25.

7. Bunger O. Über die Degenerations- und Regenerationsvorgange am Nerven nach Verletzungen. *Beitr. Pathol. Anat* 1981. **10**:321-387.

8. Morris JH, Hudson AR, and Weddell G. A study of degeneration and regeneration in the divided rat sciatic nerve based on electron microscopy. I. The traumatic degeneration of myelin in the proximal stump of the divided nerve. *Z Zellforsch Mikrosk Anat* 1972. **124**(1):76-102.

9. Morris JH, Hudson AR, and Weddell G. A study of degeneration and regeneration in the divided rat sciatic nerve based on electron microscopy. 3. Changes in the axons of the proximal stump. *Z Zellforsch Mikrosk Anat* 1972. **124**(2):131-64.

10. Thomas PK. Clinical aspects of PNS regeneration. *Adv Neurol* 1988. **47**:9-29.

11. Carroll SL, Miller ML, Frohnert PW, Kim SS, and Corbett JA. Expression of neuregulins and their putative receptors, ErbB2 and ErbB3, is induced during Wallerian degeneration. *J Neurosci* 1997. **17**(5):1642-59.

12. Dubovy P, Schwann cells—development and regeneration of the nervous system. 1998, Brno:: Masaryk University Press.

13. Stoll G and Muller HW. Nerve injury, axonal degeneration and neural regeneration: basic insights. *Brain Pathol* 1999. **9**(2):313-25.

14. Lundborg G. A 25-year perspective of peripheral nerve surgery: evolving neuroscientific concepts and clinical significance. *J Hand Surg [Am]* 2000. **25**(3):391-414.

15. Hall S. Nerve repair: a neurobiologist's view. *J Hand Surg [Br]* 2001. **26**(2):129-36.

16. Herndon JH, Neuromas, in *Operative Hand Surgery*, D.P. Green and R.N. Hotchkiss, Editors. 1993: Edinburgh, Churchill, Livingstone. p. 1387-1400.

17. Brunelli G and Brunelli F. Strategy and timing of peripheral nerve surgery. *Neurosurg Rev* 1990. **13**(2):95-102.

18. Jacobson S and Guth L. An Electrophysiological Study of the Early Stages of Peripheral Nerve Regeneration. *Exp Neurol* 1965. **11**:48-60.

19. Milesi H, Ganglberger J, and Berger A. Erfahrungen mit der Mikrochirugie peripherer Nerven. *Chir. Plast.* 1967. **3**:47.

20. Lundborg G, Nerve Injury and Repair. 1988, New York: Longman Group UK.

21. Mackinnon SE and Dellon AL, Surgery of the Peripheral Nerve. 1988, New York: Thieme Med. Publ.

22. Albert E. Einige Operationen an Nerven. *Wein Med.* 1885. **26**:1285.

23. Gluck T. Ueber Neuroplastik auf dem Wege der Transplantation. *Arch. Klin. Chir.* 1880. **25**:606-616.

24. Payr E. Beiträge zur Technik der Blutgefass and Nervennaht nebst Mitteilungen über die Verwendung eines resorbibaren Metalles in der Chirurgie. *Arch. Klin. Chir.* 1900. **62**:67.

25. Kirk EG and Lewis D. Fascial tubulization in the repair of nerve defect. *JAMA* 1915. **65**:486-92.

26. Lundborg G, Dahlin LB, Danielsen N, and Nachemson AK. Tissue specificity in nerve regeneration. *Scand J Plast Reconstr Surg* 1986. **20**(3):279-83.

27. Mackinnon SE, Dellon AL, Lundborg G, Hudson AR, and Hunter DA. A study of neurotrophism in a primate model. *J Hand Surg [Am]* 1986. **11**(6):888-94.

28. Politis MJ, Ederle K, and Spencer PS. Tropism in nerve regeneration in vivo. Attraction of regenerating axons by diffusible factors derived from cells in distal nerve stumps of transected peripheral nerves. *Brain Res* 1982. **253**(1-2):1-12.

29. Williams LR. Rat aorta isografts possess nerve regeneration-promoting properties in silicone Y chambers. *Exp Neurol* 1987. **97**(3):555-63.

30. Seddon H. Nerve grafting. *Bone Joint Surg [Br]* 1963. **45**:447-461.

31. Seddon H, Surgery of the peripheral nerves. 1972, Edinburgh: Churchill Livingstone

32. Millesi H. Interfascicular nerve grafting. *Orthop Clin North Am* 1970. **2**:419-435.

33. Chiu DT, Special article: the development of autogenous venous nerve conduit as a clinical entitiy, in *P&S Medical Review*. 1995, Columbia-Presbyterian Med. Cent.: New York.

34. Evans GR. Peripheral nerve injury: a review and approach to tissue engineered constructs. *Anat. Rec.* 2001. **263**:396-404.

35. Lundborg G. Intraneural microcirculation. *Orthop Clin North Am* 1988. **19**(1):1-12.

36. Mackinnon SE and Dellon AL. Reinnervation of distal sensory nerve environments by regenerating sensory axons. *Neuroscience* 1992. **46**(3):595-603.

37. Schmidt CE, Shastri VR, Vacanti JP, and Langer R. Stimulation of neurite outgrowth using an electrically conducting polymer. *Proc Natl Acad Sci U S A* 1997. **94**(17):8948-53.

38. Battiston B, Tos P, Cushway TR, and Geuna S. Nerve repair by means of vein filled with muscle grafts I. Clinical results. *Microsurgery* 2000. **20**(1):32-6.

39. Meek MF, Varejao AS, and Geuna S. Muscle grafts and alternatives for nerve repair. *J Oral Maxillofac Surg* 2002. **60**(9):1095-6; author reply 1096.

40. Chiu DT, Janecka I, Krizek TJ, Wolff M, and Lovelace RE. Autogenous vein graft as a conduit for nerve regeneration. *Surgery* 1982. **91**(2):226-33.

41. Walton RL, Brown RE, Matory WE, Jr., Borah GL, and Dolph JL. Autogenous vein graft repair of digital nerve defects in the finger: a retrospective clinical study. *Plast Reconstr Surg* 1989. **84**(6):944-9; discussion 950-2.

42. Risitano G, Cavallaro G, Merrino T, Coppolino S, and Ruggeri F. Clinical results and thoughts on sensory nerve repair by autologous vein graft in emergency hand reconstruction. *Chir Main* 2002. **21**(3):194-7.

43. Karacaoglu E, Yuksel F, Peker F, and Guler MM. Nerve regeneration through an epineurial sheath: its functional aspect compared with nerve and vein grafts. *Microsurgery* 2001. **21**(5):196-201.

44. Brandt J, Dahlin LB, and Lundborg G. Autologous tendons used as grafts for bridging peripheral nerve defects. *J Hand Surg [Br]* 1999. **24**(3):284-90.

45. Geuna S, Tos P, Battiston B, Guglielmone R, and Giacobini-Robecchi MG. A stereological study of long-term regeneration of rat severed sciatic nerve repaired by means of muscle-vein-combined grafts. *Ital J Anat Embryol* 2000. **105**(2):65-73.

46. Pagnotta A, Tos P, Fornaro M, Gigante A, Geuna S, et al. Neurotrophins and their receptors in early axonal regeneration along muscle-vein-combined grafts. *Microsurgery* 2002. **22**(7):300-3.

47. Rodrigues Ade C and Silva MD. Inside-out versus standard artery graft to repair a sensory nerve in rats. *Microsurgery* 2001. **21**(3):102-7.

48. Zhang F, Blain B, Beck J, Zhang J, Chen Z, et al. Autogenous venous graft with one-stage prepared Schwann cells as a conduit for repair of long segmental nerve defects. *J Reconstr Microsurg* 2002. **18**(4):295-300.

49. Voytik-Harbin SL, Brightman AO, Kraine MR, Waisner B, and Badylak SF. Identification of extractable growth factors from small intestinal submucosa. *J Cell Biochem* 1997. **67**(4):478-91.

50. Badylak SF, Record R, Lindberg K, Hodde J, and Park K. Small intestinal submucosa: a substrate for in vitro cell growth. *J Biomater Sci Polym Ed* 1998. **9**(8):863-78.

51. Hadlock TA, Sundback CA, Hunter DA, Vacanti JP, and Cheney ML. A new artificial nerve graft containing rolled Schwann cell monolayers. *Microsurgery* 2001. **21**(3):96-101.

52. Davis GE, Blaker SN, Engvall E, Varon S, Manthorpe M, et al. Human amnion membrane serves as a substratum for growing axons in vitro and in vivo. *Science* 1987. **236**(4805):1106-9.

53. Ozcan G, Shenaq S, and Spira M. Vascularized nerve tube: an experimental alternative for vascularized nerve grafts over short gaps. *J Reconstr Microsurg* 1993. **9**(6):405-13.

54. Mohammad J, Shenaq J, Rabinovsky E, and Shenaq S. Modulation of peripheral nerve regeneration: a tissue-engineering approach. The role of amnion tube nerve conduit across a 1-centimeter nerve gap. *Plast Reconstr Surg* 2000. **105**(2):660-6.

55. Mohammad JA, Warnke PH, Pan YC, and Shenaq S. Increased axonal regeneration through a biodegradable amnionic tube nerve conduit: effect of local delivery and incorporation of nerve growth factor/hyaluronic acid media. *Ann Plast Surg* 2000. **44**(1):59-64.

56. Meek MF, Coert JH, and Nicolai JP. Amnion tube for nerve regeneration. *Plast Reconstr Surg* 2001. **107**(2):622-3.

57. Mligiliche N, Endo K, Okamoto K, Fujimoto E, and Ide C. Extracellular matrix of human amnion manufactured into tubes as conduits for peripheral nerve regeneration. *J Biomed Mater Res* 2002. **63**(5):591-600.

58. Gray KJ, Shenaq SM, Engelmann UH, Fishman IJ, Jeraj K, et al. Use of human amnion for microvascular interpositional grafts. *Plast Reconstr Surg* 1987. **79**(5):778-85.

59. Strauch B. Use of nerve conduits in peripheral nerve repair. *Hand Clin* 2000. **16**(1):123-30.

60. Dellon AL and Mackinnon SE. An alternative to the classical nerve graft for the management of the short nerve gap. *Plast Reconstr Surg* 1988. **82**(5):849-56.

61. Mackinnon SE and Dellon AL. Clinical nerve reconstruction with a bioabsorbable polyglycolic acid tube. *Plast Reconstr Surg* 1990. **85**(3):419-24.

62. Weber RA, Breidenbach WC, Brown RE, Jabaley ME, and Mass DP. A randomized prospective study of polyglycolic acid conduits for digital nerve reconstruction in humans. *Plast Reconstr Surg* 2000. **106**(5):1036-45; discussion 1046-8.

63. Hudson TW, Evans GR, and Schmidt CE. Engineering strategies for peripheral nerve repair. *Clin Plast Surg* 1999. **26**(4):617-28, ix.

64. Williams LR, Longo FM, Powell HC, Lundborg G, and Varon S. Spatial-temporal progress of peripheral nerve regeneration within a silicone chamber: parameters for a bioassay. *J Comp Neurol* 1983. **218**(4):460-70.

65. Dubovy P and Svizenska I. Denervated skeletal muscle stimulates migration of Schwann cells from the distal stump of transected peripheral nerve: an in vivo study. *Glia* 1994. **12**(2):99-107.

66. Torigoe K. The role of migratory Schwann cells in nerve regeneration as studied by the film model. *J Peripher Nerv Syst* 1997. **2**(3):227-31.

67. Fornaro M, Tos P, Geuna S, Giacobini-Robecchi MG, and Battiston B. Confocal imaging of Schwann-cell migration along muscle-vein combined grafts used to bridge nerve defects in the rat. *Microsurgery* 2001. **21**(4):153-5.

68. Chernousov MA and Carey DJ. Schwann cell extracellular matrix molecules and their receptors. *Histol Histopathol* 2000. **15**(2):593-601.

69. Thanos PK, Okajima S, and Terzis JK. Ultrastructure and cellular biology of nerve regeneration. *J Reconstr Microsurg* 1998. **14**(6):423-36.

70. Son YJ, Trachtenberg JT, and Thompson WJ. Schwann cells induce and guide sprouting and reinnervation of neuromuscular junctions. *Trends Neurosci* 1996. **19**(7):280-5.

71. Dezawa M. Central and peripheral nerve regeneration by transplantation of Schwann cells and transdifferentiated bone marrow stromal cells. *Anat Sci Int* 2002. **77**(1):12-25.

72. Bunge RP. Expanding roles for the Schwann cell: ensheathment, myelination, trophism and regeneration. *Curr Opin Neurobiol* 1993. **3**(5):805-9.

73. Feneley MR, Fawcett JW, and Keynes RJ. The role of Schwann cells in the regeneration of peripheral nerve axons through muscle basal lamina grafts. *Exp Neurol* 1991. **114**(3):275-85.

74. Guenard V, Kleitman N, Morrissey TK, Bunge RP, and Aebischer P. Syngeneic Schwann cells derived from adult nerves seeded in semipermeable guidance channels enhance peripheral nerve regeneration. *J Neurosci* 1992. **12**(9):3310-20.

75. Li ST, Archibald SJ, Krarup C, and Madison RD. Peripheral nerve repair with collagen conduits. *Clin Mater* 1992. **9**(3-4):195-200.

76. Brown RE, Erdmann D, Lyons SF, and Suchy H. The use of cultured Schwann cells in nerve repair in a rabbit hind-limb model. *J Reconstr Microsurg* 1996. **12**(3):149-52.

77. Heath CA and Rutkowski GE. The development of bioartificial nerve grafts for peripheral-nerve regeneration. *Trends Biotechnol* 1998. **16**(4):163-8.

78. Gordon T, Sulaiman O, and Boyd JG. Experimental strategies to promote functional recovery after peripheral nerve injuries. *J Peripher Nerv Syst* 2003. **8**(4):236-50.

79. Ferrari G, Cusella-De Angelis G, Coletta M, Paolucci E, Stornaiuolo A, et al. Muscle regeneration by bone marrow-derived myogenic progenitors. *Science* 1998. **279**(5356):1528-30.

80. Gussoni E, Soneoka Y, Strickland CD, Buzney EA, Khan MK, et al. Dystrophin expression in the mdx mouse restored by stem cell transplantation. *Nature* 1999. **401**(6751):390-4.

81. Clarke DL, Johansson CB, Wilbertz J, Veress B, Nilsson E, et al. Generalized potential of adult neural stem cells. *Science* 2000. **288**(5471):1660-3.

82. Galli R, Borello U, Gritti A, Minasi MG, Bjornson C, et al. Skeletal myogenic potential of human and mouse neural stem cells. *Nat Neurosci* 2000. **3**(10):986-91.

83. Brazelton TR, Rossi FM, Keshet GI, and Blau HM. From marrow to brain: expression of neuronal phenotypes in adult mice. *Science* 2000. **290**(5497):1775-9.

84. Bjornson CR, Rietze RL, Reynolds BA, Magli MC, and Vescovi AL. Turning brain into blood: a hematopoietic fate adopted by adult neural stem cells in vivo. *Science* 1999. **283**(5401):534-7.

85. Petersen BE, Bowen WC, Patrene KD, Mars WM, Sullivan AK, et al. Bone marrow as a potential source of hepatic oval cells. *Science* 1999. **284**(5417):1168-70.

86. Mezey E and Chandross KJ. Bone marrow: a possible alternative source of cells in the adult nervous system. *Eur J Pharmacol* 2000. **405**(1-3):297-302.

87. Sanchez-Ramos JR, Song S, Kamath SG, Zigova T, Willing A, et al. Expression of neural markers in human umbilical cord blood. *Exp Neurol* 2001. **171**(1):109-15.

88. Woodbury D, Schwarz EJ, Prockop DJ, and Black IB. Adult rat and human bone marrow stromal cells differentiate into neurons. *J Neurosci Res* 2000. **61**(4):364-70.

89. Weimann JM, Charlton CA, Brazelton TR, Hackman RC, and Blau HM. Contribution of transplanted bone marrow cells to Purkinje neurons in human adult brains. *Proc Natl Acad Sci U S A* 2003. **100**(4):2088-93.

90. Terada N, Hamazaki T, Oka M, Hoki M, Mastalerz DM, et al. Bone marrow cells adopt the phenotype of other cells by spontaneous cell fusion. *Nature* 2002. **416**(6880):542-5.

91. Ying QL, Nichols J, Evans EP, and Smith AG. Changing potency by spontaneous fusion. *Nature* 2002. **416**(6880):545-8.

92. Zuk PA, Zhu M, Mizuno H, Huang J, Futrell JW, et al. Multilineage cells from human adipose tissue: implications for cell-based therapies. *Tissue Eng* 2001. **7**(2):211-28.

93. Zuk PA, Zhu M, Ashjian P, De Ugarte DA, Huang JI, et al. Human adipose tissue is a source of multipotent stem cells. *Mol Biol Cell* 2002. **13**(12):4279-95.

94. Halvorsen YC, Wilkison WO, and Gimble JM. Adipose-derived stromal cells--their utility and potential in bone formation. *Int J Obes Relat Metab Disord* 2000. **24 Suppl 4**:S41-4.

95. Erickson GR, Gimble JM, Franklin DM, Rice HE, Awad H, et al. Chondrogenic potential of adipose tissue-derived stromal cells in vitro and in vivo. *Biochem Biophys Res Commun* 2002. **290**(2):763-9.

96. Safford KM, Hicok KC, Safford SD, Halvorsen YD, Wilkison WO, et al. Neurogenic differentiation of murine and human adipose-derived stromal cells. *Biochem Biophys Res Commun* 2002. **294**(2):371-9.

97. Ashjian PH, Elbarbary AS, Edmonds B, DeUgarte D, Zhu M, et al. In vitro differentiation of human processed lipoaspirate cells into early neural progenitors. *Plast Reconstr Surg* 2003. **111**(6):1922-31.

98. Kang SK, Lee DH, Bae YC, Kim HK, Baik SY, et al. Improvement of neurological deficits by intracerebral transplantation of human adipose tissue-derived stromal cells after cerebral ischemia in rats. *Exp Neurol* 2003. **183**(2):355-66.

99. Mizuno H, Zuk PA, Zhu M, Lorenz HP, Benhaim P, et al. Myogenic differentiation by human processed lipoaspirate cells. *Plast Reconstr Surg* 2002. **109**(1):199-209; discussion 210-1.

100. Fujimura J, Ogawa R, Mizuno H, Fukunaga Y, and Suzuki H. Neural differentiation of adipose-derived stem cells isolated from GFP transgenic mice. *Biochem Biophys Res Commun* 2005. **333**(1):116-21.

101. Kokai LE, Rubin JP, and Marra KG. The potential of adipose-derived adult stem cells as a source of neuronal progenitor cells. *Plast Reconstr Surg* 2005. **116**(5):1453-60.

102. Safford KM and Rice HE. Stem cell therapy for neurologic disorders: therapeutic potential of adipose-derived stem cells. *Curr Drug Targets* 2005. **6**(1):57-62.

103. Toma JG, Akhavan M, Fernandes KJ, Barnabe-Heider F, Sadikot A, et al. Isolation of multipotent adult stem cells from the dermis of mammalian skin. *Nat Cell Biol* 2001. **3**(9):778-84.

104. Sieber-Blum M and Grim M. The adult hair follicle: cradle for pluripotent neural crest stem cells. *Birth Defects Res C Embryo Today* 2004. **72**(2):162-72.

105. Amoh Y, Li L, Katsuoka K, Penman S, and Hoffman RM. Multipotent nestin-positive, keratin-negative hair-follicle bulge stem cells can form neurons. *Proc Natl Acad Sci U S A* 2005. **102**(15):5530-4.

106. Schofield R. The relationship between the spleen colony-forming cell and the haemopoietic stem cell. *Blood Cells* 1978. **4**(1-2):7-25.

107. Gritti A, Vescovi AL, and Galli R. Adult neural stem cells: plasticity and developmental potential. *J Physiol Paris* 2002. **96**(1-2):81-90.

108. Scadden DT. The stem-cell niche as an entity of action. *Nature* 2006. **441**(7097):1075-9.

109. Kilpatrick TJ, Talman PS, and Bartlett PF. The differentiation and survival of murine neurons in vitro is promoted by soluble factors produced by an astrocytic cell line. *J Neurosci Res* 1993. **35**(2):147-61.

110. Ghosh A and Greenberg ME. Distinct roles for bFGF and NT-3 in the regulation of cortical neurogenesis. *Neuron* 1995. **15**(1):89-103.

111. Ma W, Maric D, Li BS, Hu Q, Andreadis JD, et al. Acetylcholine stimulates cortical precursor cell proliferation in vitro via muscarinic receptor activation and MAP kinase phosphorylation. *Eur J Neurosci* 2000. **12**(4):1227-40.

112. Burrows RC, Wancio D, Levitt P, and Lillien L. Response diversity and the timing of progenitor cell maturation are regulated by developmental changes in EGFR expression in the cortex. *Neuron* 1997. **19**(2):251-67.

113. Arsenijevic Y and Weiss S. Insulin-like growth factor-I is a differentiation factor for postmitotic CNS stem cell-derived neuronal precursors: distinct actions from those of brain-derived neurotrophic factor. *J Neurosci* 1998. **18**(6):2118-28.

114. Edlund T and Jessell TM. Progression from extrinsic to intrinsic signaling in cell fate specification: a view from the nervous system. *Cell* 1999. **96**(2):211-24.

115. Reimers D, Lopez-Toledano MA, Mason I, Cuevas P, Redondo C, et al. Developmental expression of fibroblast growth factor (FGF) receptors in neural stem cell progeny. Modulation of neuronal and glial lineages by basic FGF treatment. *Neurol Res* 2001. **23**(6):612-21.

116. Vescovi AL, Galli R, and Gritti A. The neural stem cells and their transdifferentiation capacity. *Biomed Pharmacother* 2001. **55**(4):201-5.

117. Madison RD, Archibald SJ, and Karup C, Peripheral nerve injury. In wound healing: biochemical and clinical aspects, I.K. Cohn, F. Diedelman, and W.J. Lindbald, Editors. 1992, Sauders, W.B.: Philadelphia, PA. p. 450-487.

118. Milesi H. Progress in peripheral nerve reconstruction. *World J Surg* 1990. **14**:733-747.

119. Fu SY and Gordon T. The cellular and molecular basis of peripheral nerve regeneration. *Mol Neurobiol* 1997. **14**(1-2):67-116.

120. Langer R and Vacanti JP. Tissue engineering. *Science* 1993. **260**(5110):920-6.

121. Jackson KA, Mi T, and Goodell MA. Hematopoietic potential of stem cells isolated from murine skeletal muscle. *Proc Natl Acad Sci U S A* 1999. **96**(25):14482-6.

122. Lee JY, Qu-Petersen Z, Cao B, Kimura S, Jankowski R, et al. Clonal isolation of muscle-derived cells capable of enhancing muscle regeneration and bone healing. *J Cell Biol* 2000. **150**(5):1085-100.

123. Seale P and Rudnicki MA. A new look at the origin, function, and "stem-cell" status of muscle satellite cells. *Dev Biol* 2000. **218**(2):115-24.

124. Qu-Petersen Z, Deasy B, Jankowski R, Ikezawa M, Cummins J, et al. Identification of a novel population of muscle stem cells in mice: potential for muscle regeneration. *J Cell Biol* 2002. **157**(5):851-64.

125. Romero-Ramos M, Vourc'h P, Young HE, Lucas PA, Wu Y, et al. Neuronal differentiation of stem cells isolated from adult muscle. *J Neurosci Res* 2002. **69**(6):894-907.

126. Torrente Y, Belicchi M, Pisati F, Pagano SF, Fortunato F, et al. Alternative sources of neurons and glia from somatic stem cells. *Cell Transplant* 2002. **11**(1):25-34.

127. Cao B, Zheng B, Jankowski RJ, Kimura S, Ikezawa M, et al. Muscle stem cells differentiate into haematopoietic lineages but retain myogenic potential. *Nat Cell Biol* 2003. **5**(7):640-6.

128. Deasy BM, Gharaibeh BM, Pollett JB, Jones MM, Lucas MA, et al. Long-term self-renewal of postnatal muscle-derived stem cells. *Mol Biol Cell* 2005. **16**(7):3323-33.

129. Oshima H, Payne TR, Urish KL, Sakai T, Ling Y, et al. Differential myocardial infarct repair with muscle stem cells compared to myoblasts. *Mol Ther* 2005. **12**(6):1130-41.

130. Urish KL, Vella JB, Okada M, Deasy BM, Tobita K, et al. Antioxidant Levels Represent a Major Determinant in the Regenerative Capacity of Muscle Stem Cells. *Mol Biol Cell* 2008.

131. Payne TR, Oshima H, Sakai T, Ling Y, Gharaibeh B, et al. Regeneration of dystrophin-expressing myocytes in the mdx heart by skeletal muscle stem cells. *Gene Ther* 2005. **12**(16):1264-74.

132. Kuroda R, Usas A, Kubo S, Corsi K, Peng H, et al. Cartilage repair using bone morphogenetic protein 4 and muscle-derived stem cells. *Arthritis Rheum* 2006. **54**(2):433-42.

133. Lavasani M, Lu A, Peng H, Cummins J, and Huard J. Nerve growth factor improves the muscle regeneration capacity of muscle stem cells in dystrophic muscle. *Hum Gene Ther* 2006. **17**(2):180-92.

134. Shen Q, Goderie SK, Jin L, Karanth N, Sun Y, et al. Endothelial cells stimulate self-renewal and expand neurogenesis of neural stem cells. *Science* 2004. **304**(5675):1338-40.

135. Zheng B, Cao B, Crisan M, Sun B, Li G, et al. Prospective identification of myogenic endothelial cells in human skeletal muscle. *Nat Biotechnol* 2007. **25**(9):1025-34.

136. Crisan M, Deasy B, Gavina M, Zheng B, Huard J, et al. Purification and long-term culture of multipotent progenitor cells affiliated with the walls of human blood vessels: myoendothelial cells and pericytes. *Methods Cell Biol* 2008. **86**:295-309.

137. Powell K. Stem-cell niches: it's the ecology, stupid! *Nature* 2005. **435**(7040):268-70.

138. Rizo A, Vellenga E, de Haan G, and Schuringa JJ. Signaling pathways in self-renewing hematopoietic and leukemic stem cells: do all stem cells need a niche? *Hum Mol Genet* 2006. **15 Spec No 2**:R210-9.

139. Wolf NS and Trentin JJ. Hemopoietic colony studies. V. Effect of hemopoietic organ stroma on differentiation of pluripotent stem cells. *J Exp Med* 1968. **127**(1):205-14.

140. Cao Q, Benton RL, and Whittemore SR. Stem cell repair of central nervous system injury. *J Neurosci Res* 2002. **68**(5):501-10.

141. Doetsch F. A niche for adult neural stem cells. *Curr Opin Genet Dev* 2003. **13**(5):543-50.

142. Gharaibeh B, Lu A, Tebbets J, Zheng B, Feduska J, et al. Isolation of a slowly adhering cell fraction containing stem cells from murine skeletal muscle by the preplate technique. *Nat Protoc* 2008. **3**(9):1501-9.

143. Qian X, Shen Q, Goderie SK, He W, Capela A, et al. Timing of CNS cell generation: a programmed sequence of neuron and glial cell production from isolated murine cortical stem cells. *Neuron* 2000. **28**(1):69-80.

144. Gage FH, Coates PW, Palmer TD, Kuhn HG, Fisher LJ, et al. Survival and differentiation of adult neuronal progenitor cells transplanted to the adult brain. *Proc Natl Acad Sci U S A* 1995. **92**(25):11879-83.

145. Rosser AE, Tyers P, ter Borg M, Dunnett SB, and Svendsen CN. Co-expression of MAP-2 and GFAP in cells developing from rat EGF responsive precursor cells. *Brain Res Dev Brain Res* 1997. **98**(2):291-5.

146. Colucci-D'Amato GL, Tino A, Pernas-Alonso R, ffrench-Mullen JM, and di Porzio U. Neuronal and glial properties coexist in a novel mouse CNS immortalized cell line. *Exp Cell Res* 1999. **252**(2):383-91.

147. Feldman DH, Thinschmidt JS, Peel AL, Papke RL, and Reier PJ. Differentiation of ionic currents in CNS progenitor cells: dependence upon substrate attachment and epidermal growth factor. *Exp Neurol* 1996. **140**(2):206-17.

148. Meek MF, Robinson PH, Stokroos I, Blaauw EH, Kors G, et al. Electronmicroscopical evaluation of short-term nerve regeneration through a thin-walled biodegradable poly(DLLA-epsilon-CL) nerve guide filled with modified denatured muscle tissue. *Biomaterials* 2001. **22**(10):1177-85.

149. Sterne GD, Brown RA, Green CJ, and Terenghi G. Neurotrophin-3 delivered locally via fibronectin mats enhances peripheral nerve regeneration. *Eur J Neurosci* 1997. **9**(7):1388-96.

150. Weiss SW and Goldblum JR, ENZINGER AND WEISS'S SOFT TISSUE TUMORS. 4th ed. 2001, St. Louis: Mosby.

151. Gollin SM. Mechanisms leading to chromosomal instability. *Semin Cancer Biol* 2005. **15**(1):33-42.

152. Maiese K, Boniece I, DeMeo D, and Wagner JA. Peptide growth factors protect against ischemia in culture by preventing nitric oxide toxicity. *J Neurosci* 1993. **13**(7):3034-40.

153. Maiese K, Boniece IR, Skurat K, and Wagner JA. Protein kinases modulate the sensitivity of hippocampal neurons to nitric oxide toxicity and anoxia. *J Neurosci Res* 1993. **36**(1):77-87.

154. Nozaki K, Finklestein SP, and Beal MF. Basic fibroblast growth factor protects against hypoxia-ischemia and NMDA neurotoxicity in neonatal rats. *J Cereb Blood Flow Metab* 1993. **13**(2):221-8.

155. Nozaki K, Finklestein SP, and Beal MF. Delayed administration of basic fibroblast growth factor protects against N-methyl-D-aspartate neurotoxicity in neonatal rats. *Eur J Pharmacol* 1993. **232**(2-3):295-7.

156. Masson P. Recklinghausen's neurofibromatosis, sensory neuromas and motor neuromas. Libman Anniversary. Vol. 2. 1932, International Press. 793–802.

157. Stasik CJ and Tawfik O. Malignant peripheral nerve sheath tumor with rhabdomyosarcomatous differentiation (malignant triton tumor). *Arch Pathol Lab Med* 2006. **130**(12):1878-81.

158. Brooks JS, Freeman M, and Enterline HT. Malignant "Triton" tumors. Natural history and immunohistochemistry of nine new cases with literature review. *Cancer* 1985. **55**(11):2543-9.

159. Woodruff JM, Selig AM, Crowley K, and Allen PW. Schwannoma (neurilemoma) with malignant transformation. A rare, distinctive peripheral nerve tumor. *Am J Surg Pathol* 1994. **18**(9):882-95.

160. Woodruff JM, Chernik NL, Smith MC, Millett WB, and Foote FW, Jr. Peripheral nerve tumors with rhabdomyosarcomatous differentiation (malignant "Triton" tumors). *Cancer* 1973. **32**(2):426-39.

161. Woodruff JM and Perino G. Non-germ-cell or teratomatous malignant tumors showing additional rhabdomyoblastic differentiation, with emphasis on the malignant Triton tumor. *Semin Diagn Pathol* 1994. **11**(1):69-81.

162. Locatelli P. Formation de membres surnumeraries. *C R Assoc Anat* 1925. **20**:279-282.

163. Joseph NM, Mosher JT, Buchstaller J, Snider P, McKeever PE, et al. The loss of Nf1 transiently promotes self-renewal but not tumorigenesis by neural crest stem cells. *Cancer Cell* 2008. **13**(2):129-40.

164. Pollett JB, Corsi KA, Weiss KR, Cooper GM, Barry DA, et al. Malignant Transformation of Multipotent Muscle-Derived Cells by Concurrent Differentiation Signals. *Stem Cells* 2007.

165. Kucia M and Ratajczak MZ. Stem cells as a two edged sword--from regeneration to tumor formation. *J Physiol Pharmacol* 2006. **57 Suppl 7**:5-16.

166. Prindull G and Zipori D. Environmental guidance of normal and tumor cell plasticity: epithelial mesenchymal transitions as a paradigm. *Blood* 2004. **103**(8):2892-9.

167. Rubio D, Garcia-Castro J, Martin MC, de la Fuente R, Cigudosa JC, et al. Spontaneous human adult stem cell transformation. *Cancer Res* 2005. **65**(8):3035-9.

168. Serakinci N, Guldberg P, Burns JS, Abdallah B, Schrodder H, et al. Adult human mesenchymal stem cell as a target for neoplastic transformation. *Oncogene* 2004. **23**(29):5095-8.

169. Greaves M. Molecular genetics, natural history and the demise of childhood leukaemia. *Eur J Cancer* 1999. **35**(14):1941-53.

170. Houghton J, Stoicov C, Nomura S, Rogers AB, Carlson J, et al. Gastric cancer originating from bone marrow-derived cells. *Science* 2004. **306**(5701):1568-71.

171. Prowse KR and Greider CW. Developmental and tissue-specific regulation of mouse telomerase and telomere length. *Proc Natl Acad Sci U S A* 1995. **92**(11):4818-22.

172. Stark A, Aparisi T, and Ericsson JL. Human osteogenic sarcoma: fine structure of the osteoblastic type. *Ultrastruct Pathol* 1983. **4**(4):311-29.

173. Tolar J, Nauta AJ, Osborn MJ, Panoskaltsis Mortari A, McElmurry RT, et al. Sarcoma derived from cultured mesenchymal stem cells. *Stem Cells* 2007. **25**(2):371-9.

174. Taussig DC, Pearce DJ, Simpson C, Rohatiner AZ, Lister TA, et al. Hematopoietic stem cells express multiple myeloid markers: implications for the origin and targeted therapy of acute myeloid leukemia. *Blood* 2005. **106**(13):4086-92.

175. Roy NS, Cleren C, Singh SK, Yang L, Beal MF, et al. Functional engraftment of human ES cell-derived dopaminergic neurons enriched by coculture with telomerase-immortalized midbrain astrocytes. *Nat Med* 2006. **12**(11):1259-68.

176. Schlosshauer B, Dreesmann L, Schaller HE, and Sinis N. Synthetic nerve guide implants in humans: a comprehensive survey. *Neurosurgery* 2006. **59**(4):740-7; discussion 747-8.

177. J IJ-P, Jansen K, Gramsbergen A, and Meek MF. Transection of peripheral nerves, bridging strategies and effect evaluation. *Biomaterials* 2004. **25**(9):1583-92.

178. van Deutekom JC, Floyd SS, Booth DK, Oligino T, Krisky D, et al. Implications of maturation for viral gene delivery to skeletal muscle. *Neuromuscul Disord* 1998. **8**(3-4):135-48.

179. Sanes JR, Rubenstein JL, and Nicolas JF. Use of a recombinant retrovirus to study post-implantation cell lineage in mouse embryos. *Embo J* 1986. **5**(12):3133-42.

180. Inserra MM, Bloch DA, and Terris DJ. Functional indices for sciatic, peroneal, and posterior tibial nerve lesions in the mouse. *Microsurgery* 1998. **18**(2):119-24.

181. McMurray R, Islamov R, and Murashov AK. Raloxifene analog LY117018 enhances the regeneration of sciatic nerve in ovariectomized female mice. *Brain Res* 2003. **980**(1):140-5.

182. Reynolds BA and Weiss S. Generation of neurons and astrocytes from isolated cells of the adult mammalian central nervous system. *Science* 1992. **255**(5052):1707-10.

183. Richards LJ, Kilpatrick TJ, and Bartlett PF. De novo generation of neuronal cells from the adult mouse brain. *Proc Natl Acad Sci U S A* 1992. **89**(18):8591-5.

184. Young FE. A time for restraint. *Science* 2000. **287**(5457):1424.

185. Lenoir N. Europe confronts the embryonic stem cell research challenge. *Science* 2000. **287**(5457):1425-7.

186. Huard J, Bouchard JP, Roy R, Malouin F, Dansereau G, et al. Human myoblast transplantation: preliminary results of 4 cases. *Muscle Nerve* 1992. **15**(5):550-60.

187. Fan Y, Beilharz MW, and Grounds MD. A potential alternative strategy for myoblast transfer therapy: the use of sliced muscle grafts. *Cell Transplant* 1996. **5**(3):421-9.

188. Bischoff R. Proliferation of muscle satellite cells on intact myofibers in culture. *Dev Biol* 1986. **115**(1):129-39.

189. Young HE, Steele TA, Bray RA, Detmer K, Blake LW, et al. Human pluripotent and progenitor cells display cell surface cluster differentiation markers CD10, CD13, CD56, and MHC class-I. *Proc Soc Exp Biol Med* 1999. **221**(1):63-71.

190. Young HE, Steele TA, Bray RA, Hudson J, Floyd JA, et al. Human reserve pluripotent mesenchymal stem cells are present in the connective tissues of skeletal muscle and dermis derived from fetal, adult, and geriatric donors. *Anat Rec* 2001. **264**(1):51-62.

191. Vourc'h P, Lacar B, Mignon L, Lucas PA, Young HE, et al. Effect of neurturin on multipotent cells isolated from the adult skeletal muscle. *Biochem Biophys Res Commun* 2005. **332**(1):215-23.

192. Carr LK, Steele D, Steele S, Wagner D, Pruchnic R, et al. 1-year follow-up of autologous muscle-derived stem cell injection pilot study to treat stress urinary incontinence. *Int Urogynecol J Pelvic Floor Dysfunct* 2008. **19**(6):881-3.

193. Dib N, Michler RE, Pagani FD, Wright S, Kereiakes DJ, et al. Safety and feasibility of autologous myoblast transplantation in patients with ischemic cardiomyopathy: four-year follow-up. *Circulation* 2005. **112**(12):1748-55.

194. Herreros J, Prosper F, Perez A, Gavira JJ, Garcia-Velloso MJ, et al. Autologous intramyocardial injection of cultured skeletal muscle-derived stem cells in patients with non-acute myocardial infarction. *Eur Heart J* 2003. **24**(22):2012-20.

195. Ince H, Petzsch M, Rehders TC, Chatterjee T, and Nienaber CA. Transcatheter transplantation of autologous skeletal myoblasts in postinfarction patients with severe left ventricular dysfunction. *J Endovasc Ther* 2004. **11**(6):695-704.

196. Menasche P. Cellular transplantation: hurdles remaining before widespread clinical use. *Curr Opin Cardiol* 2004. **19**(2):154-61.

197. Menasche P. Myoblast transfer in heart failure. *Surg Clin North Am* 2004. **84**(1):125-39.

198. Menasche P. Skeletal myoblast transplantation for cardiac repair. *Expert Rev Cardiovasc Ther* 2004. **2**(1):21-8.

199. Pagani FD, DerSimonian H, Zawadzka A, Wetzel K, Edge AS, et al. Autologous skeletal myoblasts transplanted to ischemia-damaged myocardium in humans. Histological analysis of cell survival and differentiation. *J Am Coll Cardiol* 2003. **41**(5):879-88.

200. Smits PC, van Geuns RJ, Poldermans D, Bountioukos M, Onderwater EE, et al. Catheter-based intramyocardial injection of autologous skeletal myoblasts as a primary treatment of ischemic heart failure: clinical experience with six-month follow-up. *J Am Coll Cardiol* 2003. **42**(12):2063-9.

201. Alessandri G, Pagano S, Bez A, Benetti A, Pozzi S, et al. Isolation and culture of human muscle-derived stem cells able to differentiate into myogenic and neurogenic cell lineages. *Lancet* 2004. **364**(9448):1872-83.

202. Schultz SS and Lucas PA. Human stem cells isolated from adult skeletal muscle differentiate into neural phenotypes. *J Neurosci Methods* 2006. **152**(1-2):144-55.

203. Reubinoff BE, Itsykson P, Turetsky T, Pera MF, Reinhartz E, et al. Neural progenitors from human embryonic stem cells. *Nat Biotechnol* 2001. **19**(12):1134-40.

204. Suzuki K, Murtuza B, Smolenski RT, Sammut IA, Suzuki N, et al. Cell transplantation for the treatment of acute myocardial infarction using vascular endothelial growth factor-expressing skeletal myoblasts. *Circulation* 2001. **104**(12 Suppl 1):I207-12.

205. Xu J, Sotereanos DG, Moller AR, Jacobsohn J, Tomaino MM, et al. Nerve wrapping with vein grafts in a rat model: a safe technique for the treatment of recurrent chronic compressive neuropathy. *J Reconstr Microsurg* 1998. **14**(5):323-8; discussion 329-30.

206. Chiu DT and Strauch B. A prospective clinical evaluation of autogenous vein grafts used as a nerve conduit for distal sensory nerve defects of 3 cm or less. *Plast Reconstr Surg* 1990. **86**(5):928-34.

207. Sotereanos DG, Giannakopoulos PN, Mitsionis GI, Xu J, and Herndon JH. Vein-graft wrapping for the treatment of recurrent compression of the median nerve. *Microsurgery* 1995. **16**(11):752-6.

208. Xu J, Varitimidis SE, Fisher KJ, Tomaino MM, and Sotereanos DG. The effect of wrapping scarred nerves with autogenous vein graft to treat recurrent chronic nerve compression. *J Hand Surg [Am]* 2000. **25**(1):93-103.

209. Schon LC, Anderson CD, Easley ME, Lam PW, Trnka HJ, et al. Surgical treatment of chronic lower extremity neuropathic pain. *Clin Orthop Relat Res* 2001(389):156-64.

210. Varitimidis SE, Vardakas DG, Goebel F, and Sotereanos DG. Treatment of recurrent compressive neuropathy of peripheral nerves in the upper extremity with an autologous vein insulator. *J Hand Surg [Am]* 2001. **26**(2):296-302.

211. Easley ME and Schon LC. Peripheral nerve vein wrapping for intractable lower extremity pain. *Foot Ankle Int* 2000. **21**(6):492-500.

212. Campbell JT, Schon LC, and Burkhardt LD. Histopathologic findings in autogenous saphenous vein graft wrapping for recurrent tarsal tunnel syndrome: a case report. *Foot Ankle Int* 1998. **19**(11):766-9.

213. Masear VR and Colgin S. The treatment of epineural scarring with allograft vein wrapping. *Hand Clin* 1996. **12**(4):773-9.

214. Gould JS, Treatment of the painful injured nerve in-continuity in *Operative nerve repair and reconstruction*. 1991, JB Lippincott: Philadelphia. p. 1541-1550.

215. Chou KH, Papadimitriou NG, Sarris I, and Sotereanos DG. Neovascularization and other histopathologic findings in an autogenous saphenous vein wrap used for recalcitrant carpal tunnel syndrome: a case report. *J Hand Surg [Am]* 2003. **28**(2):262-6.

216. Vardakas DG, Varitimidis SE, and Sotereanos DG. Findings of exploration of a vein-wrapped ulnar nerve: report of a case. *J Hand Surg [Am]* 2001. **26**(1):60-3.

217. Masear VR, Tulloss JR, St Mary E, and al. e. Venous wrapping of nerves to prevent scarring. *J Hand Surg* 1990. **15A**(Abstract):817-818.

218. Koch H, Haas F, Hubmer M, Rappl T, and Scharnagl E. Treatment of painful neuroma by resection and nerve stump transplantation into a vein. *Ann Plast Surg* 2003. **51**(1):45-50.

219. Kakinoki R, Ikeguchi R, Matsumoto T, Shimizu M, and Nakamura T. Treatment of painful peripheral neuromas by vein implantation. *Int Orthop* 2003. **27**(1):60-4.

220. Palmer TD, Willhoite AR, and Gage FH. Vascular niche for adult hippocampal neurogenesis. *J Comp Neurol* 2000. **425**(4):479-94.

221. DeGowin RL, Lewis LJ, Mason RE, Borke MK, and Hoak JC. Radiation-induced inhibition of human endothelial cells replicating in culture. *Radiat Res* 1976. **68**(2):244-50.

222. Schaner PJ, Martin ND, Tulenko TN, Shapiro IM, Tarola NA, et al. Decellularized vein as a potential scaffold for vascular tissue engineering. *J Vasc Surg* 2004. **40**(1):146-53.

223. Fields RD, Le Beau JM, Longo FM, and Ellisman MH. Nerve regeneration through artificial tubular implants. *Prog Neurobiol* 1989. **33**(2):87-134.

224. Terzis JK, Skoulis TG, and Soucacos PN. Vascularized nerve grafts. A review. *Int Angiol* 1995. **14**(3):264-77.

225. Levine MH, Yates KE, and Kaban LB. Nerve growth factor is expressed in rat femoral vein. *J Oral Maxillofac Surg* 2002. **60**(7):729-33; discussion 734.

226. Amiel GE, Komura M, Shapira O, Yoo JJ, Yazdani S, et al. Engineering of blood vessels from acellular collagen matrices coated with human endothelial cells. *Tissue Eng* 2006. **12**(8):2355-65.

227. Werts ED, Johnson MJ, and DeGowin RL. Postirradiation hemopoietic repopulation and stromal cell viability. *Radiat Res* 1977. **71**(1):214-24.

228. Oberlin E, Tavian M, Blazsek I, and Peault B. Blood-forming potential of vascular endothelium in the human embryo. *Development* 2002. **129**(17):4147-57.

229. Zambidis ET, Oberlin E, Tavian M, and Peault B. Blood-forming endothelium in human ontogeny: lessons from in utero development and embryonic stem cell culture. *Trends Cardiovasc Med* 2006. **16**(3):95-101.

230. Tang W, Zeve D, Suh JM, Bosnakovski D, Kyba M, et al. White fat progenitor cells reside in the adipose vasculature. *Science* 2008. **322**(5901):583-6.

231. Brunelli GA, Battiston B, Vigasio A, Brunelli G, and Marocolo D. Bridging nerve defects with combined skeletal muscle and vein conduits. *Microsurgery* 1993. **14**(4):247-51.

232. Battiston B, Tos P, Geuna S, Giacobini-Robecchi MG, and Guglielmone R. Nerve repair by means of vein filled with muscle grafts. II. Morphological analysis of regeneration. *Microsurgery* 2000. **20**(1):37-41.

233. Geuna S, Tos P, Battiston B, and Giacobini-Robecchi MG. Bridging peripheral nerve defects with muscle-vein combined guides. *Neurol Res* 2004. **26**(2):139-44.

234. Mosmann T. Rapid colorimetric assay for cellular growth and survival: application to proliferation and cytotoxicity assays. *J Immunol Methods* 1983. **65**(1-2):55-63.

235. Kanaya F, Firrell JC, and Breidenbach WC. Sciatic function index, nerve conduction tests, muscle contraction, and axon morphometry as indicators of regeneration. *Plast Reconstr Surg* 1996. **98**(7):1264-71, discussion 1272-4.

236. Dellon AL and Mackinnon SE. Selection of the appropriate parameter to measure neural regeneration. *Ann Plast Surg* 1989. **23**(3):197-202.

237. Bain JR, Mackinnon SE, and Hunter DA. Functional evaluation of complete sciatic, peroneal, and posterior tibial nerve lesions in the rat. *Plast Reconstr Surg* 1989. **83**(1):129-38.